R. & M. No. 3348

MINISTRY OF AVIATION

AERONAUTICAL RESEARCH COUNCIL
REPORTS AND MEMORANDA

Tests at Transonic Speeds on Wings with Wedge Sections and Sweep varying between 0° and 60°

By E. W. E. Rogers, C. J. Berry and V. G. Quincey
of the Aerodynamics Division, N.P.L.

LONDON: HER MAJESTY'S STATIONERY OFFICE
1963
PRICE £2. 0s. 0d. NET

Tests at Transonic Speeds on Wings with Wedge Sections and Sweep varying between 0° and 60°

By E. W. E. Rogers, C. J. Berry and V. G. Quincey
of the Aerodynamics Division, N.P.L.

*Reports and Memoranda No. 3348**
October, 1961

Summary.

Tests have been made in the N.P.L. 18 in. by 14 in. High-Speed Tunnel at stream Mach numbers between 0·6 and 1·2 on two finite wings of identical planform and having single-wedge and double-wedge sections of 14% and 7% thickness/chord ratio respectively. The wings were untapered and the sweepback could be set at five values: 0°, 15°, 30°, 45° and 60°. The test Reynolds number based on the streamwise chord varied with stream Mach number and wing sweepback, and was between $1·3 \times 10^6$ and $3·4 \times 10^6$.

The experiment was intended to assist in assessing the validity of the simple sweepback concepts currently in use, particularly for predicting the flow about infinite sweptback wings from two-dimensional data. The three-dimensional effects present are reduced to some extent by the type of section used, especially at transonic speeds, and the measured pressure distributions at a particular spanwise station, and the associated pressure forces (normal and chordwise) correlate quite well on the basis of the simple theory. In addition it is shown that the general flow development, including the initial growth of the leading-edge separation, and the transonic flow-attachment about the leading edge also correlate satisfactorily, as do the pressures measured on the base of the single-wedge wing.

There is some discussion on the effect of shock sweep on the conditions required for shock-induced boundary-layer separation and a modification is suggested to the curve put forward tentatively in Ref. 8.

LIST OF CONTENTS

* Replaces A.R.C. 23,180. Published with the permission of the Director, National Physical Laboratory.

LIST OF CONTENTS—*continued*

---

1. *Introduction.*

Present-day methods of designing sweptback wings are based fundamentally on the simple sweepback concepts first put forward by Betz and Busemann[1] some twenty-five years ago. Briefly these were that the characteristics of an infinite swept wing depended only on the component of the stream velocity normal to the leading edge, and the relative incidence of this component to the plane containing the wing. If the wing sweepback is ϕ, then the two important parameters influencing the flow are $U_0 \cos\phi$ and $\alpha \sec\phi$, where U_0 is the stream velocity and α the wing incidence; in a compressible flow, the velocity component may conveniently be replaced by the Mach number component $M_0 \cos\phi$, the stream Mach number being denoted by M_0. Thus, on this argument, data obtained from tests on a two-dimensional, unswept aerofoil may readily be applied to an infinite wing of arbitrary sweepback (*see* Ref. 36).

The validity of the simple sweepback theory has been demonstrated both at low stream speeds[2] and at moderate subsonic speeds[3, 4] by comparing in the correct manner pressure distributions obtained on swept wings with those from the related unswept section. In this type of test, it was generally found that the mid-semi-span of a finite swept wing of high aspect ratio could, for practical

purposes, be regarded as equivalent to a section of an infinite swept wing, so that the combined effects of the wing root and tip could be ignored. Fig. 1 shows results from certain unpublished N.P.L. tests in which the wings completely spanned the width of a high-speed wind tunnel, and serves to illustrate the nature of the agreement which may be obtained, even though, as in this case, the pressure-plotting station lies comparatively close to the end of the wing.

The view may be held, however, that the most important application of the simple sweep theory occurs in conditions when the stream Mach number is transonic or supersonic, the sweep being sufficiently high for $M_0 \cos \phi$ to remain subsonic in value; it is possible in this way, one may argue, to obtain low-drag, shock-free, subsonic-type flow over the wing even at supersonic stream Mach numbers. The advantages of such a flow are obvious and have been discussed at length elsewhere, particularly as the basis of a wing designed for economic operation at low supersonic Mach numbers (*see*, for example, Ref. 6).

One important factor in the design of such a sweptback wing is the choice of the wing section, a topic discussed in Ref. 7 in terms of results obtained from investigations on two-dimensional aerofoils. The assumption is made that the favourable characteristics of aerofoil profiles at transonic and subsonic speeds would still be present on the related infinite, swept wing at correspondingly higher speeds. Thus the simple sweep theory is used in these circumstances to enable a detailed correspondence to be established between swept and unswept sections.

One may accept such a correspondence simply as a particular instance of the sweep theory, as indeed it must be if the theory and its underlying assumptions are held to be universal in application. On the other hand, the matter is of sufficient importance to justify a more critical assessment, including, if possible, some experimental proof of the validity of the simple sweep theory for transonic-type flows.

The chief obstacle to providing the required experimental evidence is in simulating in the wind tunnel the flow conditions appropriate to an infinite swept wing, for it is at transonic and low supersonic speeds that the effects of the ends of the wing (particularly the root or upstream end) are concentrated in regions which spread farthest over the wing[16]. Thus a configuration like that shown in Fig. 1, in which the mid-semi-span position could be regarded as effectively part of an infinite wing at a stream Mach number of 0·8, ceases to be satisfactory when the stream Mach number exceeds unity. Of course, attempts can be made to overcome the dominant end effects. For example, the junction of the upstream end of the wing with the tunnel wall or supporting body may be contoured so that the required flow is maintained in the junction. In practice, this is not easy to do, particularly for a range of stream Mach number and wing incidence; limited attempts at the N.P.L. in connection with the models shown in Fig. 1 were rather unsatisfactory, though with more effort the difficulties encountered could probably have been overcome. It may be argued, however, that such a technique, corresponding as it does to the superposition of the contoured-junction flow field on that originally present on the untreated wing, artificially creates the desired pressure distribution and to this extent begs the original question of whether the infinite swept wing behaves in a similar manner to the related unswept section.

An obvious alternative is to make the wing of sufficient aspect ratio to ensure that the measuring station is beyond the region most seriously influenced by the root and tip. For a conventional wing section at transonic and low supersonic speeds the upstream boundaries of these zones correspond in certain conditions to the forward and tip shocks[8], the former, associated with intense disturbance to the flow at the root leading edge, being the most troublesome. Ideally then, the pressure-plotting

station should be outboard of the junction of the forward and rear shocks, and inboard of the region influenced by the tip shock.

These conditions have been most closely approached by Lawlor[9], whose results indicate substantial support for the simple-sweep theory. He was forced, however, to use a wing of considerable span, and, in order to maintain the test Reynolds number at a reasonably high value, a large wind tunnel. There would seem no doubt that this technique, when practicable, is very satisfactory.

For the tests described in the present report a half-wing of finite span, and mounted directly on a wall of a high-speed wind tunnel, was used. The wing contained a pressure-plotting station at about 0·7 of the semi-span, and the leading-edge sweep could be varied in steps between 0° and 60°. The effects associated with the junction of the wing and the tunnel wall were reduced in extent, rather than removed altogether, by choosing wing sections for which the maximum local velocity and most rapid flow acceleration occur away from the leading-edge region for some range of wing incidence. Two wing profiles were in fact used, one of double-wedge and one of single-wedge section. The highest local velocity occurs at the ridge-line and trailing edge respectively at low incidence, and for the double-wedge section the major disturbance at the root-wall junction usually takes the form of a shock wave originating at the ridge and running rearwards over the wing surface. There is a strong similarity between this shock and the forward shock which develops at moderate incidences close to the leading edge of wings having conventional sections, and hence for part of the test range at least the influence of the wing root may be regarded as existing to a marked degree only in the region to the rear of this ridge shock. Compared with the conventional section, with the limiting forward shock, the severe root influence for the double-wedge profile is considerably reduced in extent, partly because of the more rearward origin of the shock, and partly because the ridge shock propagates at a smaller angle with respect to the stream direction as a result of the higher local Mach numbers which occur to the rear of the ridge line. As the wing incidence is increased, the true forward shock appears however and the subsequent flow development is similar to that on swept wings having more conventional sections.

For the single-wedge section, the ridge shock is of course absent and the forward-facing surfaces are influenced mainly by the tip and forward shocks, and the effects of their intersection.

The results obtained with the wing at incidence must inevitably be affected by the finite aspect ratio of the model, at least for part of the test conditions. Moreover, as will be seen, the wing aspect ratio itself changes with the wing sweep. The present approach cannot be regarded as a satisfactory alternative to the technique employed by Lawlor, neither are the two wing sections representative of those likely to be used in modern aircraft design. Nevertheless, despite its inherent limitations the present experiment does appear to provide useful data on the application of simple sweepback ideas in transonic flows, data which up to the present have been rather scanty and which now appear to confirm many of the concepts tacitly assumed in much of the current work on swept-wing design. The final confirmation of these ideas for general section shapes must inevitably come from more precise experiments, however.

During the tests an opportunity was taken to obtain additional information to that contained in Refs. 8, 10 and 11 about the effect of shock sweep on the conditions required for shock-induced separation of the boundary layer on the wing surface. Measurements were also taken of the spanwise distribution of pressure on the base of the single-wedge wing for the complete range of sweepback, Mach number and incidence.

2. *Experimental Details.*

2.1. *The Models.*

Two wings of identical planform were used for the tests. The sweep of each wing could be varied in steps of 15° to enable the following sweepback angles to be achieved: 0°, 15°, 30°, 45° and 60°. Mechanical considerations required that the wings should pivot about the trailing edge of the root section, and this meant that the exposed wing area and the leading-edge length increased with the sweep angle (*see* Table 1).

The leading edge and trailing edges of the wings were parallel but the tip was raked, as shown in Fig. 2, so that it became streamwise when the sweepback was 30°. The pressure-plotting station lay along a chord-line, normal to the leading edge and at 0·7 of the distance from the root to the tip along that edge when the wing was at zero sweep. As the sweep is increased, this value changes, as shown in Table 1, which also includes further information on the effect of changes in the sweep on the planform geometry.

The two wing sections are illustrated in Fig. 3. The double-wedge profile has a maximum thickness/chord ratio of 7% and the ridge-line occurs at mid-chord. The single-wedge section has the same chord and is geometrically similar to, but twice the size of, the forward half of the double-wedge profile. The leading-edge semi-angle (λ) of both sections is identical and almost exactly equal to 4·0°.

The distribution of the pressure holes, situated on the upper surface only, is shown in Table 2a and Fig. 3. In terms of x/c, where c is the wing chord measured normal to the leading edge, the two distributions are not very alike, but that for the single wedge was chosen so that each hole on the forward half of the double-wedge profile had a corresponding, geometrically-linked hole on the single-wedge surface. Thus the double-wedge hole at $x/c = 0{\cdot}2$ is the counterpart of the single-wedge hole at $x/c = 0{\cdot}4$, and so on. This arrangement was of value when comparing results from the forward-facing surfaces of the two wings.

The base of the single-wedge wing was fitted with 6 pressure holes at the spanwise positions given in Table 2b. All these holes were in the chord plane of the wing, that is, mid-way between the upper and lower shoulders of the base area.

2.2. *The Tunnel.*

The N.P.L. 18 in. by 14 in. Tunnel, with a transonic working section, was used for the tests. This has slotted walls above and below the model, one-eleventh of the total area of each wall being open[12]. The side-walls are solid and formed mainly by interchangeable panels of glass set in steel frames.

The wings were mounted directly on a turntable forming part of the tunnel side-wall, and which carried a four-component strain-gauge balance. This remained locked except when measurements of the wing lift and drag were being taken. Previous experience suggested that the effect of the wall boundary layer on the model forces and on the results obtained at the pressure-plotting station would be small, and might be neglected. The influence of the wall boundary layer on the oil-flow patterns could occasionally be quite marked, though limited to a region close to the root. Care was taken to ensure that leakage around the model root was kept small, partly by fitting special cover plates, flush with the tunnel wall, around the root section, thus restricting the airflow between the tunnel and the balance box outside the working section, and partly by reducing to a minimum the deflection of the balance system (and hence the wing root) under aerodynamic load. This makes the gap necessary

between the wing and the cover plates as small as possible. It is considered that the present results are free from any serious error due to root leakage effects.

The stream Mach number was determined from the pressure measured at a previously calibrated hole in one of the centre slats, at a position well upstream of the model. All tests were made at a constant stagnation pressure of 31 in. mercury absolute for a range of stream Mach numbers between 0·6 and about 1·2. The test Reynolds number, based on the wing chord in the stream direction, changes with both sweep and test Mach number, as indicated in the following table.

Variation of Test Reynolds Number

ϕ	Reynolds number $\times 10^{-6}$, based on the streamwise chord (c_s). Stagnation pressure and temperature are 31 in. Hg and 283°K respectively		
	$M_0 = 0{\cdot}60$	1·00	1·20
0°	$1{\cdot}2_5$	$1{\cdot}6_6$	$1{\cdot}7_0$
15°	$1{\cdot}3_0$	$1{\cdot}7_1$	$1{\cdot}7_6$
30°	$1{\cdot}4_5$	$1{\cdot}9_1$	$1{\cdot}9_7$
45°	$1{\cdot}7_7$	$2{\cdot}3_4$	$2{\cdot}4_1$
60°	$2{\cdot}5_1$	$3{\cdot}3_1$	$3{\cdot}4_1$

2.3. *Boundary-Layer Transition Position on the Wings.*

Because one of the more important objects of the tests was to compare the effect of changes in wing sweep on the development of the leading-edge separation, no distributed roughness was applied to the model surfaces in the leading-edge region. As a result, at zero incidence, regions of laminar flow existed on the forward-facing surfaces of the wings alongside wedges of turbulent flow arising from small imperfections in the leading edge itself (*see* Fig. 70a). On the double-wedge wing, transition was always observed to occur at the ridge-line, so that fully turbulent flow existed over the after part of the section. At incidence, separation took place at the leading edge on the upper surface and was followed by a reattachment at some distance downstream. This separation may be quite extensive at the lower part of the Mach number range for a given sweep; thereafter a change in the type of flow occurred (*see* Section 4) and the separation was restricted to a very small region close to the leading edge. In both types of flow, the boundary layer behind the reattachment position was turbulent except in a few cases. It follows that on the upper surface, which is of most importance in the present analysis, the boundary layer was nearly always turbulent for most of the test range, particularly when it interacted with a shock wave in the region behind the ridge-line. Indeed there is no direct evidence on the upper surface of a shock wave interacting with a laminar boundary layer at the pressure-plotting station, though this point was not completely covered in the tests.

On the lower surface, separation was absent when the wing was at incidence, and hence regions of laminar flow could still persist to the ridge-line. In a few cases at the lower sweepback angles the surface pressures to the rear of the ridge suggested that laminar boundary separation occurred immediately behind the ridge. These results were not used in the present analysis.

In brief, then, it is felt that the absence of any artificial means of provoking boundary-layer transition does not affect the results to be discussed to any appreciable extent. The influence of regions of laminar flow on the balance results will probably be small and, as far as can be judged, seem to have little effect on the base pressures.

2.4. *Test Procedure.*

The incidence range for both wings was limited by a maximum permitted bending stress at the model fixing position inside the balance box and close to the wing root. This formed a very severe restriction for the weaker double-wedge model, as can be seen in Fig. 4, where the limiting incidences for three sweepback angles are plotted against stream Mach number. Because of the greater stiffness of the single-wedge wing, much higher incidences were possible with this model, but these in fact were seldom reached; a more important consideration at the higher Mach numbers was the performance of the tunnel with the model at a high angle of attack.

Under aerodynamic load, there was some deflection and twist on each wing and both quantities were measured optically at the wing tip for a representative range of conditions. Deflection and twist were small for the single-wedge model at all test conditions, and their effect on the incidence of the wing could be ignored. The deflection and twist of the double-wedge wing, however, was considerable for part of the test range and a correction was therefore required to the nominal, or root, incidence (α_n) in order to estimate the effective incidence (α) at the pressure-plotting station. In general it was possible to present the correction in terms of a ratio $\Delta\alpha/\alpha_n$, where the correction $\Delta\alpha$ must be added to the nominal incidence. The variation of this ratio with test Mach number and wing sweep is shown in Fig. 5. The correction is large at sweepback angles of 0°, 45° and 60° but at the other values of ϕ it is sufficiently small to be neglected. In some parts of the test range the induced twist was not linear with incidence, and corrections to the nominal incidence were then obtained directly from the original observations since the form used in Fig. 5 is inappropriate. The probable error in the incidence at the pressure-plotting station after the correction has been applied seems to be about 0·1° or less.

Corrections arising from the twist and deflection of the model must also be applied to the values of wing incidence used for the balance results and the oil-flow patterns. In the former case a correction equal to 0·7 of those shown in Fig. 5 was added to the nominal incidence; this represents a simple allowance for the unknown variation of twist along the wing span. In the case of the oil-flow patterns, the full corrections contained in Fig. 5 were used since it was felt that the main interest was in the flow behaviour at the pressure-plotting position.

No correction was applied to allow for the blockage of the models at either subsonic or transonic speeds. The blockage ratio, defined as the ratio of the frontal area of the model to the tunnel cross-section, is high for the single-wedge model, being equal to 2·9% at zero sweep and 1·7% when $\phi = 60°$. For the double-wedge wing, these values are approximately halved. The wall constraint arising from the model lift was also neglected.

3. *Presentation of the Results.*

It is not the aim of the present text to analyse in detail all the data obtained during the experiment with the two variable-sweep wings. The main purpose of this report is to discuss the effect of changes in sweepback on the characteristics of two related profiles in the transonic speed range. In Section 4 below, the influence of sweepback on the general flow pattern, and its development with Mach

number and incidence will be considered. Next, in Section 5, the relationship between the surface pressures obtained at the various sweepback angles will be discussed, and this is followed in Section 6 by some consideration of the way in which the sweepback angle alters the position of some of the shock waves present on the wing surface. In Section 7 the results obtained from the tests are used to provide further evidence for the effect of shock sweep on the conditions required to cause separation of the turbulent boundary layer on the wing. This is followed in Section 8 by a brief discussion of the influence of the wing sweep on the pressures measured at zero incidence at the base of the single-wedge wing. The final Section (Section 9) is concerned with the normal and axial pressure forces developed at the pressure-plotting station and deduced from the surface-pressure distributions.

4. *The Effect of Sweepback on the General Flow Development.*

The general flow pattern about the model upper surface, and the way it varies with wing sweep and incidence and with stream Mach number, is most easily studied from the sets of oil-flow photographs obtained at intervals throughout the experiment. From these patterns, the initial appearance and subsequent movement of shock waves, the onset of flow separation and like events may be detected.* From a set of oil patterns for a particular sweep angle, covering a range of Mach number and incidence, various flow boundaries may be deduced. These are shown in the several parts of Fig. 6 for the double-wedge wing and in the corresponding sections of Fig. 8 for the single-wedge wing.

4.1. *Double-Wedge Wing.*

Consider first the double-wedge wing at zero sweep (Fig. 6a). For stream Mach numbers below about 0·8, the application of incidence causes separation along the entire leading edge, the flow forming a closed bubble and reattaching on the surface at some downstream position (*see* Fig. 63a). The broken line in Fig. 6a indicates the incidence at which this reattachment takes place at $0 \cdot 1c$. At smaller incidences, the separation and subsequent reattachment still exist closer to the leading edge; from the oil-flow patterns alone it is not possible to specify accurately when separation first occurs, although it must certainly start at a very small incidence. The choice of some arbitrary reattachment position near the leading edge overcomes this difficulty to some extent and enables a more consistent set of curves to be obtained for each wing. Above a stream Mach number of about 0·8 however, large-scale leading-edge separation no longer takes place with increasing incidence, the flow becoming attached over the upper surface, with a supersonic-type expansion around the leading edge[14, 34]. Even in this flow, a small separation, with boundary-layer transition just downstream of the reattachment position still occurs in the first few percent of the chord[5]. The important difference between this flow and that occurring at the lower Mach number is that the extent of the local leading-edge separation is almost unaffected by the wing incidence, has only a limited influence on the wing flow and can frequently be disregarded. In the present report this supersonic type of flow will be referred to for convenience as 'attached leading-edge flow' to distinguish it from the large-scale 'separated leading-edge flow' that takes place at the lower Mach numbers; the former term is not strictly accurate however. The transition from separated to attached leading-edge flow which takes place

* For a discussion of the difficulties and likely inaccuracies in estimating events from a sequence of oil-flow patterns, *see* Ref. 13.

as the stream Mach number is increased at constant wing incidence (line AA′ in Fig. 6a) will be called the transonic leading-edge flow attachment. Fig. 6a shows that the Mach number for reattachment is relatively insensitive to wing incidence.

The other important events shown in Fig. 6a are related to the appearance and rearward movement of a shock wave at the ridge-line of the section, where the maximum local velocity is achieved as a result of the flow expansion over the ridge; ultimately this shock reaches the trailing edge. Before this, however, the ridge shock becomes strong enough to cause boundary-layer separation, at a stream Mach number of about 0·80.

Another shock may be present above the leading-edge separation bubble just before the leading-edge flow attachment takes place, but it is not possible to detect this from the oil patterns. A further shock almost certainly originates from the reattachment of the small leading-edge separation present at the higher Mach numbers[25]. Both shocks are of less significance in the present context than that developing behind the ridge.

Similar approximate flow boundaries have been drawn for the other sweepback angles (Figs. 6b to e). At $\phi = 15°$, these boundaries are very similar to those on the unswept wing; in addition a clear forward shock (associated mainly with the production of sufficiently high velocities at the leading edge and the presence of the wing-root junction[8]) can be detected for stream Mach numbers above those at which the transonic flow attachment begins. At lower Mach numbers, the leading-edge separation region possesses a vortex-like, rather than a bubble-type, structure over the inner half of the span (Fig. 65). The general effect of the sweep is to increase slightly the stream Mach numbers at which the important flow events occur and this trend is much more marked at a sweepback angle of 30°. (Fig. 6c.) For $\phi = 45°$, the flow boundaries are somewhat altered in shape and it is now possible to distinguish between the beginning of the leading-edge flow attachment at some spanwise station and its completion along the entire leading edge. Finally at 60° sweepback (Fig. 6e), the leading-edge separation and its associated vortex are present over the whole Mach number range of the tests, within which transonic flow attachment does not take place.

The flow-boundary diagrams of Fig. 6 are severely restricted by the incidence range permitted with the double-wedge wing, and because of the distortion of the model under load and the rather limited number of oil-flow patterns available, these boundaries should only be regarded as approximate. Nevertheless, it seems appropriate to replot these results in terms of the reduced incidence ($\alpha \sec \phi$) and stream Mach number ($M_0 \cos \phi$), as in Fig. 7. In general the curves for a particular event tend to group together, suggesting that to some extent simple-sweep theory can be used to account for the differences in the various parts of Fig. 6. The agreement between the curves indicating the reattachment of the leading-edge separation at $0{\cdot}1c$ is good, particularly for values of $M_0 \cos \phi$ below about 0·7. The correlation of the transonic flow-attachment boundaries is less satisfactory, mainly on account of the rather high value of $M_0 \cos \phi$ achieved by the 45° swept wing.

4.2. *Single-Wedge Wing.*

The limited nature of the data from the double-wedge wing may be supplemented by making a corresponding analysis of the single-wedge results, and the main boundaries for this wing are contained in Figs. 8a to e. The smaller elastic distortion of the model under aerodynamic load makes it possible to determine these boundaries with greater accuracy. As an example of how these diagrams were compiled, the set of points used to draw Fig. 8a are displayed in Fig. 9; each point was obtained from a surface oil-flow pattern.

For the single-wedge wing, the boundary corresponding to flow reattachment at $0{\cdot}1c$ has again been drawn. The leading-edge flow-attachment process occurs first over only part of the span at moderate incidences, full-span attachment being attained with increasing stream Mach number. This spanwise variation cannot be attributed to the twisting of the model, and must therefore be a three-dimensional effect. One interesting aspect of this spanwise variation is that the attached flow occurs first on the inner part of the wing at sweep angles of 0° and 15°, and on the outer part of the wing when the sweep is 30° and 45°. Immediately after the leading-edge flow attachment associated with increasing stream Mach number, shock-induced separation occurs at the foot of the strong rear and outboard shocks ($\phi = 0°$, 15° and 30°) or the forward shock ($\phi = 45°$). With further increase in Mach number, the strength of these shocks decreases, because of the strong isentropic compression which exists between the leading edge and the shock, and the separation ultimately ceases.

4.3. *Comparison of Leading-Edge Separation Boundaries.*

The effect of wing sweep on the leading-edge separation and transonic flow-reattachment boundaries is illustrated directly in Fig. 10. Broken lines have been drawn on this diagram showing the Mach numbers and incidences at which the flow reattachment takes place at the mid-semi-span; such boundaries are perhaps as representational as possible for the present results of true two-dimensional flow.

The various horizontal boundaries, which represent a stage in the development of the leading-edge separation, are replotted in terms of $M_0 \cos\phi$ and $\alpha \sec\phi$ in Fig. 11. The five curves collapse in a satisfactory manner and the average value of $\alpha \sec\phi$ is close to that for the double-wedge wing (Fig. 7). It seems reasonable to conclude that the initial development of the separation bubble or vortex on the single-wedge wing depends very largely on the Mach number component normal to the leading edge and on the associated incidence, $\alpha \sec\phi$. The oil patterns show in fact that initially the separation is often remarkably uniform along the span. The reattachment line of the bubble or vortex lies parallel to the leading edge except at the extremes of the span and thus it might be expected that a close approximation to the infinite-swept-wing flow may be achieved. Only at the higher incidences, as the separated region grows rearward and so becomes appreciable compared with the span, does the wing sweep appear to modify the reattachment-line position. For $\phi = 0°$, the reattachment line moves rapidly to the trailing edge, whilst remaining roughly parallel to the leading edge, but becoming more and more influenced by the strong vortex, originating at the tip leading edge and spreading inboard over the wing. When the wing is swept at 30° or greater, the vortex sweep soon becomes larger than that of the leading edge as the wing incidence is increased. Hence it is only the initial stages of the separation growth that may be related by the simple theory; the subsequent development is influenced by the finite span of the models.

Because Fig. 7 and Fig. 11 agree, it is also possible to argue that on the present evidence, the initial development of the separation region is independent of the section shape behind the maximum-thickness position. The flow reattaches at $0{\cdot}1$ of the wing chord at almost the same value of $\alpha \sec\phi$ for both profiles, and not as might perhaps be expected, at the same fraction of the forward-facing surfaces. In the absence of separation, the local pressure gradients due to the wing profile, when expressed in terms of the total wing chord, must be twice as large for the double-wedge wing. The gradients due to the model lift however are presumably related simply to the model chord, and in the leading-edge region more specifically by the stagnation-point position and the circulation. The former may well determine the shape of the local separation bubble.

4.4. *Comparison of Transonic Flow-Reattachment Boundaries.*

As was remarked earlier, the more or less vertical boundaries of Fig. 10 correspond to the inception and completion of leading-edge flow attachment, the shaded area of partial attachment representing a departure from the assumed two-dimensional flow conditions. It might be expected then that the observed flow-attachment boundaries would give a less striking confirmation of the simple-sweep theory than is contained in Fig. 11. Fig. 12 shows that there is in fact some variation in the values of $M_0 \cos\phi$ at which the leading-edge attachment begins, and is completed, though the range of Mach number component involved is not large. As the wing sweep increases, the boundaries shift progressively to the right. It may be thought more realistic to consider the boundaries for flow reattachment at the mid-semi-span position, shown as broken lines in Fig. 10. These are replotted in terms of the reduced Mach number and incidence in Fig. 12c; the improvement over the two earlier diagrams is small however. It is perhaps unwise to dwell too much on the magnitude of the variation in $M_0 \cos\phi$ shown in Fig. 12 and to accept instead the results as evidence that the transonic leading-edge attachment is strongly influenced by the component of stream Mach number normal to the wing leading edge. Such a finding is in agreement with the broader analysis of results from many different sweptback wings made by Stanbrook and Squire[15].

The leading-edge flow-attachment boundaries for the double-wedge wing may be transferred from Fig. 7 to Figs. 12a and b in order to compare the two sections. The most serious discrepancy occurs at $\phi = 30°$, and corresponds to about 0·04 in stream Mach number at $\alpha = 3°$. The existence of this variation may readily be confirmed from the oil-flow patterns; for example, at $\alpha = 3°$ the flow is attached over part of the span of the double-wedge wing at a stream Mach number of 0·89, but completely detached on the single-wedge model at $M_0 = 0{\cdot}90$. Uncertainties in the exact values of M_0 and α cannot account for this magnitude of difference. At a sweepback of 45° there is reasonable agreement in the values of $M_0 \cos\phi$ at which transonic flow attachment first takes place, and is completed, suggesting that the apparently large values of $M_0 \cos\phi$ for this sweep in Fig. 7 may be correct.

Briefly then, it may be concluded that complete leading-edge separation ceases and gives place to attached flow around the leading edge when the Mach number normal to that edge exceeds about 0·8. This value is somewhat higher than found elsewhere for circular-arc aerofoils ($\phi = 0°$) for a range of leading-edge angles[13, 14, 17]. The differences between the curves for the various sweep angles are rather greater for the flow-attachment phenomenon than for the leading-edge separation development discussed earlier, and part of these differences may be associated with the finite span of the wings. The dominant part played by the parameters $M_0 \cos\phi$ and $\alpha \sec\phi$ is unquestionable however.

5. *The Effect of Sweepback on the Surface Pressure Distributions.*

5.1. *The Validity of the Results.*

In the preceding paragraphs we have been concerned with the effects of changes in the leading-edge sweep on the general flow pattern; it is now appropriate to consider how the wing sweep influences the pressures measured at the pressure-plotting station, and to attempt to correlate these on the basis of the simple-sweep theory. To do this, it must be assumed that the measuring station can be regarded as part of an infinite swept wing, even though the aspect ratio and spanwise position of the station vary with the sweepback angle (*see* Table 1). In considering this point, attention in this section of the report will be concentrated mainly on the results obtained with the unswept

double-wedge wing, partly because of the existence of comparable two-dimensional data, and partly because it will be shown later that the results from the swept double-wedge wing and from the single-wedge model correlate quite well with those from the unswept double-wedge section.

Though there already exists a considerable amount of data on two-dimensional wedges in the transonic speed range, covering a wide variation in the leading-edge semi-angle (λ), there appears to be no information on an aerofoil having exactly the same value of λ as the present model ($4{\cdot}0°$). The most closely related profiles are those tested by Sandemann[18], Knechtel[19] and others, which have semi-angles of $3{\cdot}4°$ and $4{\cdot}5°$. A comparison for stream Mach numbers very close to $0{\cdot}60$ between the present results for $\phi = 0°$ and those from Ref. 18 is given in the upper part of Fig. 13a. H is the stream total pressure and p the local static pressure. The small variations in λ do not appear to affect the surface pressure distributions greatly and the results from the finite wing lie close to the two-dimensional data. Only the points from the thicker wedge of Ref. 18 are included behind the ridge-line in this comparison, because those obtained with the wedge of $3{\cdot}4°$ semi-angle were modified to the rear of the ridge by a laminar boundary-layer separation.

This comparison has been extended to higher stream Mach numbers in the lower diagram of Fig. 13a. Over the front part of the profile there is a considerable disagreement between the present results and those reported by Sandemann, lower local Mach numbers being attained on the wing. According to the results given by Vincenti[20] the effect of the finite aspect ratio should be to *increase* the local Mach numbers on the forward part of the section, a trend in the opposite direction to that shown in the diagram. In fact, the distribution of pressure over the front part of Sandemann's $4{\cdot}5°$ wedge does not agree with similar measurements made on an identical profile by Knechtel[19], whilst, as will be seen, these later results are in excellent agreement with those obtained from the present finite wing. It must be concluded therefore that these particular results given in Ref. 18 are to some extent suspect,* and that a more valid comparison will be obtained by using the data of Ref. 19. A theoretical curve[22] for the distribution of pressure at a stream Mach number of unity may also be used to check the present results, again in a satisfactory manner. At transonic speeds the pressures over the rear half of the double-wedge will depend on the expansion angle at the ridge, which is equal to 2λ. This explains the progressive decrease in pressures with increasing thickness apparent in Fig. 13a.

It seems clear that at zero incidence the results from the pressure-plotting station may be regarded as largely equivalent to those obtained on a true two-dimensional model. Consideration must now be given to the effects of placing the wing at incidence; the influence of the finite span would then be expected to reduce the lift measured at the pressure-plotting station compared with the two-dimensional value, and this of course implies a discrepancy in the local pressure distributions. In the upper part of Fig. 13b the pressure distribution obtained on the double-wedge wing at a corrected incidence of $3{\cdot}0°$ and a stream Mach number of $0{\cdot}70$ are compared with results due to Sandemann[18] and Knechtel[19] at the same incidence. The points from Ref. 18 are in very close agreement with the present results over most of the model surface, whereas Knechtel's data show marked differences on the upper surface. The agreement with the tests of Ref. 18 is less encouraging than it appears at first sight, because the lift obtained from the integration of this pressure distribution for the $3{\cdot}4°$ wedge is about 15% lower than that measured on a strain-gauge balance

* The difference between Sandemann's and Knechtel's results is probably attributable to tunnel interference. This matter is discussed briefly in Refs. 23 and 24, and it would appear that the tunnel used in Ref. 18 was rather too open for the particular models tested.

attached to the complete aerofoil. The reason for this is not clear but it does suggest that the proper comparison in the present context is once more with Knechtel's data. It thus appears that the pressures at the pressure-plotting station are, as expected, modified by the finite wing span. The effect is not large however, and though a serious criticism of the present experimental technique, may not influence unduly the general conclusions to be drawn in the present text.

A further comparison with Knechtel's results is made in the lower part of Fig. 13b. The stream Mach number is very nearly equal to 1·05 for both cases, but the incidence of the two-dimensional wing is 2·0° and for the finite double-wedge wing the corrected value is 2·2°. The apparent agreement over the front part of the profile is therefore again slightly misleading and may be more correctly visualised as corresponding to a 10% loss in lift for double-wedge wing. A further loss in lift occurs over the rear portion of the section, but in this case it is probably mainly attributable to effects associated with the different expansion angles (8° and 9°) at the ridge-line. These correspond to local Mach numbers just behind the ridge of 1·365 and 1·400 respectively, the values of p/H being 0·330 and 0·314.

The comparisons shown in Fig. 13 are intended only to establish in general terms the possible magnitude of the influence of the finite span of the wings on the measured pressure distribution. In certain test conditions the effect may be rather less than that indicated; in other cases it may well be more. Exact knowledge can only come from information on the spanwise distribution of the lift for all flows. Three-dimensional effects cannot be avoided entirely in tests of this type and it is to be hoped that such as do exist are sufficiently small not to affect the main conclusions. At transonic stream speeds other effects associated with the finite span of the model will be present; for example, the forward shock from the root-wall junction or the tip shock will cross the pressure-plotting station when the wing incidence is high enough. In this condition the flow ahead of these two shocks ought to behave very largely as if the wing span were infinite. As was mentioned earlier, the choice of a double-wedge section for the wing profile tends to delay the appearance of the true forward shock and to reduce considerably the interference effects associated with the wing-root junction. The effects cannot be removed altogether in this way.

5.2. *Results from the Single-Wedge Wing.*

The overall effects of increasing stream Mach number, wing incidence and leading-edge sweep may be seen from Figs. 47 to 55; for example, the development of the separated flow region with increasing incidence at a Mach number of 0·7 is illustrated in Fig. 47. When leading-edge reattachment occurs, there is a change in the shape of the upper-surface pressure distribution; in particular a marked isentropic compression exists upstream of the shock (Fig. 54) and when the latter is near the wing leading edge it may cause boundary-layer separation. The reattachment of this shock-induced separation may often be linked to characteristic changes in the shape of the surface pressure distribution; observed reattachment positions on the unswept wing are marked in Fig. 48a where it seems that the separation region corresponds to the moderately steep compression zone to the rear of the shock.

At zero sweepback, with attached leading-edge flow at fixed incidence the pressure on the surface ahead of the shock is largely independent of M_0, as can be seen from the results plotted in Fig. 14, though there is a tendency for the local Mach number (M_L) to decrease slightly as the stream Mach number increases and the shock moves rearward. At the same time, the shock pattern becomes more clearly defined, resolving into an inclined shock from both the tip and root leading edges with a

short intersection shock between them at about the wing semi-span. Above a Mach number of about 0·90, it is the highly-swept tip shock that passes across the pressure-plotting station and this change is reflected in the pressure distributions by a sudden reduction in the strength of the recompression as the stream Mach number rises (*see* Fig. 54a). The shock movement with increasing incidence apparent in Fig. 50a, for example, is due to the increasing sweep of the tip shock as the local Mach numbers in the tip region rise. No boundary-layer separation takes place behind the tip shock.

There is much similarity between this pattern of events and that for the swept wing. At $\phi = 45°$, and particularly 60°, the vortex formed from the leading-edge separation exhibits a marked suction effect on the adjacent surfaces. (Fig. 48e.)

The transition to attached leading-edge flow does not take place within the test range for the 60° swept wing but for moderate incidences occurs near $M_0 = 1{\cdot}15$ for $\phi = 45°$. A typical change in the surface pressures over the forward part of the single-wedge section may be seen in Fig. 54d as the stream Mach number is increased from 1·11 to 1·20. At $M_0 = 1{\cdot}16$ a change from attached to separated leading-edge flow occurs as the incidence is raised due to the shape of the flow boundary; the corresponding pressure distributions are contained in Fig. 52d. Both the oil patterns and pressure distributions show that as the sweep increases the forward shock becomes of greater importance in the wing flow and there is a corresponding reduction in the influence of the tip shock.

These pressure distributions may be compared on the basis of simple-sweep theory by replotting in terms of p/H_e, where H_e is the equivalent total head of a stream of Mach number $M_0 \cos\phi$ and having the same static pressure as the free stream. Thus

$$\frac{p}{H_e} = \frac{p}{H}\frac{H}{H_e} = \frac{p}{H}\left[\frac{\left(\frac{p}{H}\right)_{\text{for } M=M_0\cos\phi}}{\left(\frac{p}{H}\right)_{\text{for } M=M_0}}\right]$$

$$= \frac{p}{H}\left[\frac{1+\frac{1}{5}M_0^2}{1+\frac{1}{5}M_0^2\cos^2\phi}\right]^{7/2}.$$

This is equivalent to making the comparison in terms of $C_p \cos^2\phi$. Figs. 15a and b show such a comparison when the wing is at zero incidence and $M_0 \cos\phi$ is 0·60 and 0·80, respectively. The agreement is good, except at the highest stream Mach numbers, where there appears to be a pressure gradient along the chord, perhaps associated with the large blockage of the model (2·9%). In Fig. 15a, the irregularity in the pressures near $x/c = 0{\cdot}6$ is probably due to the reflection of the bow wave of the model from the tunnel wall on to the model surface. Despite differences of this kind the general level and trend of the results is consistent with the theoretical approach.

When the incidence normal to the leading edge is increased to 4·0° discrepancies begin to occur in the separated-flow region near the leading edge. (Fig. 15c.) For $\phi = 0°$ and 15°, the values of p/H_e there agree closely and to the rear of $x/c = 0{\cdot}3$, agreement is still obtained when the sweepback is increased to 30° and 45°. Over the forward part of the chord however, there is a tendency for the separated-flow region to occupy a smaller fraction of the chord at the higher sweepback angles, and this trend is most noticeable at $\phi = 60°$. At this sweepback, the pressures over the rear part of the profile are rather different in level and shape, and it may be possible to attribute this to the influence of a flow distortion in the tunnel itself; a similar effect was commented upon in connection with Fig. 15a.

The evidence of Fig. 15c, though not conclusive, suggests that the flow in the separation region does not conform exactly to the model used in the simple-sweep theory, and is influenced to some extent by the actual wing sweep. The main differences appear to be in the position of the reattachment line when this is well away from the leading-edge region; it might be expected that the reattachment, linked as it is to the boundary-layer flow on the model would be susceptible to the magnitude of the spanwise velocity component, and also, for large-scale separations, the finite span of the wing.

Fig. 15 contains data obtained at fractional Mach numbers and incidences, chosen specially for comparison purposes. Unfortunately, no such direct comparisons were made at high incidence on the single-wedge model when the flow was attached over the forward part of the chord. It is possible, however, to construct such a comparison by cross-plotting the available results. This is done in Fig. 16, where the variation of p/H_e is plotted against $\alpha \sec \phi$ for chordwise positions of $0{\cdot}05c$, $0{\cdot}17c$ and $0{\cdot}32c$. The stream Mach number component normal to the leading edge varies slightly, but is close to $0{\cdot}85$. At low values of this reduced incidence, the shock wave, when it exists, is ahead of the hole position and influences the degree of correlation obtained. The sudden fall in pressure which occurs near $\alpha \sec \phi = 3°$ for $x/c = 0{\cdot}05$ is caused by the passage of the shock past the pressure hole, which is subsequently in a supersonic flow field extending back from the leading edge and which should be largely unaffected by the wing root and tip. This flow transition takes place at higher incidences at the more rearward stations. With further increase in incidence, there is a steady fall in local pressure as the expansion around the leading edge becomes stronger.

Within this supersonic flow region there appears to be an effect associated with the wing sweep, which is comparatively small at the most forward station and becomes more marked at $x/c = 0{\cdot}32$. If the flow behaved in a manner predicted by the simple-sweep theory, the lines for the various sweepback angles should be coincident; the differences shown in Fig. 16 must therefore be attributed to some modification to the assumed conditions for this attached type of flow.

The actual variation in the values of p/H_e on the wing surface for the four sweepback angles of this comparison may be estimated from Fig. 16 for a constant value of $\alpha \sec \phi$, say $7{\cdot}0°$, as in Fig. 17. It is apparent that as the sweep increases, there is a correspondingly larger supersonic recompression behind the leading edge than would be predicted by the simple theory. This result is of considerable importance because of the fundamental assumption made in the design of aerofoil sections for swept wings that the two-dimensional characteristics are retained unchanged when the section is used as part of a swept infinite wing. More particularly, one of the desirable features of the type of profile advocated by Pearcey[7] is an isentropic compression along the aerofoil surface between the leading edge and the shock, whose effect is to reduce the shock strength compared with the more conventional type of section, which generally has a constant or rising local Mach number up to the shock. It appears on the evidence of Fig. 17 that this recompression will in fact be retained on the swept infinite wing and may well be reinforced.

One other aspect of this compression merits comment. In the case of the two-dimensional aerofoil the flow compression may be accounted for (and indeed may even be designed) by considering the expansion waves originating from close to the leading edge; these reflect from the sonic line and return to the aerofoil surface as compression waves. The reflection at the sonic line follows from the unique nature of this boundary. Difficulties exist, however, when this physical argument is applied to the swept infinite wing; and though these may in some degree be overcome by careful consideration of the nature of the 'reflection', the practical tests of the application of the simple-sweep

theory to the details of the pressure distributions must come from experiment, and up to the present such information has been rather scarce. Fig. 17 is encouraging then in suggesting that the swept-wing analogy seems to be largely true. Obviously more experimental work is required to determine the exact nature of the relationship between the aerofoil and the swept infinite wing; the practical difficulties mentioned earlier must not be underestimated however.

It will also be apparent from Fig. 16 that the value of $\alpha \sec \phi$ at which the shock passes the pressure hole is also influenced by the leading-edge sweep. Too much significance should not be placed upon this effect. At sweepbacks of 45° and 30° the forward shock crosses the pressure-plotting station; the position of this shock depends on the distance of the station from the root and the absolute value of the local Mach number on the wing surface. Hence it will not correlate on the basis of the simple-sweep theory. At $\phi = 0°$ and 15° the tip shock crosses the pressure-plotting station; once more its chordwise position there depends on the local Mach number and the planform geometry and a similar lack of correspondence would be expected. Once the shock has passed beyond the pressure hole, the flow in front of the shock should be largely independent of the wing root and tip, and influenced only by the leading-edge sweep. It is true that even in this condition it is possible for disturbances from the subsonic flow on the lower surface to propagate around the wing leading edge, and hence in this sense the effect of the tip and root may still be transmitted on to the upper surface; such an influence is likely to be very small however.

5.3. *Results from the Double-Wedge Wing.*

An analysis similar to that discussed in the preceding section may be made for the double-wedge wing, though the range of test conditions available is far more restricted. The development of the pressure distribution with both stream Mach number and wing incidence can be seen in Figs. 42 to 46. The pressures over the forward-facing surfaces of the profile are very similar to those obtained on the corresponding surfaces of the single-wedge wing (*see* Section 5.4 below). At the ridge-line the flow is able to expand, and if the stream Mach number is high enough, supersonic flow at almost constant local Mach number is maintained over part or all of the rearward surfaces. The most noticeable feature of the flow development with increasing stream Mach number at a fixed incidence is in fact the extension of this supersonic flow region away from the ridge towards the trailing edge. On the unswept wing at zero incidence, this occurs at just above $M_0 = 0{\cdot}75$. The flow undergoes an expansion of very nearly 8·0° at the ridge-line and if it is assumed that sonic velocity is reached just upstream of the ridge, the local Mach number on the rearward surface immediately behind the ridge should be 1·365. This corresponds to the lowest pressure achieved in the theoretical pressure distribution contained in the lower part of Fig. 13a. As can be seen, the experimental pressures are somewhat higher corresponding to a local Mach number of about $1{\cdot}34_5$. The supersonic flow region terminates in a shock wave, the flow behind the wave being further compressed until the trailing edge is reached. The extent to which boundary-layer separation develops behind the shock is shown in the flow-boundary diagrams of Fig. 6. When incidence is applied to the wing, separation takes place at the leading edge and the development of the surface pressures is similar in many ways to that for the single-wedge wing, except that for the double-wedge section the bubble or vortex may extend to influence the rearward part of the upper surface.

A comparison in terms of the simple-sweep theory of some of the results from the double-wedge wing is made in Fig. 18. At zero incidence and for a Mach number component normal to the leading edge of 0·85 (Fig. 18a), the correlation is good over most of the surface; behind the shock, however,

there is a marked divergence, which becomes progressively larger as the wing sweep increases. This effect will be referred to later. It is perhaps significant that the longitudinal pressure gradient which seemed to be present on the results from the single-wedge wing at the highest stream Mach numbers, is less conspicuous for the double-wedge wing of smaller blockage. Fig. 18a may be regarded as typical of the comparisons that can be made at zero incidence.

The remaining parts of Fig. 18 show comparisons in which the wing incidence is held at approximately constant values of $\alpha \sec \phi$; the incidence has been corrected for the aerodynamic twist of the wing, and to this extent there may be some uncertainty in the precise values of α. Despite this, the general agreement must be regarded as satisfactory. Of the obvious differences, the change in the level of the 60° swept-wing results in Fig. 18b may possibly be due to the reflection of the model bow wave from the tunnel walls and thus similar to the distortion noted in Fig. 15c. In Fig. 18c, there would appear to be small differences in the extent of the leading-edge separation region as ϕ changes, a feature noted and commented upon for the single-wedge results. Unfortunately, a stray shock from the tunnel walls intersects the model at $\phi = 45°$ and M_0 close to unity and for this reason the experimental results on part of the forward half of the chord for $\phi = 45°$ are not given in Fig. 18c. In this figure, the flow at the leading edge is separated and forms a bubble or vortex, according to the value of ϕ; the corresponding comparison for attached leading-edge flow is made in Fig. 18d, where the value of $M_0 \cos \phi$ is now 0·90. In this case there are two main regions of disagreement. Close to the leading edge, the pressure recovery is associated with the tip shock for $\phi = 0°$ and 15°, and a forward shock, lying closer to the leading edge, for $\phi = 30°$. Since both the types of shock wave are essentially due to the finite span of the wing, there is no reason why their positions in Fig. 18d should coincide. A similar discrepancy was commented upon in Section 5.2. As at zero incidence (Fig. 18a) there is a marked effect of wing sweep on the pressures to the rear of the ridge shock situated in this case at about $0{\cdot}75c$.

Perhaps one of the most noticeable features of Figs. 18a and d is the good agreement obtained in the supersonic flow between the ridge and the shock. The variation with stream Mach number of the actual pressures measured at $0{\cdot}51c$ for zero model incidence is shown in Fig. 19; the sudden fall in pressure corresponds to the development and passage of the ridge shock wave past the pressure station. Once this has occurred there is little subsequent change in the measured pressure. These results are replotted in the lower part of Fig. 20a in terms of p/H_e and $M_0 \cos \phi$ and collapse into a single band, thus illustrating in a more general way than Figs. 18a and d that the flow to the rear of the ridge behaves very closely in the manner demanded by the simple-sweep theory. The local flow is therefore dominated by the Mach number component normal to the ridge-line. In the upper part of the figure similar results are plotted for the wing at an uncorrected incidence of 2°; again the agreement is good. Fortunately, the pressures in the supersonic flow region are not greatly dependent on the wing incidence so that the effect of neglecting both the corrections to the nominal incidences at some sweepback angles and the fact that the comparison should have been made at a constant value of $\alpha \sec \phi$ are not important. The comparison shown in Fig. 20a is very striking and a similar plot may be made for any position on the model surface. Results for three other stations are shown in Figs. 20b and c, corresponding to $x/c = 0{\cdot}30$, $0{\cdot}70$ and $0{\cdot}95$; the wing incidence is 0° in each case. For the first two of these positions the agreement is again good, though the scatter is perhaps a little more evident than for $x/c = 0{\cdot}51$. In particular, the points obtained at the highest values of $M_0 \cos \phi$ for a sweepback angle of 30° deviate from the main trend and this may be due to tunnel-interference effects at the upper end of the transonic speed range.

The most marked discrepancies occur for the position near the trailing edge of the model (Fig. 20c), and this figure reflects the differences already apparent in Figs. 18a and d for the region behind the shock. The pressure at $x/c = 0{\cdot}95$ is influenced first by the extension of the separated-flow region behind the shock to the vicinity of the hole (event A in Fig. 20c), then by the passage of the shock itself (event B), and finally by any upstream separation associated with the shock. For $\phi = 0°$ and 15°, the separation behind the shock reaches the pressure hole at $M_0 \cos\phi = 0{\cdot}81$; the shock passes the hole at $M_0 \cos\phi = 0{\cdot}96$. Thereafter the pressures remain relatively constant. When the sweepback is increased to 30°, the pressure hole is influenced by the separation at a rather lower value of $M_0 \cos\phi$ (0·79), the pressure-hole position being passed at $M_0 \cos\phi = 0{\cdot}99$. Even when the shock is close to the trailing edge its upstream influence persists to the pressure-plotting station for all test Mach numbers. This explains the large difference in the values of p/H_e for $M_0 \cos\phi$ greater than 0·9 between sweepback angles of 0° and 30°. At $\phi = 45°$, the shock wave does not pass the pressure hole, which is not influenced by any true flow separation due to the shock wave upstream, but rather by a thick, but attached, boundary layer drifting in a spanwise direction towards the tip.

The comparison shown in Fig. 20c is therefore influenced by both the pressures which develop in the separated or very thick three-dimensional boundary-layer flow to the rear of the shock, and also by the influence which the flow viscosity has on the rate at which the shocks move towards the trailing edge. It would thus appear that there may be a marked divergence from the conditions implied in the simple-sweep theory in some events dominated by viscous effects, and hence a lack of correlation on the basis of the simple theory. Though the results shown in Figs. 18a and d and Fig. 20c are merely representative of the present tests, they may well indicate a much more general trend of this sort, which though not unexpected, may nevertheless be of considerable importance.

Though diagrams like that shown in Fig. 16 for the single-wedge wing may be constructed for the double-wedge model, the range of incidence over which this can be done is very limited, and it is not possible to confirm the type of result indicated in Fig. 17.

5.4. *Comparison of the Forebody Pressures on the Two Models.*

It is perhaps of interest at this stage to compare the pressures obtained on the two models over the forward-facing surfaces, in order to see what effect the geometry of the model behind the maximum-thickness position has. For the unswept wings, the agreement is very good (Fig. 21a) even close to the shoulder. Part of the small differences which develop at the higher stream Mach number may be attributable to the interference arising from the larger blockage of the single-wedge model. Similar comparisons are made in Figs. 21b and c for sweep angles of 30° and 60°; again the correlation is very close. From this it may be concluded that at zero incidence, the forebody pressures are relatively unaffected by the flow conditions behind the maximum-thickness position.

When the models are placed at incidence, the degree of correlation shown in Fig. 21 is lost, mainly because of the increasing influence of the flow separation that takes place at the leading edge. As discussed in Section 4 the initial extent of the separation region seems to depend on the actual chord of the wing and not on the geometric representation used in Fig. 21; for small-scale separations at least, the shape of the rear part of the profile does not influence appreciably the position of the reattachment line. This particular point is illustrated in Fig. 22 for zero sweep and a stream Mach number of 0·70; the single- and double-wedge results appear to form a sequence as the incidence is increased. The correlation is not quite exact, as Fig. 23 shows, and becomes less precise as the reattachment position moves towards the mid-chord point which is the ridge-line on the

double-wedge section. A definition of the reattachment position based on the pressure distribution shape and indicated in the inset to this figure is somewhat to the rear of the position deduced from oil-flow patterns, but the trend with increasing incidence is little different.

It will be apparent from the pressure distributions obtained on the two wings that the speed of sound is achieved on the model surface at a short distance ahead of the ridge, and not as the inviscid theory[22, 31, 35] predicts, exactly at the ridge. This discrepancy has been noted in most experimental tests made on double-wedge sections and for two-dimensional flows is attributed to the propagation of the influence of the wedge shoulder through the model boundary layer (*see*, for example, Ref. 21). On the other hand, in the tests made by Vincenti[20] on an unswept double-wedge wing of aspect ratio 4, it was found that the sonic point was farther forward than for the comparable two-dimensional model, particularly over the outer half of the semi-span. The location of the sonic point for the present single- and double-wedge wings is shown in Fig. 24, which also includes data from the swept wings corresponding to the achievement of a local Mach number equal in value to $\sec\phi$; that is, to the component of the local flow velocity normal to the leading edge becoming sonic. With increase in $M_0 \cos\phi$, the sonic point moves forward slightly but the position is at no stage to the rear of that given in Refs. 20 and 26 for the two-dimensional wedge of $4{\cdot}5°$ semi-angle, some results for which are included as triangular symbols in Fig. 24. It is suggested that this figure provides further evidence that at zero incidence the finite span of the wings does not greatly influence the flow at the pressure-plotting station over an important part of the test range; in addition it emphasises that for the region near the ridge-line the flow component normal to that line plays a dominant part.

6. *The Effect of Sweepback on the Shock Positions.*

Though some discrepancies exist due to the presence of separated flow to the rear, there is some degree of correlation between the positions of the ridge shock on the after part of the double-wedge section, as may be seen in Figs. 18a and 20b, for example. This point may be taken further by considering the way the shock position at zero incidence varies with wing sweepback and stream Mach number (Fig. 25). In the left-hand diagram are the positions of the outboard part of the ridge shock at the pressure-plotting station as determined from the oil-flow patterns. The abscissa is the stream Mach number. For $\phi = 45°$, the measuring position is very close to the junction of the swept, inboard part of the shock and its outer region of reduced sweep, so that there is rather more uncertainty in these particular values. The four points at the highest values of M_0 for $\phi = 30°$ are influenced by the strong outflow and possible separation to the rear of the shock, whose aft movement is correspondingly delayed.

In the right-hand diagram these results are plotted in terms of the component Mach number $M_0 \cos\phi$ and fall into a single band suggesting that the position of the ridge shock, when it is well away from the root region and roughly parallel to the ridge, is largely determined in accordance with the predictions of the simple-sweep theory.

This particular part of the ridge shock is of course the one most likely to correlate on this basis, and it is not possible to relate the more highly-swept inboard portion of the ridge shock, or the forward shock, in a similar manner, even if an allowance is made for the change in the spanwise position of the pressure-plotting station as the wing sweepback is increased. As has been said earlier, this is mainly because these shocks are associated with the flow conditions at the root of the wing and their direction of propagation depends on the absolute value of the local Mach number.

7. *The Effect of Sweepback on the Conditions required for Shock-Induced Boundary-Layer Separation.*

The conditions that seem to be required for the separation of a turbulent boundary layer on a swept wing at transonic and low supersonic speeds have been discussed in some detail in Refs. 8, 10 and 11, mainly for wings having a leading-edge sweep of about 50°. One of the objects of the present tests was to obtain further information on the effect of leading-edge sweepback, and hence shock sweepback, on the separation conditions. In the earlier work, it appeared that the most important parameter was the component of local Mach number normal to the shock front (M_n). For a shock having an effective sweep of about 40°, separation occurred when this component exceeded about 1·39. This is rather higher than the local Mach numbers found to cause separation on conventional two-dimensional aerofoils[27] and it was concluded that a genuine effect of the shock sweep was present.

The effective shock sweep is the angle between the normal to the local flow direction and the shock front. Because on an infinite swept wing the local flow tends to turn towards the root as the velocities increase the effective shock sweep is less than the geometric shock sweep (ϕ_s). If the inward turning is denoted by θ, then the effective shock sweep is $\phi_s - \theta$ and M_n is then equal to $M_L \cos(\phi_s - \theta)$, where M_L is the local Mach number. For most of the earlier results ϕ_s had a value of about 60° and θ about 20°, thus giving the effective shock sweep quoted earlier. A few results of rather doubtful validity were available for effective shock sweeps near 20°, and in addition, some careful analysis of the condition causing separation for an unswept shock on a finite swept wing was reported in Ref. 11. A tentative curve, based on this data, for the way in which the critical Mach number component might vary with effective shock sweep was put forward in Ref. 8.

In the present tests flow separation occurred behind the outboard part of the ridge shock on the double-wedge wing for all sweepback angles except 60°, and the corresponding pressure distributions and oil-flow patterns were analysed. The results are presented in Fig. 26, where the effective shock sweep ($\phi_s - \theta$) is plotted against M_n. Separated flow to the rear of the shock is denoted by a filled symbol. The present results are not completely in accord with the tentative curve of Ref. 8, particularly at the low values of effective shock sweep, and a modification to the earlier curve is shown as a full line. The main reason for this disparity lies in the values of M_n for separation at zero shock sweep obtained in the present tests ($1 \cdot 29_5$) and in Ref. 11 ($1 \cdot 23$). Both values were determined with some precision and the different shape of the two curves in Fig. 26 would seem to arise from an effect of section shape on the value of M_n required to cause separation on the unswept wing[27]. It may be argued however that in the present case separation occurs on the unswept wing when the shock is relatively close to the ridge ($x/c \simeq 0 \cdot 6$), and the boundary layer may then still be disturbed by the rapid flow acceleration that takes place at the ridge. The separation condition may therefore be somewhat different (and M_n possibly higher) than when the event occurs nearer the trailing edge. Unfortunately, the position of incipient separation does not vary much with incidence on the unswept model, but with $\phi = 30°$ (and $\phi_s - \theta \simeq 15°$), it occurs for a wider range of chordwise positions, between $x/c_n = 0 \cdot 65$ and $0 \cdot 80$ approximately. Though the evidence is somewhat sparse, there seems to be little or no effect of shock position on the critical value of M_n and it appears reasonable to consider that this would still be the case at zero effective shock sweep.

As with all analyses of this type, the accuracy of any particular point is not very high because of errors which can arise for example in estimating the flow direction at the shock front or in determining precisely when separation begins[13]. However, from the way in which a large number of points

group, it is possible to make an assessment of the required separation condition. Fig. 26 is reasonably satisfactory from this point of view, and the boundary is comparatively well defined. It may be further tested by considering data from other shock waves which cross the pressure-plotting station in the present tests. In particular, the results for the tip, forward and intersection shocks on the single-wedge wing are set out in Fig. 27 and both the boundaries from Fig. 26 have been transferred to this diagram. The new points are extremely scattered and in themselves are insufficient to define a boundary; they do tend, however, to confirm the revised boundary of Fig. 26 especially at high and low shock sweeps. In the intermediate sweep range, no points are available mainly because separation was not obtained on the wing surface for $\phi = 30°$.

The present results thus appear to confirm the apparently unique value of M_n required to produce separation at high values of the effective shock sweep, and suggest that this value decreases as the effective shock sweep is reduced. At low values of shock sweep, it is possible that the section shape may more strongly influence the separation condition.

Some details of the surface pressures close to the beginning of separation on the unswept wing are contained in Figs. 28 and 29, the former displaying the pressure distributions during the initial development of the separation, and the latter the variation of the measured pressure at $x/c = 0{\cdot}80$. From the oil patterns, separation could sometimes, though not always, be detected at $M_0 = 0{\cdot}800$, but by $M_0 = 0{\cdot}805$ it had certainly occurred, the flow reattaching near $x/c = 0{\cdot}7$. This reattachment position moved to $0{\cdot}8c$ at $M_0 = 0{\cdot}810$ and to the trailing edge for all stream Mach number above $0{\cdot}82$. The appropriate loci of the local pressures p_1, upstream, and p_2, downstream, of the shock are sketched in Fig. 27; the locus of p_2 is difficult to draw because of the wide spacing of the pressure holes, but it seems that this pressure approaches $0{\cdot}528H$ (corresponding to the local speed of sound) when the separation is well developed. The most marked effect of the separation on the surface pressures occurs for Mach numbers above $0{\cdot}83$ (*see* Fig. 29), and by $M_0 = 0{\cdot}86$ the readings at $x/c = 0{\cdot}95$ have been affected.

8. *The Effect of Sweepback on the Base Pressures of the Single-Wedge Wing.*

The base-pressure results are given in Table 3 and some of these data are also presented graphically. At zero wing incidence, the ratio of the base pressure (p_b) to the free-stream static pressure (p_0) varies with both Mach number and wing sweep, as can be seen in Fig. 30a for a station near the mid-semi-span. These results collapse to a considerable degree when plotted against $M_0 \cos\phi$ (Fig. 30b), thus suggesting that the base flow also behaves in many respects in the manner required by the simple-sweep theory. The dominant parameter is presumably the stream Mach number component normal to the trailing edge, but since the present wing is untapered this is equivalent to $M_0 \cos\phi$. The correspondence is not exact however; for example, the kink present on the curve for $\phi = 30°$ is less evident at the other sweepback angles. In general though, there is a marked tendency to conform to the pattern of the unswept wing.

The trend with $M_0 \cos\phi$ in Fig. 30b is similar to, though less pronounced, than that obtained by Cleary and Stevens[28] using an unswept wing of aspect ratio 4. The wing section in this case was of 4% thickness/chord ratio over the forward half followed by a parallel afterbody. The results of Ref. 28 were later used by Goin[29] as part of a more general analysis of base pressure effects on finite wings. His work included tests at Mach numbers of $1{\cdot}41$ and $1{\cdot}62$ on untapered wings with a leading-edge sweep of 45°, a range of thickness/chord ratios, and profiles having a wedge forebody

followed by a parallel section back to the trailing edge. The base pressure ratios from these experiments, measured at the mid-semi-span position, are included in Fig. 30b, and yield similar values of p_b/p_0 in the region where $M_0 \cos\phi$ is near unity.

9. *Pressure Forces on the Wings.*

Much of the preceding discussion has been concerned with the details of the pressure distributions measured at the pressure-plotting station. These distributions may of course be integrated to give the pressure forces acting on this particular section of the wing; in this way it is possible to illustrate to some extent the overall effect of the discrepancies which occur in the correlations of the pressure distributions on the basis of the simple-sweep theory. The two forces of interest are the normal force, acting perpendicularly to the chord plane of the wing, and the chordwise force, which acts along the wing chord in a direction at right angles to the leading edge. The direction of the chordwise force will thus change as the wing sweep alters. The non-dimensional coefficients corresponding to these forces will be formed by dividing by the wing chord, c, normal to the leading edge, and the kinetic pressure of the free stream. These coefficients will be called C_N and C_c respectively. For the single-wedge profile it is convenient to base C_c on twice the actual chord of the wing; i.e. to regard it as the forward part of a double-wedge wing of the same maximum thickness. Moreover, since contributions to C_c will come from the forward-facing surfaces and from the base region, that due to the forward-facing surfaces only will be designated C_{cf} to distinguish it from the overall force coefficient C_c.

9.1. *Chordwise Force.*

The chordwise force coefficient resulting from the pressures acting on the forward faces of the single-wedge wing (C_{cf}) may be obtained by a simple mechanical integration if it is assumed that free-stream static pressure occurs on the base of the wedge. The results for zero incidence are plotted in Fig. 31a. At low Mach number, C_{cf} is negative, but becomes positive as the stream Mach number increases and the position on the wing surface at which the free-stream static pressure is attained moves rearward. According to the simple-sweep theory, the results set out in Fig. 31a should collapse if $C_{cf} \sec^2\phi$ is plotted against $M_0 \cos\phi$, as in Fig. 31b. The correlation is reasonably good, but as the sweep is increased, the rise in C_{cf} takes place at progressively earlier values of $M_0 \cos\phi$. This means that at the higher sweepback angles, the free-stream static pressure is achieved farther aft than on the corresponding unswept section. Because C_{cf} is proportional to the difference between two pressure loops of about the same size, and since small errors in the stream static pressure affect the relative magnitude of the two loops, the final answer is very sensitive to inaccuracies of this type. It is not clear how much of the effect of sweepback noticeable in Fig. 31b is inherent and how much may be attributed to tunnel interference, particularly in view of the variation in model blockage with sweepback. Despite doubts of this kind, Fig. 31b does indicate that to a considerable extent the sweepback theory is successful in correlating the chordwise force results.

The accuracy of the integration at zero sweep may be checked by comparing the present results with those obtained by Knechtel[19] on a single-wedge model having a parallel afterbody. The semi-angle of this wedge was 4·4° compared with 4·0° for the variable-sweep single-wedge section, but this difference may be overcome by replotting the results in terms of the transonic similarity parameters $\tilde{C}_{cf}$ and ξ_0 which are defined in Fig. 32. The results of Fig. 31a are in excellent agreement with those of Ref. 19, and correspond well with the theoretical curve due to Cole[30]. With the model

sketched in Fig. 32, Knechtel did not obtain the rather large negative values of C_{cf} found in the present tests for comparatively low values of M_0. Comparable values were obtained by him, however, when the afterbody was removed and this difference in his results seems to be associated with the presence of a pressure gradient along the surface of the wedge at the lower stream Mach numbers when the afterbody is present. Again this could be attributed to the increase in the model blockage in the latter condition. For present purposes it is sufficient to note that the results for $\phi = 0°$ on the single-wedge wing agree well with those obtained elsewhere and with theory, and afford further evidence that at zero incidence and sweep the pressure-plotting station is acting effectively as part of an infinite wing.

The complete pressure drag of the single-wedge profile will include the contribution of the base region. Values of C_c for zero incidence at several sweep angles are presented in Fig. 33. The shape of these curves is greatly influenced by the base-pressure component as will be seen by comparing the relative magnitudes of C_{cf} and C_c in Figs. 31a and 33 respectively. The base pressure ratios (p_b/p_0) used in estimating C_c are contained in Fig. 30a. Fig. 30, in fact, demonstrates that the base pressure is strongly influenced by the Mach number component $M_0 \cos\phi$ and correlates approximately if plotted against this parameter. It would be expected then, that the base contribution to the pressure force would also correlate in a similar manner and since the forebody contribution is known to behave in this fashion too, it follows that some degree of correlation should be obtained by replotting the data contained in Fig. 33 in terms of $C_c \sec^2\phi$ and $M_0 \cos\phi$. This is done in Fig. 34; though the scatter is rather large, there is some measure of agreement between the four sweepback angles.

A similar analysis for the complete chordwise pressure-force coefficient C_c, may be made from the double-wedge pressure distributions, and for zero incidence the resultant curves are set out in Figs. 35 and 36. The earlier rise in C_c with $M_0 \cos\phi$ as the sweepback is increased is again evident (Fig. 35b), but this effect can now be attributed in part to the failure of the pressures close to the trailing edge to behave in accordance with simple-sweep theory. This effect has already been discussed in connection with Fig. 20c and was attributed there to boundary-layer separation or thickening. Nevertheless, the correlation shown in Fig. 35b is reasonably satisfactory. In Fig. 36 the present results at zero incidence and sweep are compared with those obtained by Knechtel[19] on a double-wedge section of $4{\cdot}5°$ semi-angle and with the theory for low supersonic speeds due to Vincenti and Wagoner[31] and for subsonic speeds by Trilling[32]. The values of $\tilde{C}_c$ for the present wing tend to increase at rather lower values of ξ_0 compared with those given in Ref. 19 and this may be due to the onset of shock-induced separation on the 7% thick section when M_0 exceeds $0{\cdot}80$. The corresponding value of stream Mach number for Knechtel's slightly thicker profile is not known. On the other hand the present results in this region are in agreement with those obtained by Humphreys, and reported in Ref. 23, on a double-wedge profile of $5{\cdot}74°$ semi-angle and 10% thickness/chord ratio. The values of C_c for this wing were converted to $\tilde{C}_c$ in Ref. 18, from which the points shown in Fig. 34 have been taken. Sandemann's own results tend to be rather larger at low free-stream Mach numbers and again near $M_0 = 1{\cdot}0$. The latter effect would be expected from the differences in surface pressure distribution displayed in Fig. 13a.

As in the case of the single-wedge wing the evidence of Fig. 36 may be used to suggest that the influence of the finite wing span at zero incidence and sweep is small.

In Fig. 35a, the stream Mach number corresponding to the initial movement of the ridge shock back from the ridge, as indicated by extrapolating the shock positions plotted in Fig. 25a, has been

indicated for $\phi = 0°$, 30° and 45°. All three events seem to correspond to a similar position close to the beginning of the drag rise, which suggests that the wave drag at the section does not appear until the shock forms and moves rearward. Again this is in accordance with the simple theory. At $\phi = 60°$, the ridge shock does not form within the Mach number range of the tests and C_c is almost constant as M_0 increases.

9.2. *Normal Force.*

To indicate the effect of leading-edge sweep on the normal force acting at the pressure-plotting station, the section values of C_N were obtained by mechanical integration for the single-wedge model at an incidence of 4·0°. These results are shown in Fig. 37, which also includes the corresponding normal-force coefficients measured on the complete wing using the strain-gauge balance. It will be seen that the integrated results differ somewhat from those obtained with the balance, indicating that the pressure-plotting station was not at exactly the position to give the average normal force on the wing. At this particular incidence, the flow may change with increasing stream Mach number from separated to attached leading-edge flow, and as sketched in Fig. 37 there would appear to be related changes in the section normal-force coefficient.

These results were obtained for a wing incidence of 4·0°, and the effective incidence normal to the leading edge is therefore $4·0 \sec \phi$ degrees. It follows that the correct comparison of these results, to show whether the simple-sweep theory holds for the normal force as the wing sweep changes, is in terms of $C_N \sec \phi$ and $M_0 \cos \phi$. This comparison is made in Fig. 38. In general the correlation is reasonably satisfactory, though there is some tendency for a rise in section normal force to take place at a progressively lower value of $M_0 \cos \phi$ as the sweep increases. Since these results have been obtained on a wing of finite span, it is necessary to assess how this affects the correlation; at present this can only be done by comparing the present results for $\phi = 0°$ with other experimental results on two-dimensional single wedges at incidence. Unfortunately, such material is rather scarce. The present results agree well with those obtained by Bugler and Hanslip[33] but since this wedge was tested in a hydraulic channel the validity of the comparison is uncertain. Values of C_N for a single-wedge section may of course be estimated from the pressures measured on the front half of the double-wedge aerofoil tested by Knechtel[19], but because the reattachment position of the leading-edge separation seems to depend on the aerofoil chord rather than its shape, the reattachment line would be relatively too far aft at a given incidence and Mach number and the lift on the forward half of the section too high. This objection no longer applies once transonic leading-edge flow attachment has occurred, but the normal force at the pressure-plotting station of the finite wing will then be strongly influenced by the position at which the tip shock crosses the station. As a result the values of C_N are much smaller than are obtained by considering only the front part of Knechtel's wedge or by making a comparison with similar results presented in Ref. 26. Both these sets of points appear to lie on a single curve parallel to, but considerably higher than, that for the single-wedge wing. It is perhaps worth pointing out that the discrepancy is accentuated in Fig. 38 by the false zero in the scale for $C_N/\cos \phi$; the actual difference between the two curves amounts to about a 20% loss in normal force compared with the two-dimensional values.

Similar considerations leading to a loss in normal force would be expected to apply to the double-wedge wing and in Fig. 39 a comparison is made between values of C_N/α obtained on the finite wing at two fixed values of the nominal incidence, values corresponding to corrected incidences of about 1·1° and 2·2°. These two curves do not coincide, indicating that the section normal-force

curve is not linear with incidence, possibly due to changes in the spanwise distribution of the load, as well as changes in the local flow pattern. The marked dip in the curves for stream Mach numbers between 0·85 and 0·95 is associated with the differential movement of the ridge shocks on the upper and lower surfaces, and as would be expected, tends to diminish as the incidence increases. This phenomenon is reflected in the overall lift curve for the wing as measured on the balance, and may be clearly seen in Fig. 60; it would appear to be restricted to zero wing sweepback. The four other curves included in Fig. 39 are from different two-dimensional tests on double-wedge aerofoils; rather surprisingly these show considerable scatter at moderate subsonic Mach numbers. Again the most reliable values are probably those due to Knechtel[19], which suggest that in this Mach number range the normal force from the finite wing is only about 60% of the two-dimensional value. Most of this loss comes from the forward half of the profile, as can be seen in Fig. 13b. As the stream Mach number approaches 1·2 the values of C_N/α increase rapidly and approach those obtained by Vincenti, Dugan and Phelps[26] for a two-dimensional wing; this stream Mach number is very close to that for shock attachment and presumably the three-dimensional effects diminish rapidly with the shrinking subsonic flow region. As Ref. 20 shows, the attachment Mach number is independent of the aspect ratio of the wing.

The values of C_N/α for the other angles of sweep may now be compared with those for $\phi = 0°$, but since the normal force does not always vary linearly with incidence (*see* the inset to Fig. 40), particularly when there is a pronounced vortex separation, it is best to make the comparison at as constant a value of $\alpha \sec \phi$ as possible. The reduced incidence must also change at constant nominal wing incidence for certain sweepbacks because of the twist of the model under load. A comparison of C_N/α for the range of sweepback is shown in Fig. 40 where, as would be expected, there is a reduction in C_N/α as the sweep increases. These results are replotted in Fig. 41 in terms of $(C_N \sec \phi/\alpha)$ and $M_0 \cos \phi$. The effect of the incidence at which the comparison is made is of some importance at high sweepback angles as can be seen from the set of points for $\alpha \sec \phi \simeq 1·3°$ for $\phi = 60°$ in Fig. 41; these are closer to the general trend of the results than those for $\alpha \sec \phi \simeq 2·6°$, suggesting that the non-linear lift may exercise a marked influence on the comparison. Apart from this aspect the correlation is reasonably good.

10. *Concluding Remarks.*

The results discussed in the foregoing pages represent an attempt to contribute to the problems associated with the simple-sweep analogy at transonic speeds. The technique used is one which may be criticised on many grounds, the most important probably being the finite span of the wings, and the failure to deal adequately with the flow at the wing root. Such shortcomings must be admitted; nevertheless it is felt that the correlations that have been obtained do suggest that in certain conditions these difficulties were not dominant. The present text has tended to be rather selective in its treatment of the basic results in an effort to concentrate on the limited objective of estimating the effect of the wing sweep on the flow and section characteristics.

In general it would appear that the simple-sweep theory predicts remarkably well the behaviour of the swept wings, and many of the defects can plausibly be attributed to three-dimensional flows. The infinite swept wing, so difficult to represent in wind-tunnel tests, seems likely on this evidence to behave very closely to the theoretical manner. This agreement would seem to apply not only to the overall flow characteristics, but to the detailed development of the flow about the wing section and the appearance of shock waves and the accompanying wave drag.

The present results should therefore be encouraging to those concerned with the design of sweptback wings and their sections. Obviously further and more precise tests are required to establish the matter beyond doubt, but it is hoped that the present contribution may help to indicate the broad directions in which more data are needed.

11. *Acknowledgements.*

The authors wish to acknowledge the assistance given both in the experiment itself, and in the subsequent analysis, by Miss B. M. Davis. The models were made by Mr. D. Dillaway, who was also responsible for the precise fitting that accompanied each change of sweep.

REFERENCES

No.	*Author(s)*	*Title, etc.*
1	A. Busemann	Aerodynamischer Auftrieb bei Überschallgeschwindigkeit. Atti di Convegni 5, Acc. d'Italia (Proc. 5th Volta Congress), pp. 328 to 360 (1935). *Luftfahrtforschung*, Vol. 212, pp. 210 to 219. 1935.
2	L. W. Hunton	Effects of finite span on the characteristics of two 45° sweptback wings of aspect ratio 6. N.A.C.A. Tech. Note 3008. September, 1953.
3	A. Busemann	Pfeilflügel bei Hochgeschwindigkeit. *Lilienthal-Gesellschaft Bericht*, 164. 1943.
4	H. J. Walker and W. C. Maillard	A correlation of airfoil section data with the aerodynamic loads measured on a 45° sweptback wing model at subsonic Mach numbers. N.A.C.A. Research Memo. A55C08, TIL/4684. May, 1955.
5	O. Bardsley and W. A. Mair ..	Separation of the boundary layer at a slightly blunt leading edge in supersonic flow. *Phil. Mag.*, Vol. XLIII, p. 334. 1952.
6	J. A. Bagley	Some aerodynamic principles for the design of swept wings. R.A.E. Report Aero. 2650. A.R.C. 23,173. May, 1961.
7	H. H. Pearcey	The design of wing sections for swept wings at transonic speeds. Paper given at 2nd I.C.A.S. Conference, Zürich (1960). *Advances in Aeronautical Sciences*, Vol. 3, p. 277.
8	E. W. E. Rogers and I. M. Hall ..	An introduction to the flow about plane sweptback wings at transonic speeds. *J. R. Ae. Soc.*, Vol. 64, p. 449. 1960.
9	E. F. Lawlor	Wind tunnel tests at Mach numbers between 0·6 and 1·4 of a 60° swept wing having an aerofoil section designed for subcritical flow at a Mach number of 1·2. Part I: 9% thick section with 'triangular' pressure distribution. A.R.C. C.P.582. May, 1961.
10	I. M. Hall and E. W. E. Rogers ..	Experiments with a tapered sweptback wing of Warren 12 planform at Mach numbers between 0·6 and 1·6. A.R.C. R. & M. 3271. Part II. July, 1960.
11	E. W. E. Rogers, I. M. Hall and C. J. Berry	An investigation of the flow about a plane half-wing of cropped-delta planform and 6 per cent symmetrical section at stream Mach numbers between 0·8 and 1·41. A.R.C. R. & M. 3286. September, 1960.
12	I. M. Hall	The operation of the N.P.L. 18 in. × 14 in. wind tunnel in the transonic speed range. A.R.C. C.P. 338. January, 1957.
13	E. W. E. Rogers, C. J. Berry and J. E. G. Townsend	A study of the effect of leading-edge modifications on the flow over a 50 deg sweptback wing at transonic speeds. A.R.C. R. & M. 3270. May, 1960.

REFERENCES—*continued*

No.	*Author(s)*	*Title, etc.*
14	W. F. Lindsey and E. J. Landrum	Compilation of information on the transonic attachment of flows at the leading edges of airfoils. N.A.C.A. Tech. Note 4204. February, 1958.
15	A. Stanbrook and L. C. Squire ..	Possible types of flow at swept leading edges. A.R.C. 21,464. April, 1959.
16	W. Jacobs	Transonic flow past swept and unswept wings between parallel walls. F.F.A. Report 55, Sweden. February, 1954.
17	B. D. Henshall and R. F. Cash .. .	An experimental investigation of leading-edge flow separation from a 4 per cent thick two-dimensional biconvex aerofoil. A.R.C. R. & M. 3091. February, 1957.
18	R. J. Sandemann	The transonic characteristics of a family of two-dimensional symmetrical double-wedge profiles. Part I: Details of the programme and the zero-lift results. A.R.L. Aerodynamics Report 114. 1959. Part II: Results obtained for lifting profiles. A.R.L. Aerodynamics Report 115. 1959.
19	E. D. Knechtel	Experimental investigation at transonic speeds of pressure distributions over wedge and circular-arc airfoil sections and evaluation of perforated-wall interference. N.A.S.A. Tech. Note D-15. August, 1959.
20	W. G. Vincenti	Measurements of the effects of finite span on the pressure distribution over double-wedge wings at Mach numbers near shock attachment. N.A.C.A. Tech. Note. 3522. September, 1955.
21	H. W. Liepmann and A. E. Bryson	Transonic flow past wedge sections. *J. Ae. Sci.*, Vol. 17, p. 745. 1950.
22	J. R. Spreiter, D. W. Smith and B. J. Hyett	A study of the simulation of flow with free-stream Mach number 1 in a choked wind tunnel. N.A.S.A. Tech. Report R-73. 1960.
23	M. D. Humphreys	An investigation of a lifting 10-percent-thick symmetrical double-wedge airfoil at Mach numbers up to 1. N.A.C.A. Tech. Note 3306. November, 1954.
24	W. J. Nelson and F. Bloetscher ..	An experimental investigation of the zero-lift pressure distribution over a wedge airfoil in closed, slotted, and open-throat tunnels at transonic Mach numbers. N.A.C.A. Research Memo. L52C18, TIB/3241. June, 1952.
25	H. A. Stine, C. B. Wagoner and A. L. Lugn	A study of the asymmetric transonic flow past a sharp leading edge. N.A.S.A. Tech. Report R-66. 1960.

REFERENCES—*continued*

No.	*Author(s)*	*Title, etc.*
26	W. G. Vincenti, D. W. Dugan and E. R. Phelps	An experimental study of the lift and pressure distribution on a double-wedge profile at Mach numbers near shock attachment. N.A.C.A. Tech. Note 3225. July, 1954.
27	G. E. Gadd	Interactions between normal shock waves and turbulent boundary layers. A.R.C. R. & M. 3262. February, 1961.
28	J. W. Cleary and G. L. Stevens ..	The effects at transonic speeds of thickening the trailing edge of a wing with a 4-percent-thick circular-arc airfoil. N.A.C.A. Research Memo. A51J11, TIB/2951. December, 1951.
29	K. L. Goin	Effects of planform, airfoil section, and angle of attack on the pressures along the base of blunt-trailing-edge wings at Mach numbers of 1·41, 1·62 and 1·96. N.A.C.A. Research Memo. L52D21, TIB/3324. September, 1952.
30	J. D. Cole	Drag of finite wedge at high subsonic speeds. *J. Math. Phys.*, Vol. 30, p. 79. 1951.
31	W. G. Vincenti and C. B. Wagoner	Transonic flow past a wedge profile with detached bow wave. N.A.C.A. Report 1095. 1952.
32	L. Trilling	Transonic flow past a wedge at zero angle of attack. U.S.A.F. W.A.D.C. Tech. Report 52-61. 1952.
33	J. W. Bugler and N. C. Hanslip ..	Lift and drag of single wedge sections in two-dimensional transonic flow. College of Aeronautics Report No. 131. A.R.C. 22,157. May, 1960.
34	G. P. Wood	Experiments on transonic flow around wedges. N.A.C.A. Tech. Note 2829. November, 1952.
35	A. E. Bryson	An experimental investigation of transonic flow past two-dimensional wedge and circular-arc sections using a Mach-Zehnder interferometer. N.A.C.A. Report 1094. 1952.
36	R. T. Jones and D. Cohen ..	Aerodynamics of wings at high speeds. Section A of Vol. VII of *High Speed Aerodynamics and Jet Propulsion*. Oxford University Press. 1957.

TABLE 1

Principal Dimensions and Characteristics of Wing Planform

ϕ	c (in.)	c_s (in.)	$\bar{s}$ (in.)	l (in.)	A	S (sq. in.)	$\bar{\eta}_p$ (%)	η_l (%)
0°	4·00	4·00	11·15	10·00	5·57	44·60	62·7	70·0
15°	4·00	4·14	11·29	11·07	5·45	46·74	64·8	72·9
30°	4·00	4·62	10·65	12·31	4·61	49·21	66·3	75·6
45°	4·00	5·66	9·30	14·00	3·29	52·60	68·4	78·6
60°	4·00	8·00	7·31	16·93	1·83	58·45	71·6	82·3

ϕ Sweepback angle of wing with respect to stream direction

c Chord normal to leading edge

c_s Chord in stream direction

$\bar{s}$ Mean semi-span of wing

l Length of leading edge

A Aspect ratio of wing

S Area of wing

$\bar{\eta}_p$ Mean spanwise position of pressure-plotting station

η_l Spanwise position of pressure-plotting station along leading edge

TABLE 2

Positions of Pressure Holes

(*a*) On wedge surfaces

Hole No.	x/c	
	Double wedge	Single wedge
1	0·05	0·05
2	0·12	0·10
3	0·20	0·17
4	0·30	0·24
5	0·40	0·32
6	0·45	0·40
7	0·47	0·50
8	0·49	0·60
9	0·51	0·70
10	0·53	0·80
11	0·55	0·85
12	0·60	0·90
13	0·70	0·94
14	0·80	0·96
15	0·88	0·98
16	0·95	0·995

(*b*) On base of single-wedge wing, where η_b denotes the position of the hole from the root, as a fraction of the span of the base

Hole No.	Spanwise position (η_b)
1	0·10
2	0·26
3	$0{\cdot}42_5$
4	0·59
5	0·75
6	$0{\cdot}91_5$

TABLE 3

Base Pressure on Single-Wedge Wing

Tabulated quantities are p_b/p_0 where p_b is the base pressure and p_0 is the tunnel static pressure.

(a) $M_0 = 0{\cdot}70$, $\phi = 0°$

Hole No.	η	$\alpha = 0°$	2°	4°	6°	8°
6	$0{\cdot}91_5$	0·766	0·765	0·788	0·793	0·735
5	0·75	0·726	0·736	0·767	0·784	0·776
4	0·59	0·703	0·708	0·749	0·771	0·787
3	$0{\cdot}42_5$	0·703	0·703	0·752	0·827	0·855
2	0·26	0·728	0·727	0·770	0·850	0·875
1	0·10	0·759	0·759	0·788	0·852	0·867

(b) $M_0 = 0{\cdot}80$, $\phi = 0°$

6		0·664	0·682	0·708	0·709	0·678
5		0·627	0·644	0·663	0·672	0·663
4		0·611	0·624	0·642	0·653	0·641
3		0·609	0·621	0·663	0·655	0·647
2		0·621	0·634	0·673	0·687	0·687
1		0·645	0·656	0·702	0·756	0·750

(c) $M_0 = 0{\cdot}90$, $\phi = 0°$

6		0·477	0·516	0·548	0·581	0·552
5		0·427	0·476	0·510	0·572	0·554
4		0·436	0·452	0·494	0·565	0·550
3		0·466	0·448	0·484	0·552	0·548
2		0·493	0·477	0·497	0·558	0·566
1		0·529	0·518	0·538	0·628	0·608

(d) $M_0 = 1{\cdot}00$, $\phi = 0°$

6		0·413	0·397	0·380	0·363	0·340
5		0·413	0·402	0·393	0·378	0·359
4		0·411	0·402	0·402	0·391	0·372
3		0·411	0·405	0·411	0·406	0·389
2		0·413	0·408	0·420	0·422	0·408
1		0·402	0·411	0·418	0·413	0·386

(e) $M_0 = 1{\cdot}11$, $\phi = 0°$

6		0·456	0·432	0·404	0·384	0·369
5		0·453	0·436	0·419	0·402	0·391
4		0·451	0·438	0·432	0·415	0·406
3		0·453	0·443	0·440	0·432	0·421
2		0·458	0·449	0·449	0·445	0·438
1		0·443	0·456	0·447	0·419	0·404

TABLE 3—*continued*

(*f*) $M_0 = 1{\cdot}16$, $\phi = 0°$

Hole No.	$\alpha = 0°$	2°	3°
6	0·484	0·458	0·433
5	0·479	0·463	0·447
4	0·479	0·465	0·454
3	0·479	0·470	0·461
2	0·484	0·477	0·470
1	0·472	0·484	0·474

(*g*) $M_0 = 0{\cdot}70$, $\phi = 15°$

Hole No.	$\alpha = 0°$	2°	4°	6°	8°
6	0·797	0·799	0·804	0·840	0·829
5	0·753	0·751	0·772	0·826	0·832
4	0·738	0·739	0·770	0·852	0·895
3	0·732	0·731	0·762	0·837	0·886
2	0·732	0·731	0·761	0·812	0·850
1	0·740	0·736	0·768	0·804	0·829

(*h*) $M_0 = 0{\cdot}80$, $\phi = 15°$

6	0·707	0·708	0·733	0·786	0·775
5	0·657	0·657	0·692	0·768	0·763
4	0·636	0·639	0·685	0·797	0·849
3	0·628	0·629	0·676	0·780	0·827
2	0·627	0·627	0·679	0·757	0·800
1	0·632	0·637	0·713	0·753	0·780

(*i*) $M_0 = 0{\cdot}90$, $\phi = 15°$

6	0·617	0·624	0·620	0·635	0·642
5	0·595	0·598	0·598	0·612	0·615
4	0·573	0·576	0·579	0·587	0·619
3	0·558	0·556	0·559	0·586	0·642
2	0·546	0·542	0·555	0·596	0·668
1	0·561	0·568	0·605	0·651	0·646

(*j*) $M_0 = 1{\cdot}00$, $\phi = 15°$

6	0·455	0·452	0·455	0·465	0·459
5	0·442	0·435	0·442	0·450	0·446
4	0·432	0·426	0·433	0·442	0·435
3	0·426	0·420	0·432	0·446	0·442
2	0·423	0·418	0·433	0·433	0·426
1	0·417	0·423	0·423	0·420	0·412

TABLE 3—*continued*

(*k*) $M_0 = 1{\cdot}11$, $\phi = 15°$

Hole No.	$\alpha = 0°$	2°	4°	6°	8°
6	0·488	0·486	0·464	0·432	0·393
5	0·473	0·466	0·451	0·423	0·391
4	0·462	0·456	0·445	0·432	0·419
3	0·456	0·449	0·445	0·443	0·440
2	0·449	0·449	0·438	0·436	0·432
1	0·447	0·456	0·432	0·434	0·425

(*l*) $M_0 = 1{\cdot}16$, $\phi = 15°$

6	0·514	0·507	0·479		
5	0·497	0·511	0·467		
4	0·486	0·474	0·461		
3	0·477	0·467	0·458		
2	0·472	0·465	0·451		
1	0·467	0·481	0·451		

(*m*) $M_0 = 0{\cdot}70$, $\phi = 30°$

6	0·876	0·876	0·894	0·925	0·915
5	0·813	0·815	0·846	0·915	0·915
4	0·793	0·799	0·826	0·873	0·882
3	0·788	0·794	0·823	0·850	0·858
2	0·793	0·799	0·830	0·843	0·843
1	0·831	0·828	0·833	0·833	0·842

(*n*) $M_0 = 0{\cdot}80$, $\phi = 30°$

6	0·827	0·830	0·855	0·896	0·884
5	0·748	0·765	0·792	0·867	0·878
4	0·723	0·727	0·764	0·825	0·832
3	0·723	0·734	0·771	0·803	0·798
2	0·749	0·757	0·785	0·797	0·792
1	0·760	0·766	0·757	0·772	0·774

(*o*) $M_0 = 0{\cdot}90$, $\phi = 30°$

6	0·764	0·771	0·794	0·852	0·832
5	0·699	0·696	0·744	0·811	0·842
4	0·673	0·674	0·717	0·787	0·805
3	0·680	0·690	0·723	0·767	0·777
2	0·700	0·710	0·730	0·755	0·750
1	0·621	0·625	0·639	0·657	0·649

TABLE 3—*continued*

(p) $M_0 = 1{\cdot}00$, $\phi = 30°$

Hole No.	$\alpha = 0°$	2°	4°	6°	8°
6	0·686	0·675	0·681	0·709	0·596
5	0·616	0·609	0·624	0·647	0·634
4	0·561	0·563	0·590	0·612	0·648
3	0·536	0·526	0·556	0·571	0·620
2	0·500	0·501	0·522	0·545	0·584
1	0·492	0·490	0·495	0·503	0·507

(q) $M_0 = 1{\cdot}11$, $\phi = 30°$

6	0·497	0·527	0·518	0·495	0·447
5	0·449	0·486	0·484	0·445	0·382
4	0·397	0·438	0·417	0·389	0·391
3	0·367	0·389	0·391	0·384	0·406
2	0·384	0·404	0·417	0·434	0·514
1	0·469	0·479	0·486	0·497	0·499

(r) $M_0 = 1{\cdot}16$, $\phi = 30°$

6	0·539	0·532	0·541	0·497	
5	0·502	0·495	0·500	0·449	
4	0·461	0·447	0·433	0·403	
3	0·412	0·431	0·435	0·408	
2	0·417	0·428	0·456	0·458	
1	0·467	0·467	0·481	0·516	

(s) $M_0 = 0{\cdot}70$, $\phi = 45°$

6	0·957	0·954	0·955	0·941	0·919
5	0·884	0·886	0·896	0·911	0·916
4	0·877	0·881	0·888	0·899	0·908
3	0·883	0·886	0·888	0·891	0·896
2	0·886	0·886	0·886	0·887	0·889
1	0·884	0·877	0·873	0·868	0·865

(t) $M_0 = 0{\cdot}80$, $\phi = 45°$

6	0·941	0·941	0·945	0·920	0·893
5	0·846	0·848	0·864	0·882	0·894
4	0·835	0·844	0·857	0·867	0·882
3	0·845	0·849	0·856	0·861	0·868
2	0·848	0·850	0·855	0·856	0·859
1	0·826	0·827	0·820	0·818	0·818

TABLE 3—*continued*

(*u*) $M_0 = 0{\cdot}90$, $\phi = 45°$

Hole No.	$\alpha = 0°$	2°	4°	6°	8°
6	0·920	0·923	0·933	0·889	0·855
5	0·804	0·811	0·837	0·848	0·869
4	0·793	0·803	0·823	0·837	0·855
3	0·805	0·811	0·825	0·828	0·838
2	0·807	0·811	0·821	0·823	0·828
1	0·726	0·730	0·717	0·722	0·723

(*v*) $M_0 = 1{\cdot}00$, $\phi = 45°$

6	0·895	0·899	0·919	0·891	0·838
5	0·819	0·827	0·836	0·823	0·836
4	0·755	0·764	0·780	0·790	0·813
3	0·770	0·777	0·776	0·772	0·785
2	0·732	0·742	0·749	0·746	0·751
1	0·608	0·617	0·613	0·617	0·613

(*w*) $M_0 = 1{\cdot}11$, $\phi = 45°$

6	0·812	0·812	0·825	0·754	0·750
5	0·680	0·678	0·683	0·715	0·752
4	0·665	0·680	0·702	0·724	0·747
3	0·665	0·683	0·698	0·709	0·743
2	0·661	0·672	0·672	0·672	0·685
1	0·566	0·583	0·583	0·592	0·592

(*x*) $M_0 = 1{\cdot}20$, $\phi = 45°$

6	0·741	0·744	0·758		
5	0·618	0·613	0·613		
4	0·581	0·611	0·649		
3	0·603	0·608	0·618		
2	0·567	0·577	0·591		
1	0·509	0·514	0·545		

(*y*) $M_0 = 0{\cdot}70$, $\phi = 60°$

6	0·981	0·976	0·964	0·957	0·959
5	0·940	0·940	0·940	0·943	0·954
4	0·934	0·936	0·937	0·940	0·950
3	0·933	0·936	0·936	0·937	0·944
2	0·933	0·934	0·936	0·937	0·940
1	0·898	0·900	0·905	0·911	0·914

TABLE 3—*continued*

(*z*) $M_0 = 0{\cdot}80$, $\phi = 60°$

Hole No.	$\alpha = 0°$	2°	4°	6°	8°
6	0·979	0·972	0·954	0·944	0·945
5	0·919	0·919	0·920	0·925	0·939
4	0·915	0·915	0·916	0·922	0·932
3	0·912	0·913	0·915	0·917	0·926
2	0·910	0·912	0·915	0·916	0·916
1	0·863	0·865	0·873	0·881	0·881

(*aa*) $M_0 = 0{\cdot}90$, $\phi = 60°$

6	0·979	0·974	0·943	0·925	0·930
5	0·888	0·898	0·898	0·906	0·925
4	0·890	0·892	0·895	0·904	0·915
3	0·888	0·890	0·895	0·898	0·906
2	0·885	0·886	0·890	0·892	0·892
1	0·820	0·821	0·832	0·842	0·840

(*bb*) $M_0 = 1{\cdot}00$, $\phi = 60°$

6	0·996	0·989	0·931	0·901	0·901
5	0·826	0·842	0·848	0·861	0·897
4	0·864	0·871	0·870	0·887	0·897
3	0·870	0·880	0·887	0·893	0·897
2	0·860	0·859	0·861	0·863	0·861
1	0·743	0·749	0·768	0·779	0·779

(*cc*) $M_0 = 1{\cdot}11$, $\phi = 60°$

6	0·907	0·899	0·853	0·869	0·920
5	0·864	0·873	0·879	0·890	0·916
4	0·856	0·860	0·869	0·873	0·914
3	0·836	0·847	0·853	0·869	0·864
2	0·817	0·827	0·836	0·825	0·845
1	0·687	0·700	0·734	0·752	0·750

(*dd*) $M_0 = 1{\cdot}20$, $\phi = 60°$

6	0·849	0·838	0·803	0·854	
5	0·854	0·860	0·870	0·877	
4	0·817	0·834	0·844	0·864	
3	0·803	0·817	0·824	0·824	
2	0·795	0·792	0·788	0·780	
1	0·655	0·652	0·676	0·686	

TABLE 4

Balance Results for Single-Wedge Wing

It should be noted that the wing drag includes the contribution from the raked tip edge which is a blunt forward-facing surface at $\phi = 0°$ to 30° and a blunt base at $\phi = 45°$ and 60°.

(a) $\phi = 0°$

α	$M_0 = 0{\cdot}70$	0·80	0·90	1·00	1·11
0° C_L	0	0	0	0	0
0° C_D	0·123	0·135	0·163	0·171	0·156
2° C_L	0·214	0·226	0·228	0·234	0·255
2° C_D	0·123	0·131	0·162	0·174	0·158
4° C_L	0·440	0·466	0·493	0·566	0·548
4° C_D	0·121	0·136	0·168	0·185	0·171
6° C_L	0·701	0·735	0·872	0·804	0·762
6° C_D	0·129	0·162	0·186	0·222	0·213
8° C_L	0·929	1·037	1·075	0·996	0·937
8° C_D	0·169	0·216	0·242	0·276	0·261
10° C_L	1·008	1·350			
10° C_D	0·218	0·291			
12° C_L	1·012	1·092			
12° C_D	0·267	0·298			

(b) $\phi = 15°$

0° C_L	0	0	0	0	0
0° C_D	0·106	0·118	0·122	0·145	0·137
2° C_L	0·187	0·198	0·200	0·206	0·222
2° C_D	0·108	0·117	0·122	0·146	0·138
4° C_L	0·389	0·415	0·428	0·466	0·470
4° C_D	0·109	0·114	0·132	0·156	0·153
6° C_L	0·627	0·672	0·731	0·725	0·684
6° C_D	0·112	0·116	0·153	0·184	0·186
8° C_L	0·857	0·904	1·031	0·927	0·864
8° C_D	0·142	0·149	0·196	0·230	0·232
10° C_L	0·949	0·969			
10° C_D	0·188	0·197			
12° C_L	0·951	1·024			
12° C_D	0·233	0·252			

TABLE 4—*continued*

(*c*) $\phi = 30°$

α	$M_0 = 0{\cdot}70$	0·80	0·90	1·00	1·11	
0° C_L	0	0	0	0	0	
0° C_D	0·070	0·070	0·074	0·093	0·109	
2° C_L	0·155	0·165	0·171	0·167	0·173	
2° C_D	0·070	0·070	0·073	0·095	0·102	
4° C_L	0·328	0·344	0·365	0·365	0·373	
4° C_D	0·072	0·074	0·078	0·103	0·120	
6° C_L	0·532	0·566	0·589	0·572	0·564	
6° C_D	0·085	0·089	0·095	0·124	0·147	
8° C_L	0·727	0·723	0·813	0·784	0·749	
8° C_D	0·120	0·123	0·134	0·162	0·185	
10° C_L	0·829	0·821	0·859	0·959	0·923	
10° C_D	0·164	0·166	0·172	0·208	0·225	
12° C_L	0·882	0·880	0·980			
12° C_D	0·209	0·211	0·233			

(*d*) $\phi = 45°$

α	$M_0 = 0{\cdot}70$	0·80	0·90	1·00	1·11	1·20
0° C_L	0	0	0	0	0	0
0° C_D	0·037	0·037	0·037	0·040	0·048	0·052
2° C_L	0·126	0·130	0·136	0·143	0·143	0·149
2° C_D	0·038	0·038	0·040	0·041	0·051	0·054
4° C_L	0·267	0·275	0·287	0·301	0·297	0·299
4° C_D	0·046	0·046	0·048	0·051	0·061	0·065
6° C_L	0·436	0·446	0·462	0·470	0·462	
6° C_D	0·065	0·066	0·068	0·074	0·082	
8° C_L	0·615	0·625	0·644	0·646	0·635	
8° C_D	0·097	0·099	0·102	0·107	0·115	
10° C_L	0·760	0·798	0·815	0·794	0·788	
10° C_D	0·140	0·149	0·152	0·152	0·158	
12° C_L	0·833	0·833	0·833	0·884		
12° C_D	0·184	0·186	0·190	0·199		

TABLE 4—*continued*

(*e*) $\phi = 60°$

α	$M_0 = 0{\cdot}70$	0·80	0·90	1·00	1·11	1·20
0° C_L	0	0	0	0	0	0
0° C_D	0·019	0·019	0·019	0·020	0·021	0·021
2° C_L	0·090	0·092	0·096	0·097	0·102	0·105
2° C_D	0·020	0·020	0·020	0·021	0·023	0·023
4° C_L	0·195	0·199	0·208	0·210	0·221	0·222
4° C_D	0·028	0·028	0·029	0·030	0·031	0·032
6° C_L	0·316	0·321	0·329	0·334	0·343	0·343
6° C_D	0·044	0·044	0·045	0·047	0·048	0·049
8° C_L	0·448	0·453	0·465	0·467	0·476	
8° C_D	0·070	0·070	0·071	0·073	0·075	
10° C_L	0·587	0·593	0·608	0·609	0·604	
10° C_D	0·104	0·105	0·107	0·109	0·109	
12° C_L	0·729	0·736	0·722			
12° C_D	0·149	0·112	0·148			

TABLE 5

Balance Results for Double-wedge Wing

α_1 is the approximate mean incidence for the model when distorted by aerodynamic load.

(*a*) $\phi = 0°$

	$M_0 = 0{\cdot}70$	0·80	0·90	1·00	1·11
α_1	−1·0°	−1·0°	−1·0°	−1·0°	−0·9°
C_L	−0·094	−0·103	−0·045	−0·082	−0·078
C_D	0·013	0·019	0·0391	0·0551	0·0509
α_1	+0·1°	+0·1°	+0·1°	+0·1°	+0·1°
C_L	+0·012	+0·014	+0·004	+0·016	+0·017
C_D	0·011	0·018	0·0384	0·0535	0·0503
α_1	1·2°	1·2°	1·3°	1·1°	1·1°
C_L	0·107	0·120	0·045	0·108	0·106
C_D	0·012	0·017	0·0368	0·0527	0·0492
α_1	2·3°	2·3°	2·4°	2·3°	2·2°
C_L	0·204	0·226	0·113	0·216	0·222
C_D	0·015	0·020	0·0371	0·0541	0·0507
α_1	3·3°	3·4°	3·5°	2·8°	2·7°
C_L	0·307	0·340	0·311	0·291	0·279
C_D	0·020	0·028	0·0427	0·0560	0·0537
α_1	4·4°	4·0°			
C_L	0·413	0·403			
C_D	0·029	0·033			

(*b*) $\phi = 15°$

α_1	−0·9°	−0·9°	−0·9°	−0·9°	−0·9°
C_L	−0·072	−0·081	−0·070	−0·068	−0·063
C_D	0·0106	0·0137	0·0283	0·0472	0·0455
α_1	+0·1°	+0·1°	+0·1°	+0·1°	0·1°
C_L	+0·006	+0·008	+0·006	+0·009	+0·013
C_D	0·0092	0·0122	0·0268	0·0470	0·0437
α_1	1·1°	1·1°	1·1°	1·1°	1·1°
C_L	0·089	0·097	+0·087	+0·089	+0·090
C_D	0·0089	—	0·0266	0·0456	0·0425
α_1	2·1°	2·1°	2·1°	2·1°	2·1°
C_L	0·173	0·183	0·179	0·173	0·171
C_D	0·0115	0·0144	0·0285	0·0470	0·0440
α_1	3·1°	3·1°	3·1°	3·1°	3·1°
C_L	0·257	0·271	0·275	0·269	0·259
C_D	0·0158	0·0193	0·0327	0·0501	0·0472
α_1	5·1°	4·1°			
C_L	0·428	0·367			
C_D	0·0310	0·0263			

TABLE 5—*continued*

(*c*) $\phi = 30°$

	$M_0 = 0{\cdot}70$	0·80	0·90	1·00	1·11
α_1	−0·9°	−0·9°	−0·9°	−0·9°	−0·9°
C_L	−0·053	−0·055	−0·057	−0·045	−0·046
C_D	0·0085	0·0091	0·0126	0·0266	0·0315
α_1	+0·1°	+0·1°	+0·1°	+0·1°	+0·1°
C_L	+0·012	+0·012	+0·014	+0·014	+0·014
C_D	0·0079	0·0083	0·0118	0·0258	0·0311
α_1	1·1°	1·1°	1·1°	1·1°	1·1°
C_L	0·073	0·079	0·086	0·077	0·075
C_D	0·0083	0·0077	0·0112	0·0256	0·0305
α_1	2·1°	2·1°	2·1°	2·1°	2·1°
C_L	0·143	0·149	0·161	0·155	0·138
C_D	0·0093	0·0095	0·0130	0·0283	0·0319
α_1	4·1°	4·1°	4·1°	3·1°	3·1°
C_L	0·285	0·299	0·316	0·220	0·212
C_D	0·0187	0·0189	0·0232	0·0308	0·0354
α_1	6·1°	5·1°			
C_L	0·440	0·358			
C_D	0·0360	0·0244			

(*d*) $\phi = 45°$

α_1	−0·8°	−0·8°	−0·8°	−0·8°	−0·8°
C_L	−0·041	−0·042	−0·043	−0·044	−0·039
C_D	0·0084	0·0082	0·0086	0·0098	0·0130
α_1	+0·1°	0°	0·1°	0·1°	0·1°
C_L	+0·009	+0·005	+0·009	+0·010	+0·009
C_D	0·0079	0·0077	0·0078	0·0093	0·0133
α_1	1·0°	1·0°	1·0°	1·0°	0·9°
C_L	0·059	0·057	0·061	0·063	0·060
C_D	0·0077	0·0073	0·0074	0·0092	0·0132
α_1	2·0°	1·9°	1·9°	1·8°	1·8°
C_L	0·111	0·109	0·115	0·119	0·112
C_D	0·0088	0·0090	0·0090	0·0100	0·0147
α_1	3·8°	3·7°	3·6°	2·7°	2·6°
C_L	0·223	0·221	0·225	0·174	0·172
C_D	0·0125	0·0162	0·0158	0·0131	0·0193
α_1	5·7°	5·5°	4·5°	3·5°	3·5°
C_L	0·346	0·343	0·286	0·235	0·222
C_D	0·0299	0·0293	0·0219	0·0176	0·0219

TABLE 5—*continued*

(*e*) $\phi = 60°$

	$M_0 = 0{\cdot}70$	0·80	0·90	1·00	1·11
α_1	−0·8°	−0·7°	−0·7°	−0·7°	−0·6°
C_L	−0·018	−0·026	−0·026	−0·031	−0·026
C_D	0·0081	0·0083	—	—	0·0081
α_1	0°	0°	+0·1°	+0·1°	+0·1°
C_L	+0·008	+0·006	+0·008	+0·007	+0·006
C_D	0·0077	0·0073	0·0075	0·0077	0·0075
α_1	+1·0°	+0·9°	+0·8°	+0·9°	0·8°
C_L	0·043	0·041	0·043	0·043	0·041
C_D	0·0077	0·0071	0·0071	0·0075	0·0077
α_1	1·8°	1·7°	1·6°	1·6°	1·5°
C_L	0·079	0·081	0·079	0·079	0·079
C_D	0·0107	0·0095	0·0085	0·0087	0·0087
α_1	2·7°	2·6°	2·3°	2·4°	2·2°
C_L	0·120	0·120	0·118	0·122	0·122
C_D	0·0114	0·0109	0·0109	0·0109	0·0112
α_1	4·4°	4·2°	4·5°	3·9°	3·6°
C_L	0·212	0·208	0·257	0·210	0·208
C_D	0·0193	0·0195	0·0248	0·0187	0·0185
α_1	6·1°				
C_L	0·310				
C_D	0·0354				

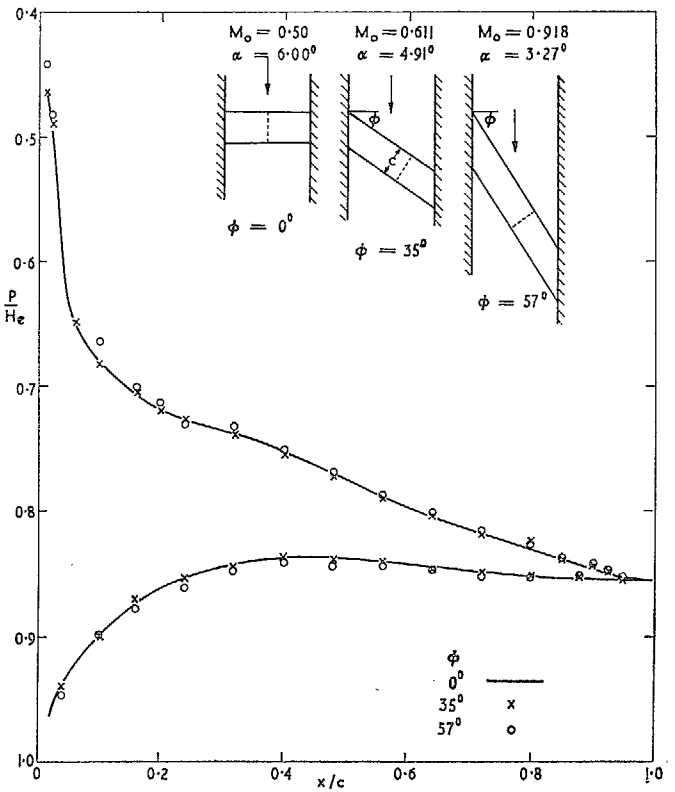

FIG. 1. Validity of simple-sweepback theory for component Mach number of 0·5 normal to leading edge and $\alpha \sec \phi = 6{\cdot}0°$. H_e is the effective total pressure of this component and p the local static pressure.

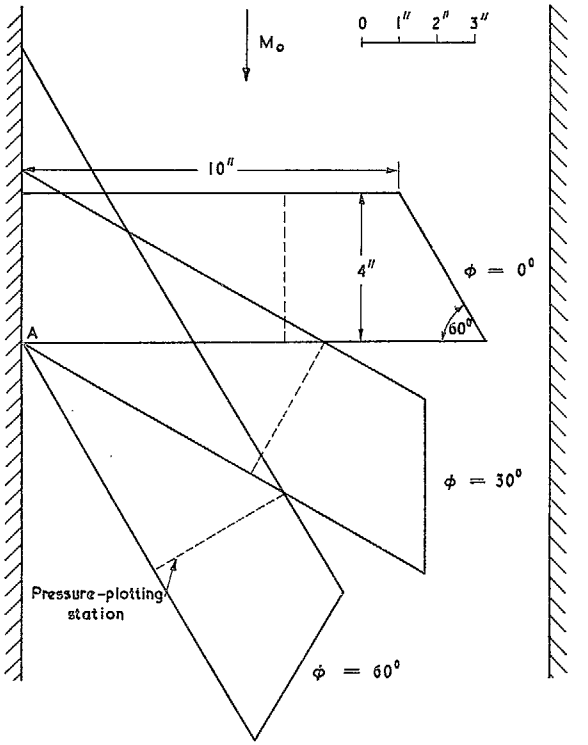

The wing pivots about the root trailing edge (Point A). For details of planform dimensions see Table 1.

FIG. 2. Wing planform at three sweepback angles.

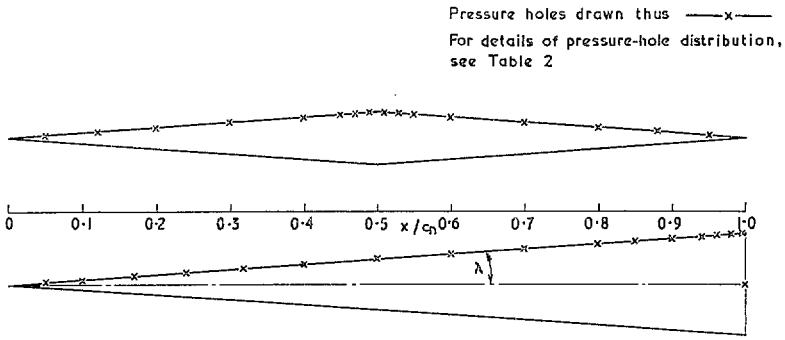

FIG. 3. Wing profiles and pressure-hole distribution. For both sections λ is 4·0°.

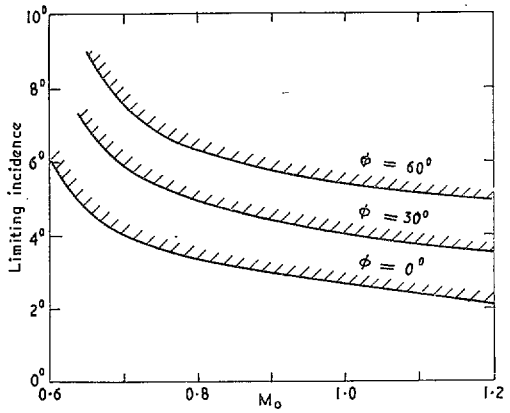

FIG. 4. Approximate incidence boundaries used with double-wedge wing.

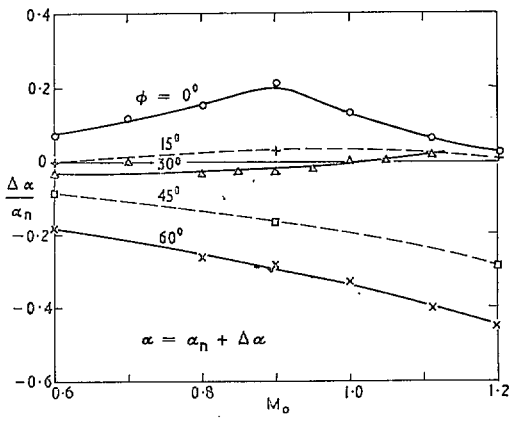

FIG. 5. Corrections to root incidence to allow for aerodynamic twist of double-wedge wing; α_n is the nominal (root) incidence, α is the value at the pressure-plotting station.

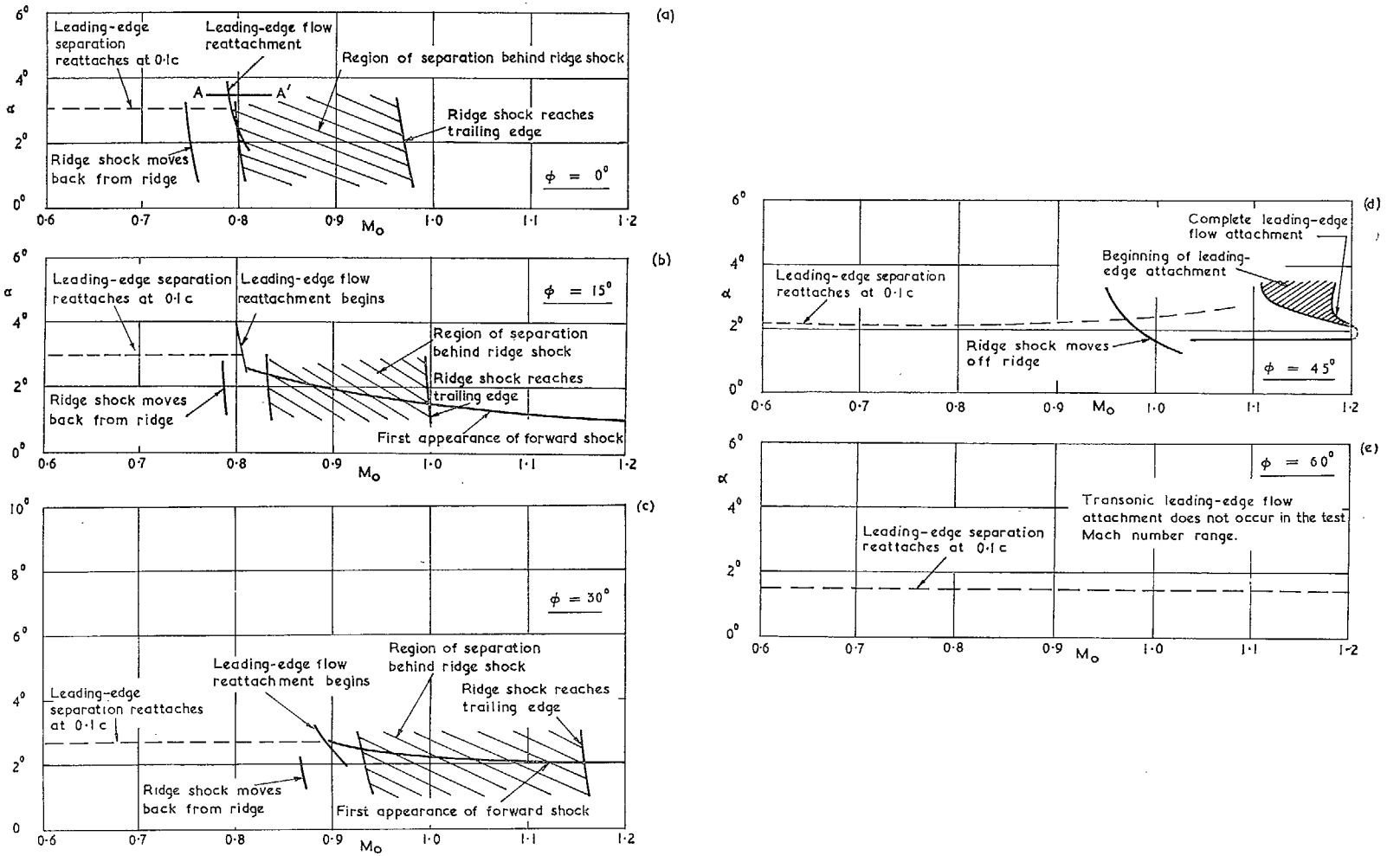

FIG. 6. Approximate flow boundaries for double-wedge wing.

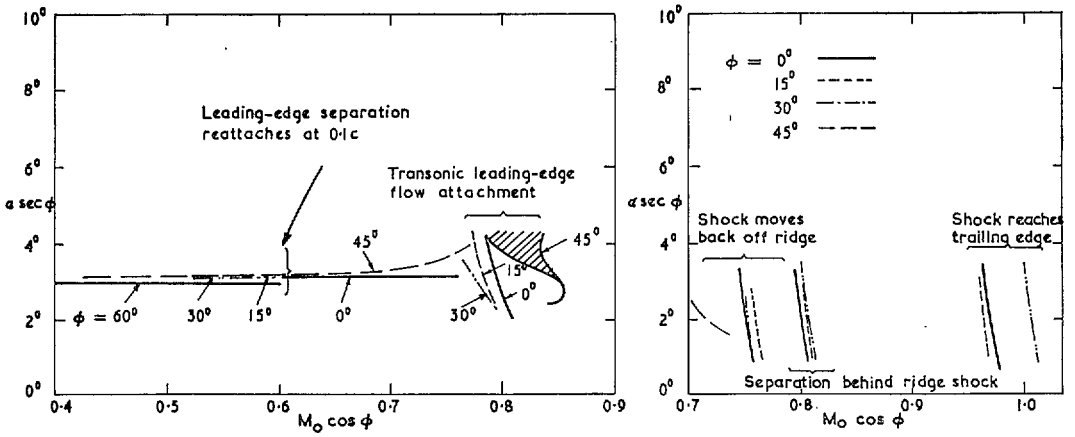

FIG. 7. Some reduced-flow boundaries for double-wedge wing.

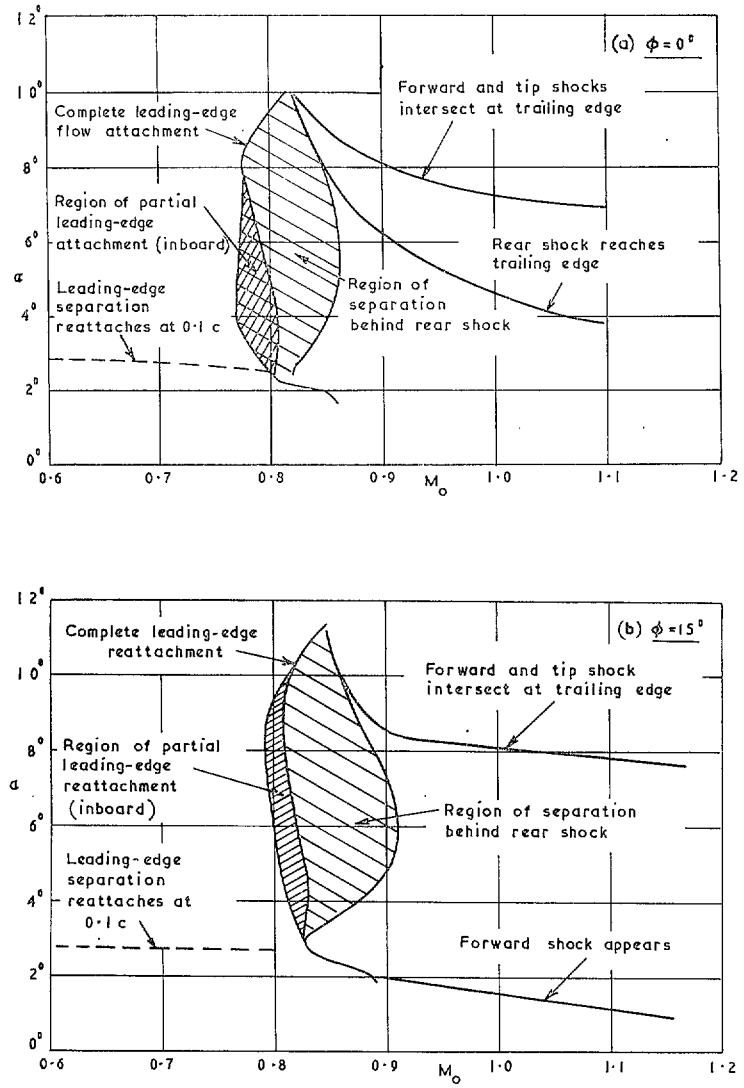

FIGS. 8a and b. Flow boundaries for single-wedge wing.

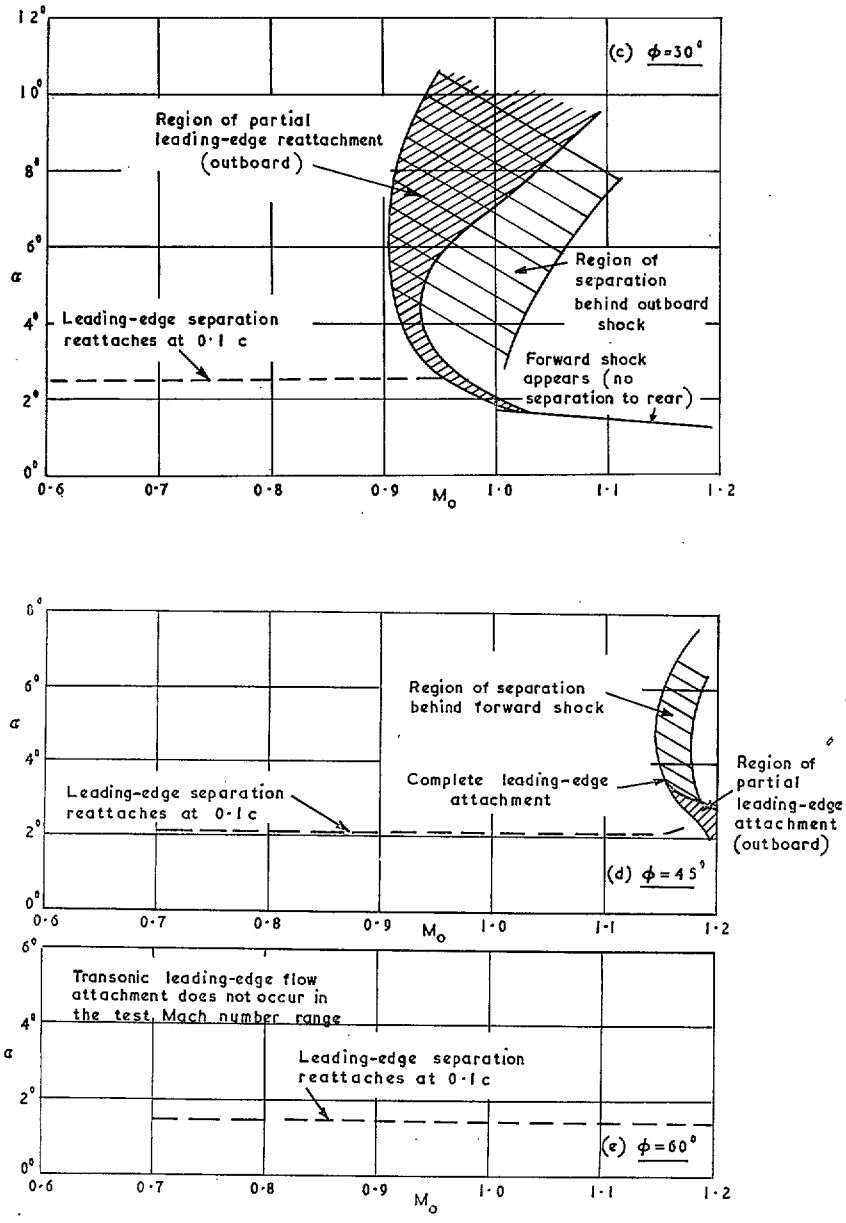

FIGS. 8c, d and e. Flow boundaries for single-wedge wing.

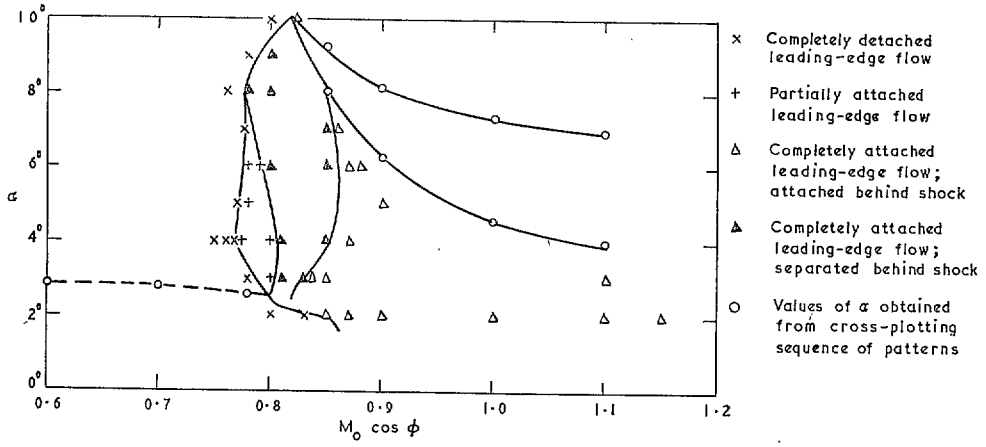

FIG. 9. Set of points used to establish flow boundaries of Fig. 8a.

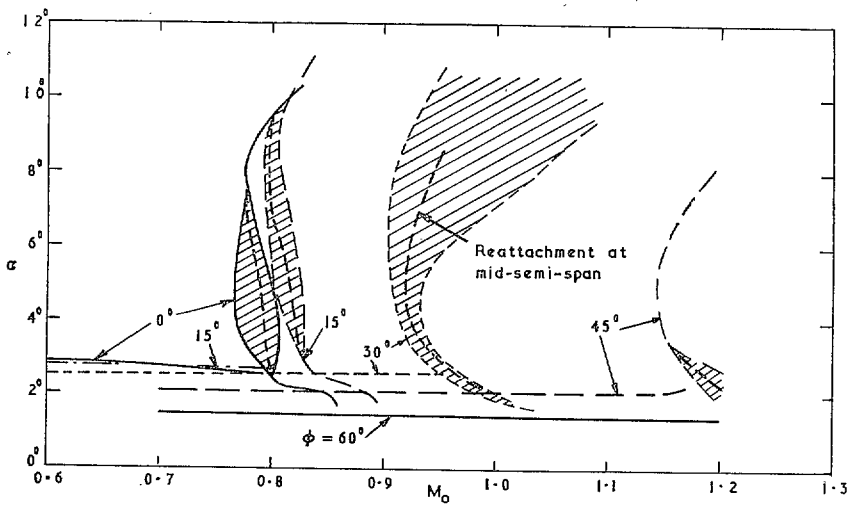

FIG. 10. Comparison of leading-edge separation and reattachment boundaries: single-wedge section.

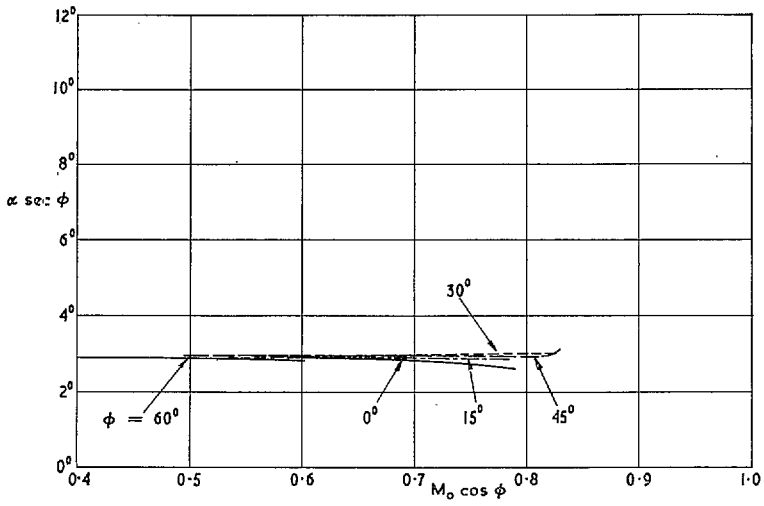

FIG. 11. Comparison of boundaries showing reattachment of leading-edge separation at $0 \cdot 1c$ in Fig. 10: single-wedge section.

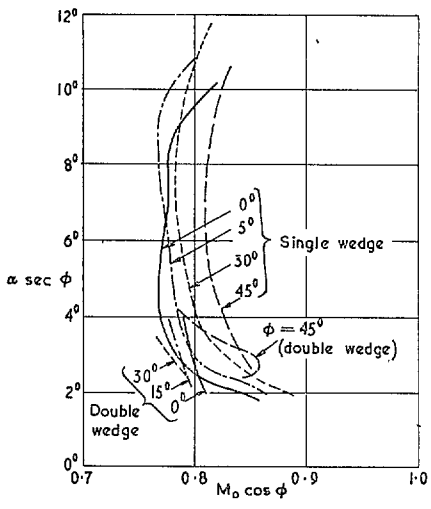

(a) Beginning of leading-edge reattachment.

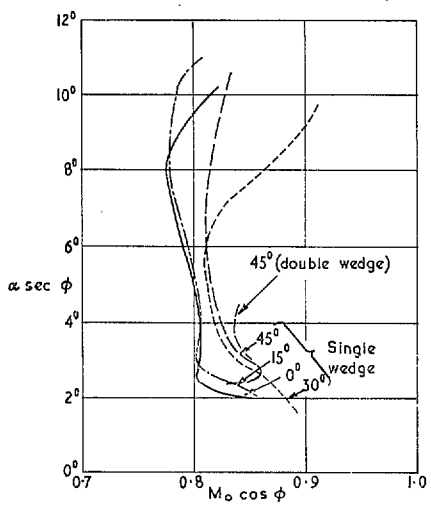

(b) Complete leading-edge attachment.

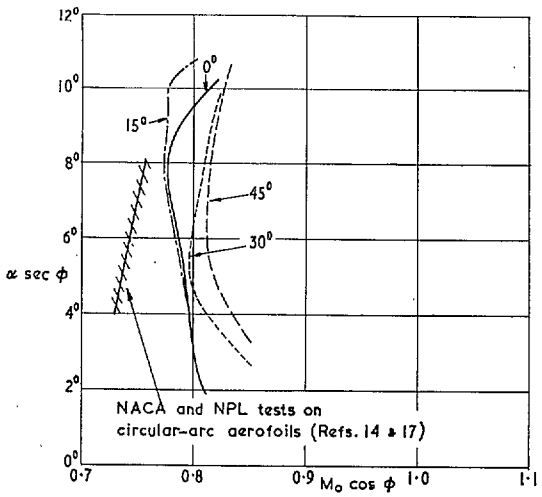

(c) Leading-edge flow attachment at mid-semi-span of single-wedge wings.

FIG. 12. Flow boundaries for single- and double-wedge wings.

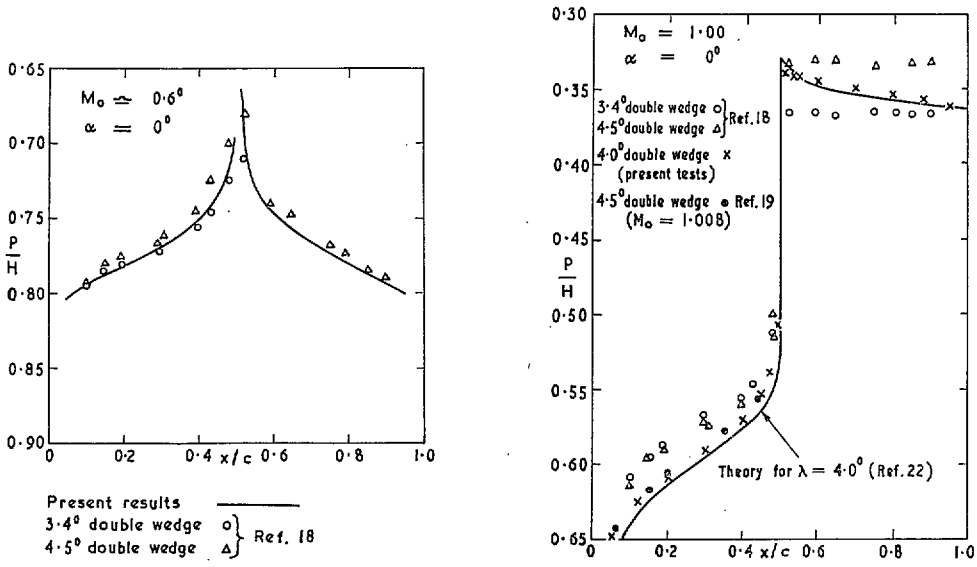

FIG. 13a. Comparison of present results for $\phi = 0°$ with two-dimensional data at zero incidence.

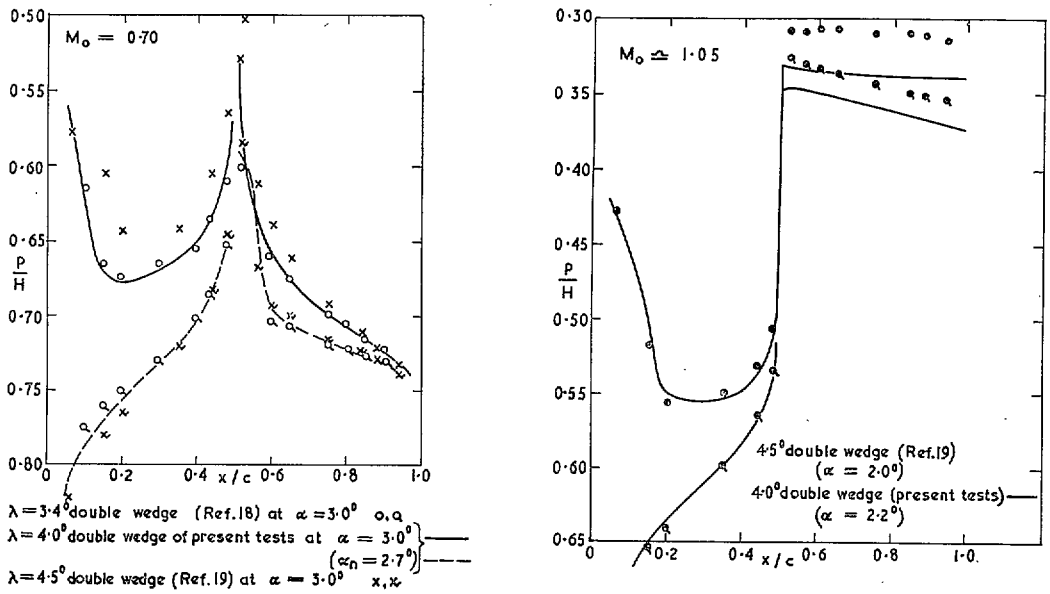

FIG. 13b. Comparison of present results for $\phi = 0°$ with two-dimensional data at incidence.

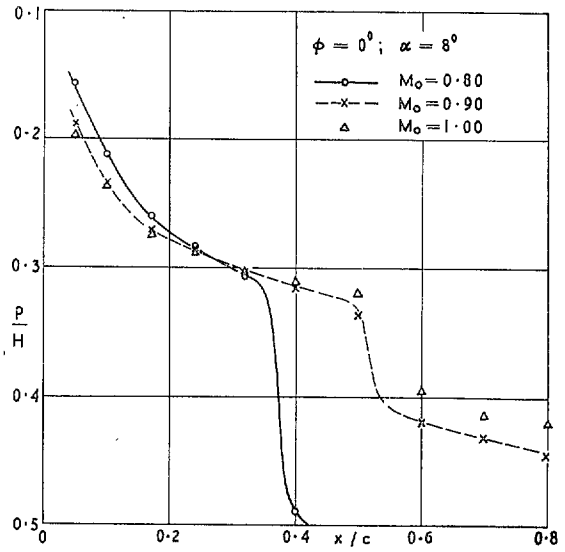

FIG. 14. Effect of Mach number on the pressures ahead of the shock on the upper surface of the single-wedge wing.

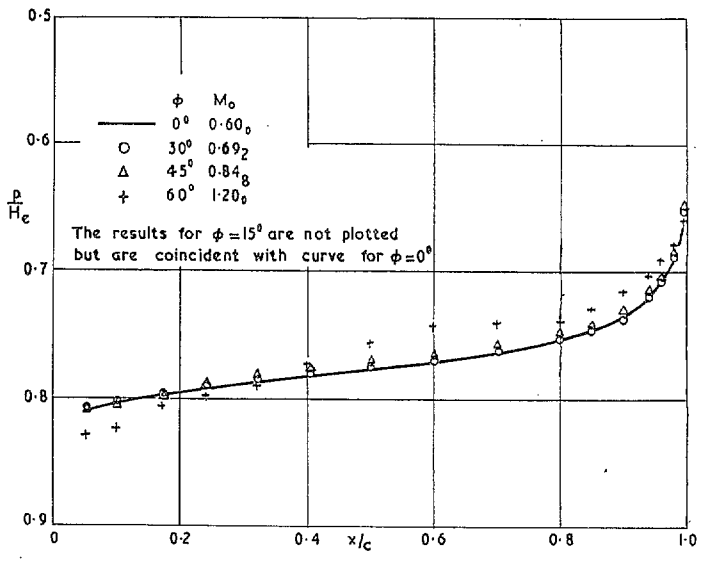

FIG. 15a. Comparison of pressures on forward face of single wedge at zero incidence and $M_0 \cos \phi = 0{\cdot}60$.

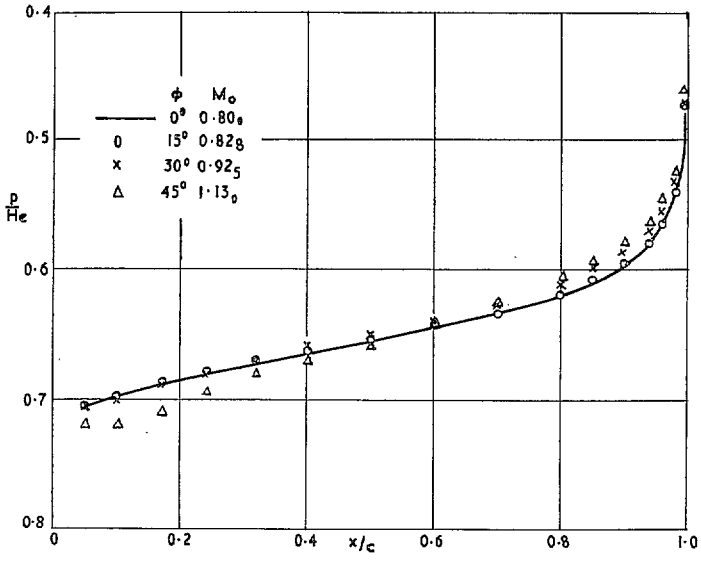

FIG. 15b. Comparison of pressure on forward face of single wedge at zero incidence and $M_0 \cos \phi = 0{\cdot}80$.

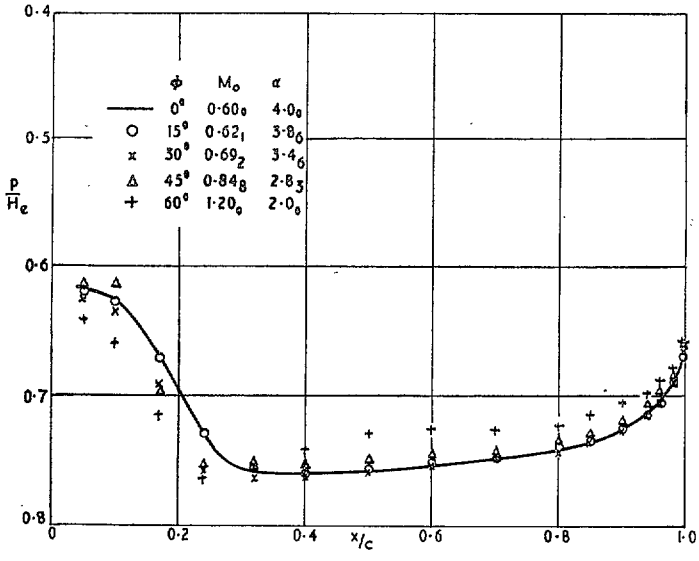

FIG. 15c. Comparison of pressures on forward face of single wedge at $\alpha \sec \phi = 4{\cdot}0°$ and $M_0 \cos \phi = 0{\cdot}60$.

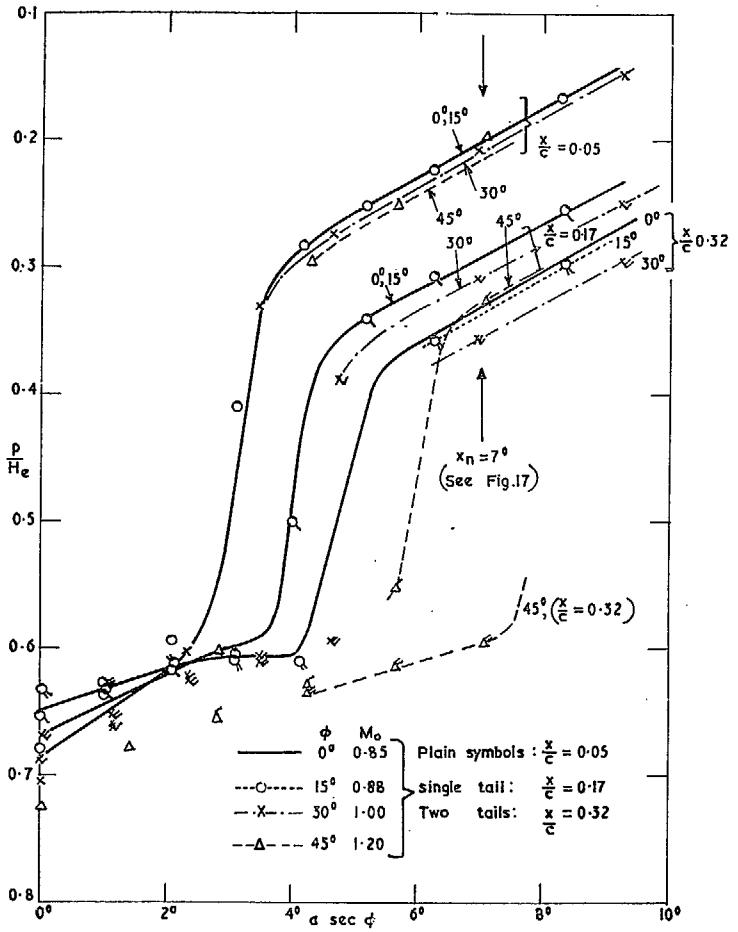

FIG. 16. Variation of local values of p/H_e with sweepback for attached leading-edge flow at $M_0 \cos \phi = 0{\cdot}85$.

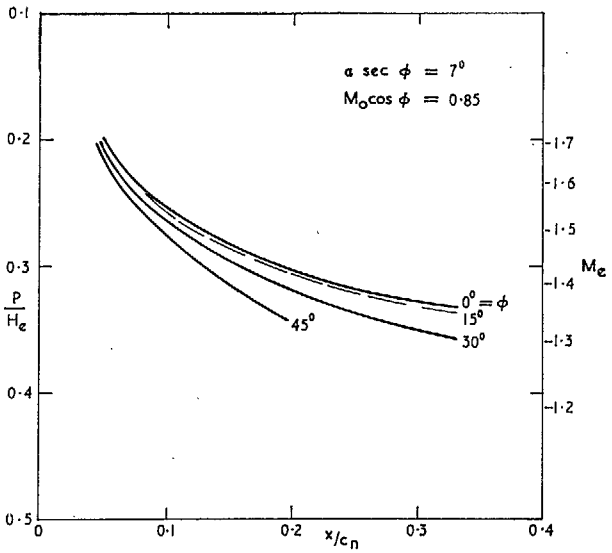

FIG. 17. Reconstruction, from Fig. 16, of the chordwise distribution of p/H_e at four sweepback angles. M_e is the Mach number corresponding to p/H_e. Supersonic attached flow was not obtained in the test Mach number range with $\phi = 60°$.

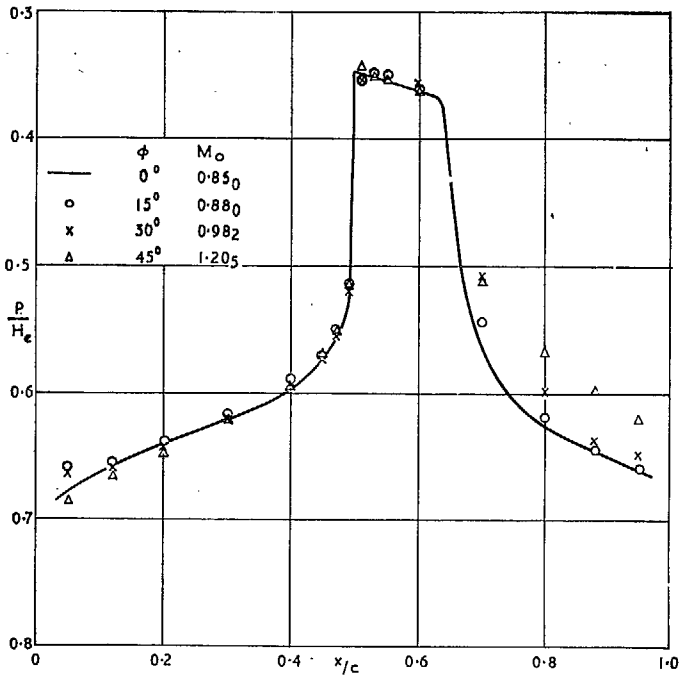

FIG. 18a. Comparison of pressures on double-wedge wing at zero incidence and $M_0 \cos \phi = 0{\cdot}85$.

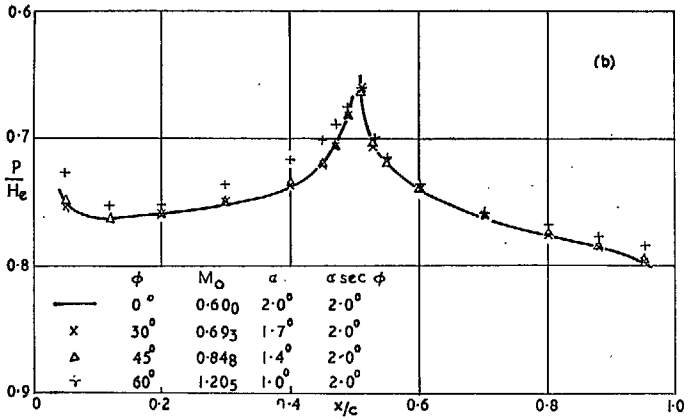

FIG. 18b. Comparison of upper-surface pressures on double-wedge wing at $M_0 \cos \phi = 0{\cdot}60$, $\alpha \sec \phi = 2{\cdot}0°$.

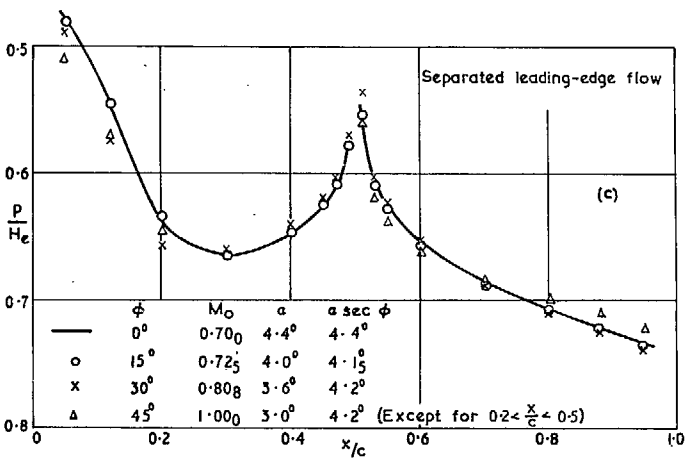

FIG. 18c. Comparison of upper-surface pressures on double-wedge wing at $M_0 \cos \phi \simeq 0{\cdot}70$, $\alpha \sec \phi \simeq 4{\cdot}2°$.

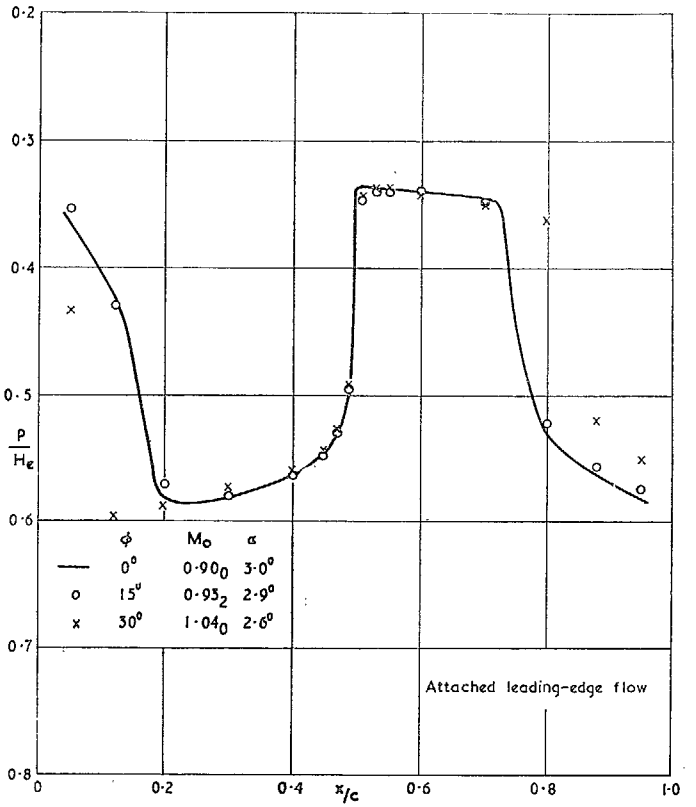

FIG. 18d. Comparison of upper-surface pressures on double-wedge wing at $M_0 \cos \phi = 0{\cdot}90$, $\alpha \sec \phi \simeq 3{\cdot}0$.

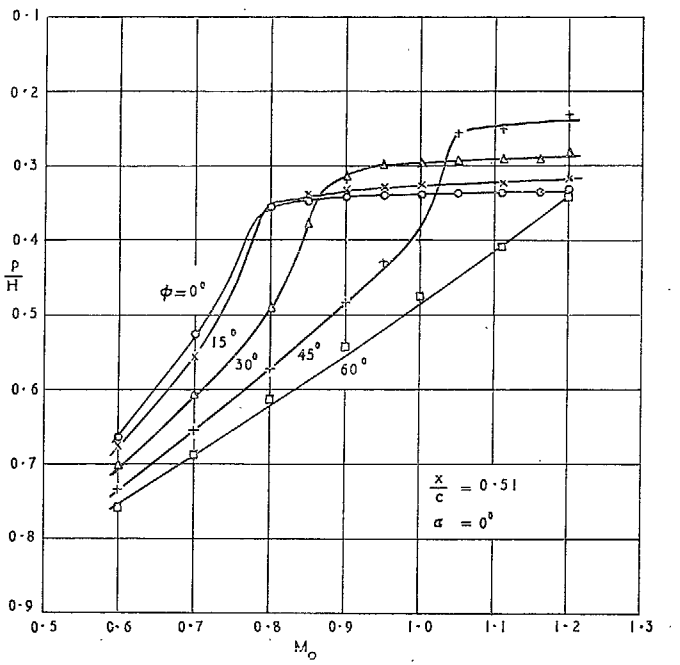

FIG. 19. Variation of surface pressure just behind ridge.

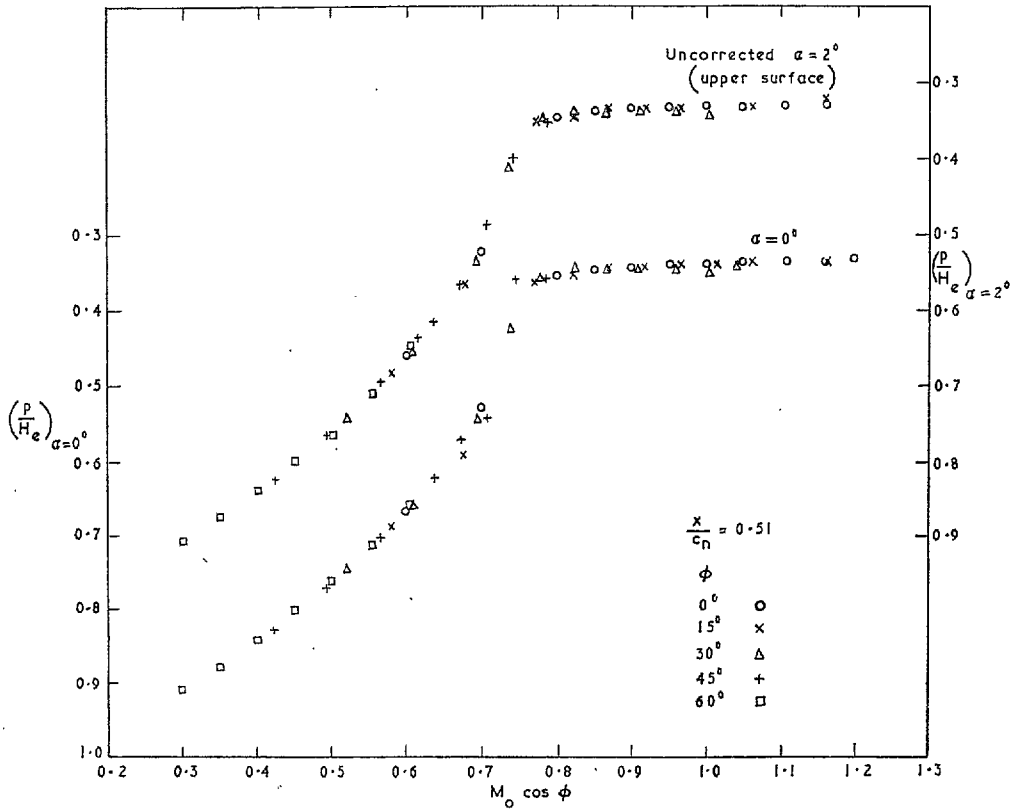

FIG. 20a. Correlation of surface pressures immediately behind the ridge-line of the double-wedge wing.

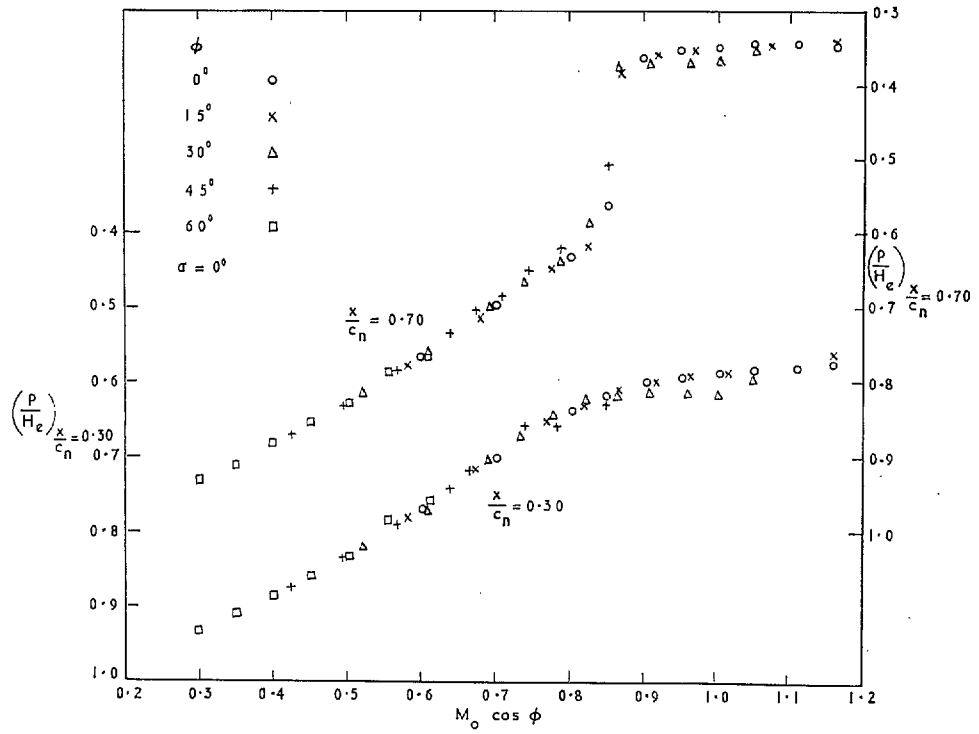

FIG. 20b. Correlation of surface pressures on the forward and rearward facing surfaces of the double-wedge wing.

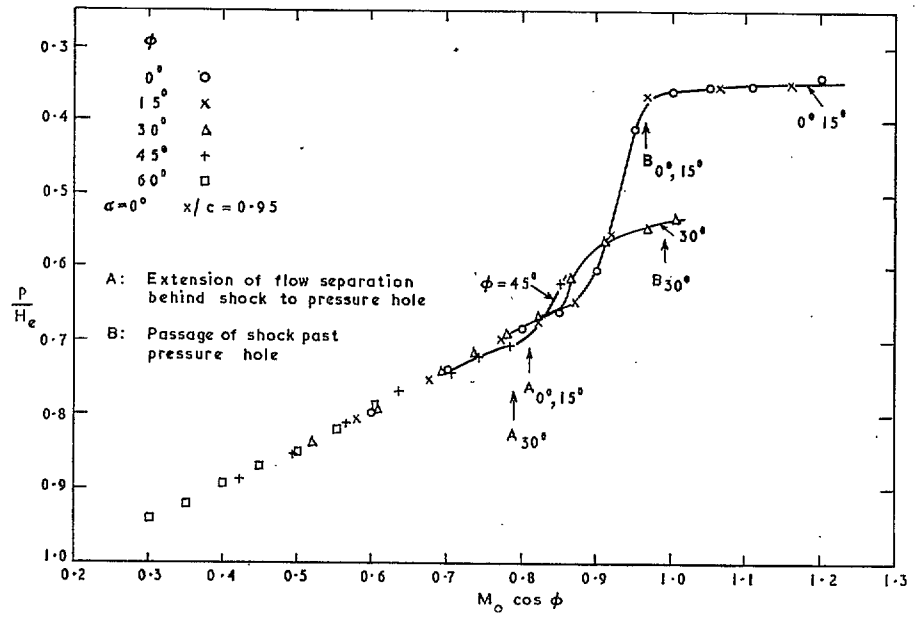

FIG. 20c. Correlation of surface pressure close to the trailing edge of the double-wedge wing.

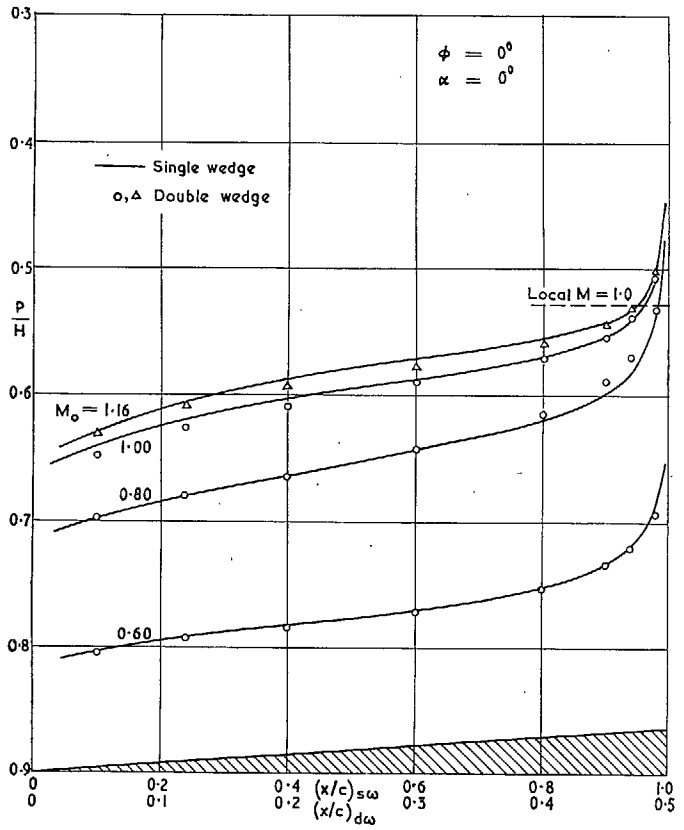

FIG. 21a. Comparison of forebody pressures at zero sweep.

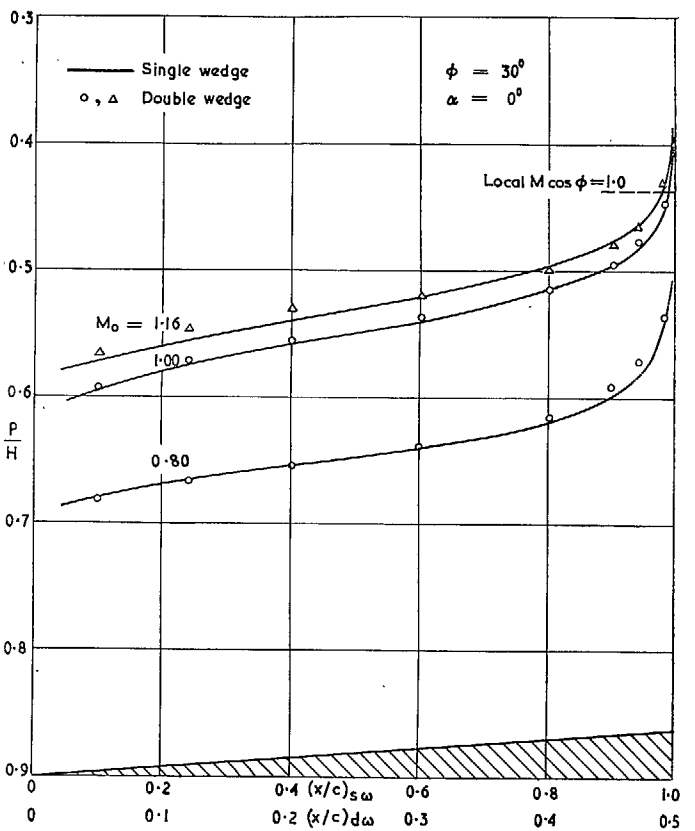

FIG. 21b. Comparison of forebody pressures at $\phi = 30°$.

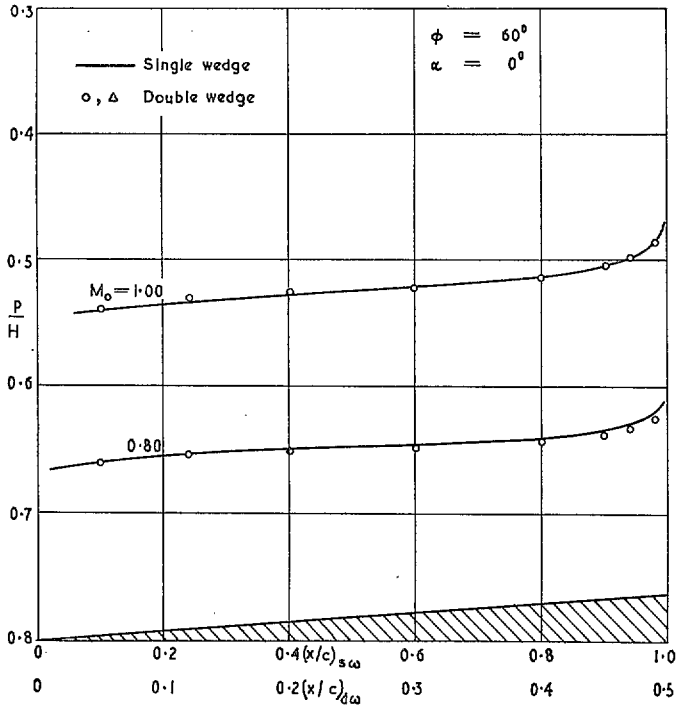

FIG. 21c. Comparison of forebody pressures at $\phi = 60°$.

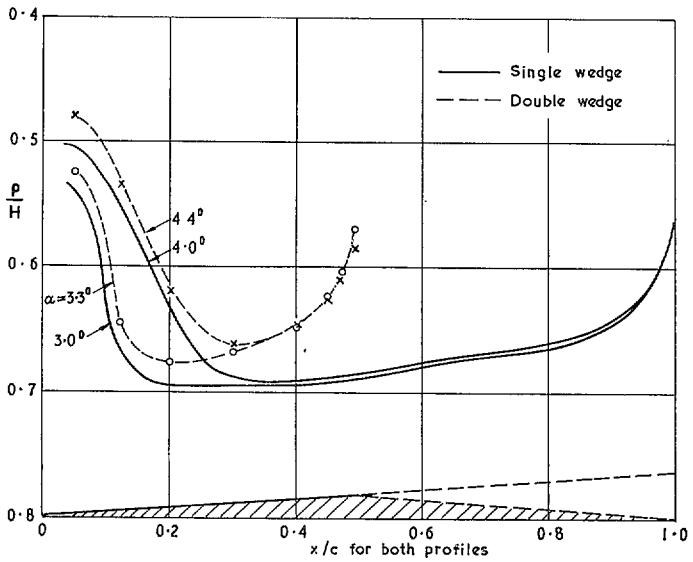

FIG. 22. Comparison of pressures on forward-facing surfaces of double and single wedges at zero sweep and $M_0 = 0{\cdot}70$.

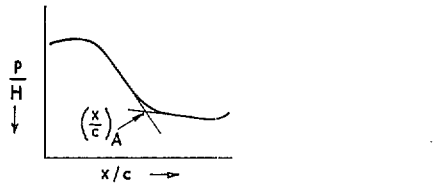

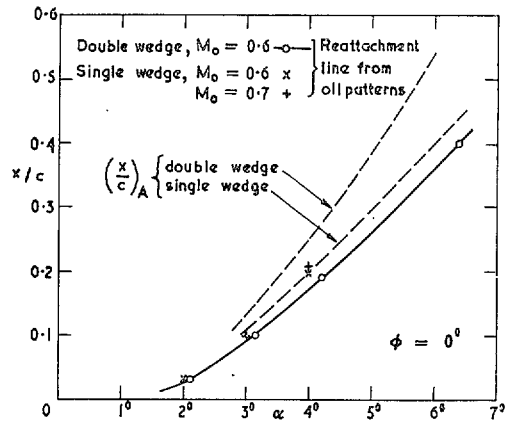

FIG. 23. Development of separation region with increasing incidence on the unswept wings.

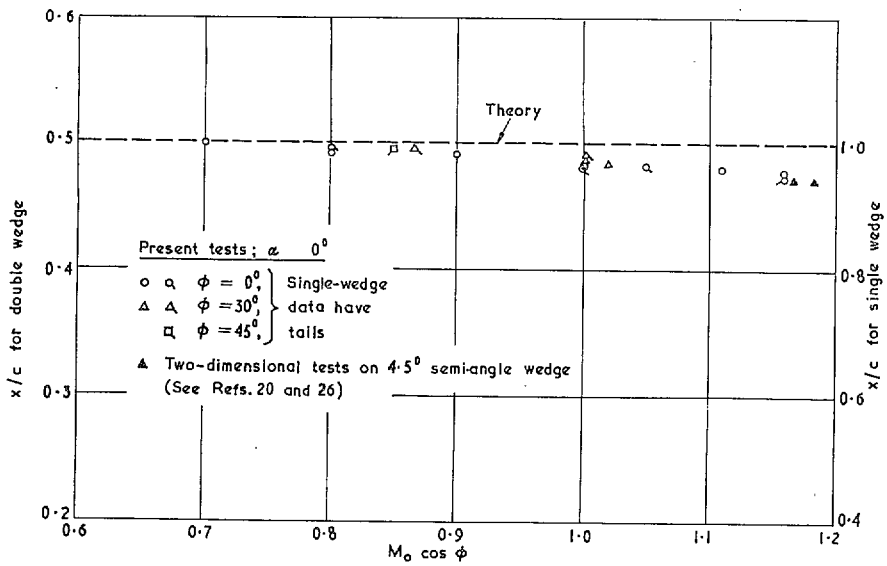

FIG. 24. Location of sonic point for single- and -double-wedge models. For swept models sonic point is defined as position at which local Mach number reaches sec ϕ.

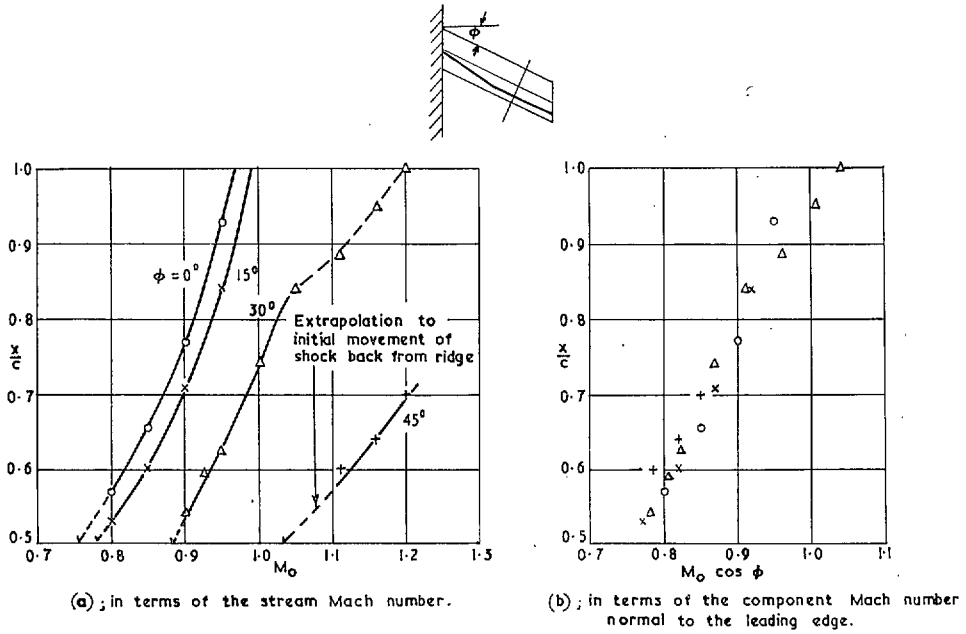

FIG. 25. Position of the ridge shock on the after part of the double-wedge wing at zero incidence.

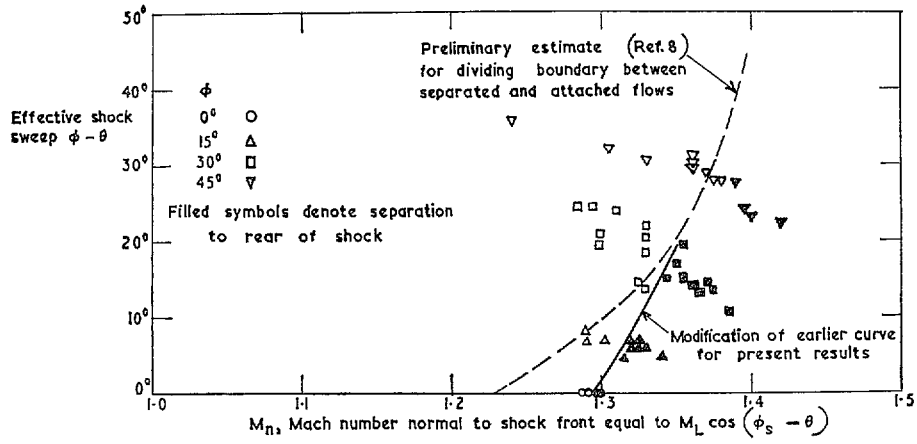

FIG. 26. Conditions for boundary-layer separation to rear of outboard shock on double-wedge wing.

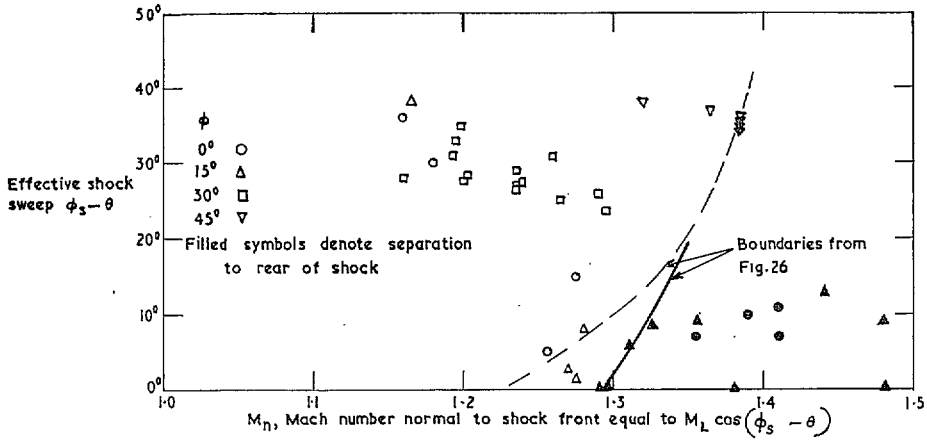

FIG. 27. Results of separation analysis on single-wedge wing: forward, tip and intersection shocks.

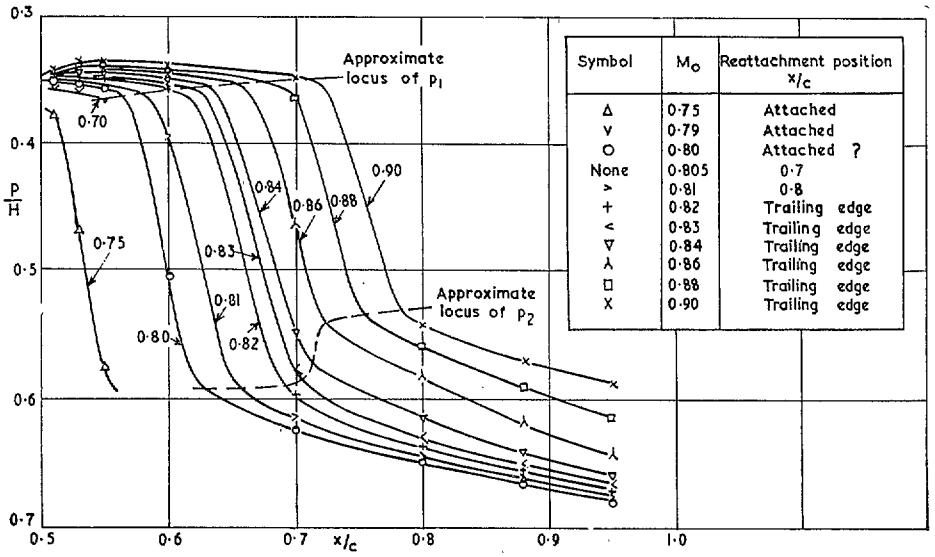

FIG. 28. Pressure distributions over the rear part of the double-wedge wing near a shock-induced separation condition ($\phi = 0°$, $\alpha = 2{\cdot}4°$).

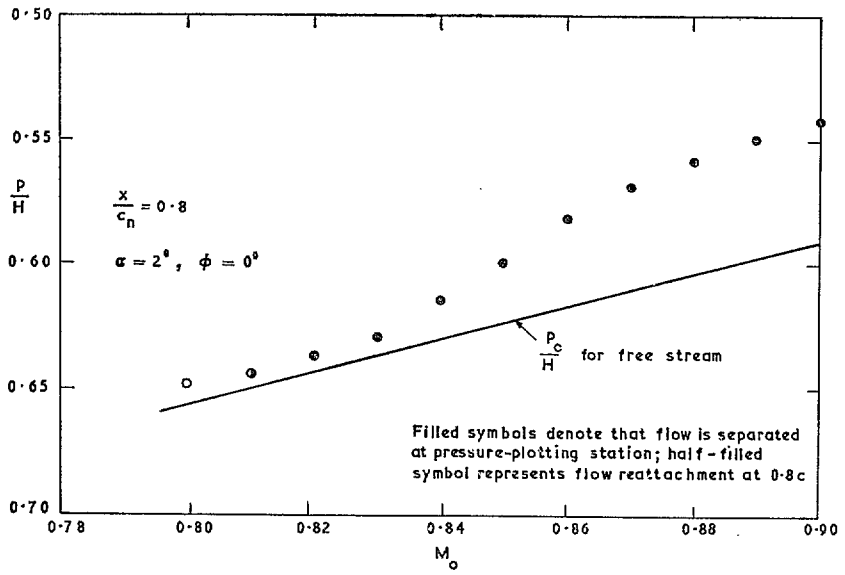

FIG. 29. Influence of shock-induced boundary-layer separation on the pressure at a point behind the shock.

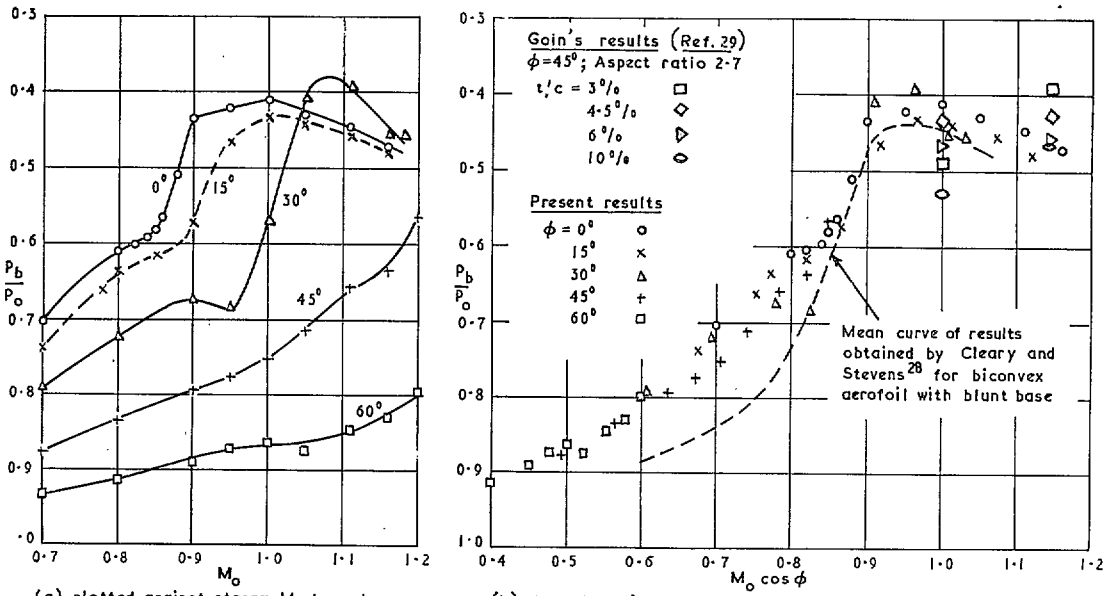

(a) plotted against stream Mach number

(b) plotted against component of stream Mach number normal to the leading edge

FIG. 30. Effect of wing sweep on base pressures measured on single-wedge wing ($\eta = 0{\cdot}59$; $\alpha = 0°$).

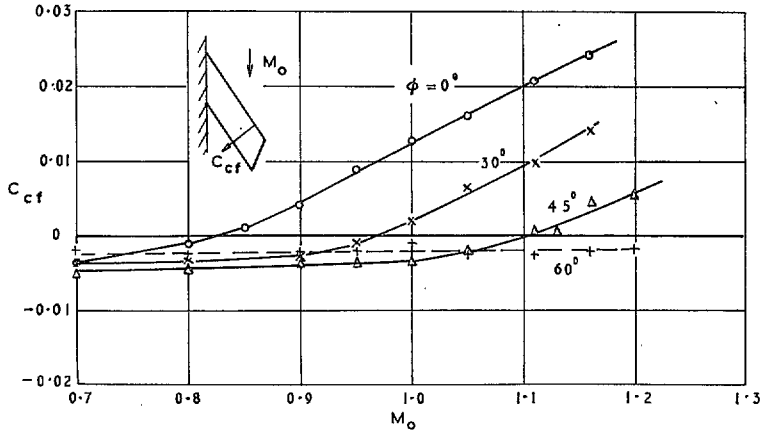

FIG. 31a. Chordwise pressure-force coefficients on forward faces of single-wedge profile at zero incidence (coefficients determined for front half of 7% thick double-wedge section).

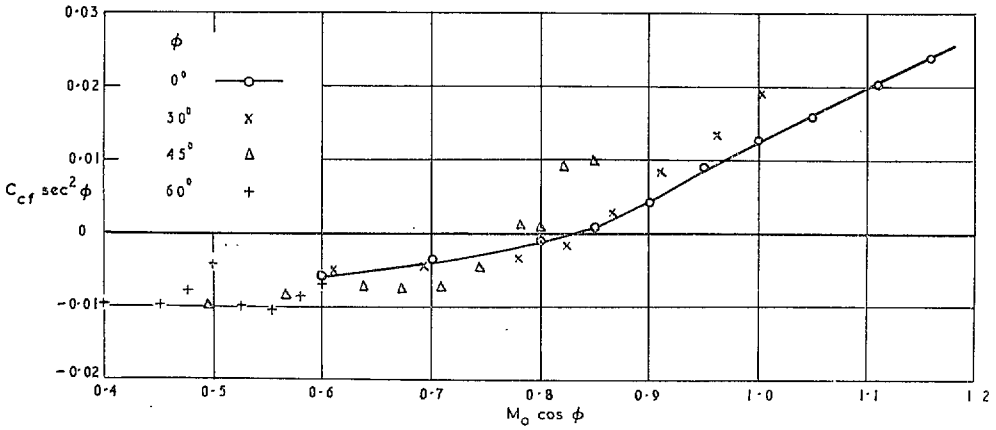

FIG. 31b. Correlation of reduced chordwise pressure-force coefficients for single-wedge profile at zero incidence (coefficients determined for front half of 7% thick double-wedge section).

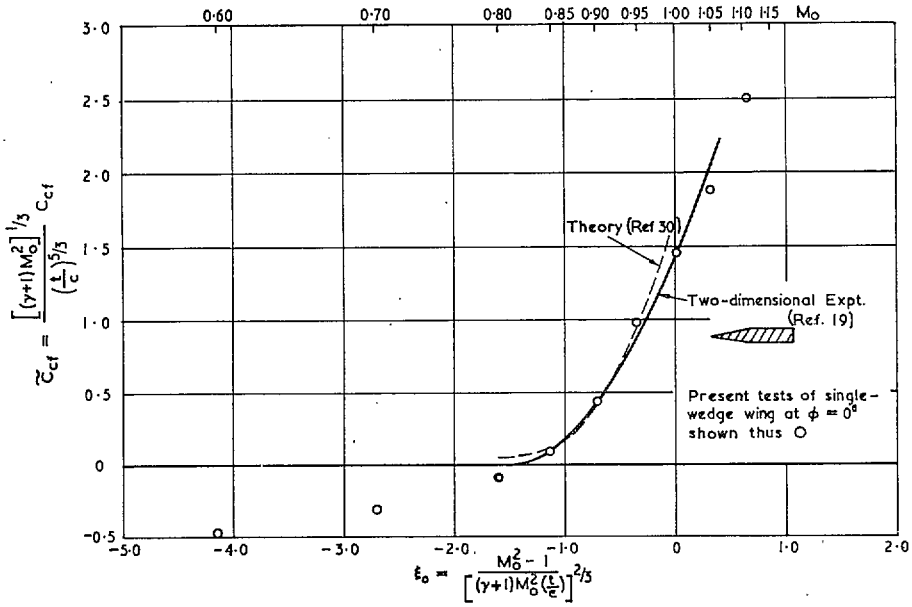

FIG. 32. Variation of chordwise pressure-force coefficient with Mach number for $\phi = 0°$ plotted in transonic similarity form. (Single-wedge models.)

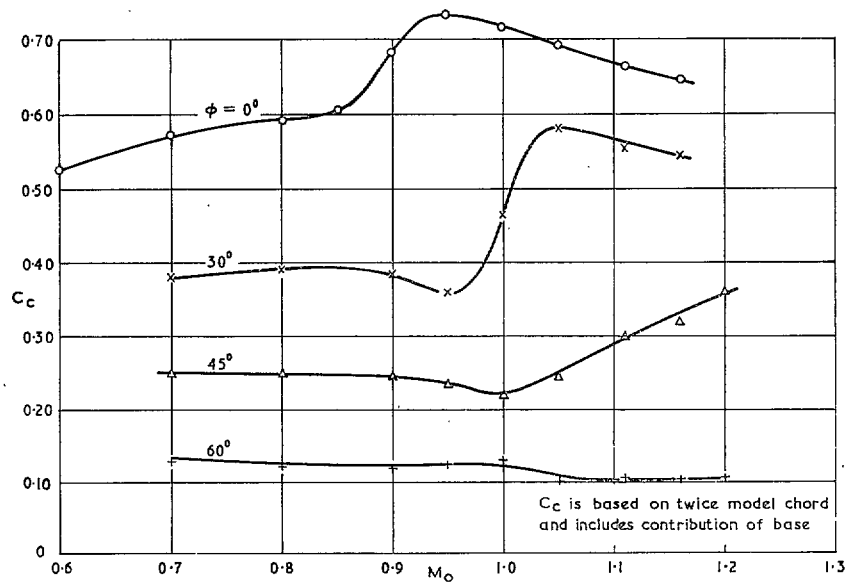

FIG. 33. Chordwise force coefficient of complete single-wedge profile at zero lift.

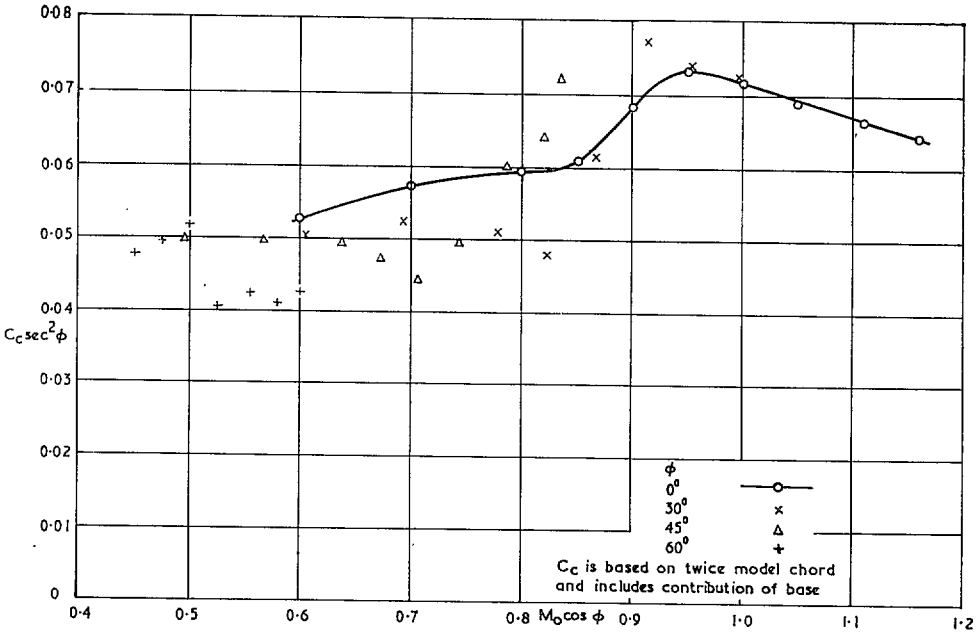

FIG. 34. Correlation of complete chordwise force coefficient for single-wedge profile at zero lift.

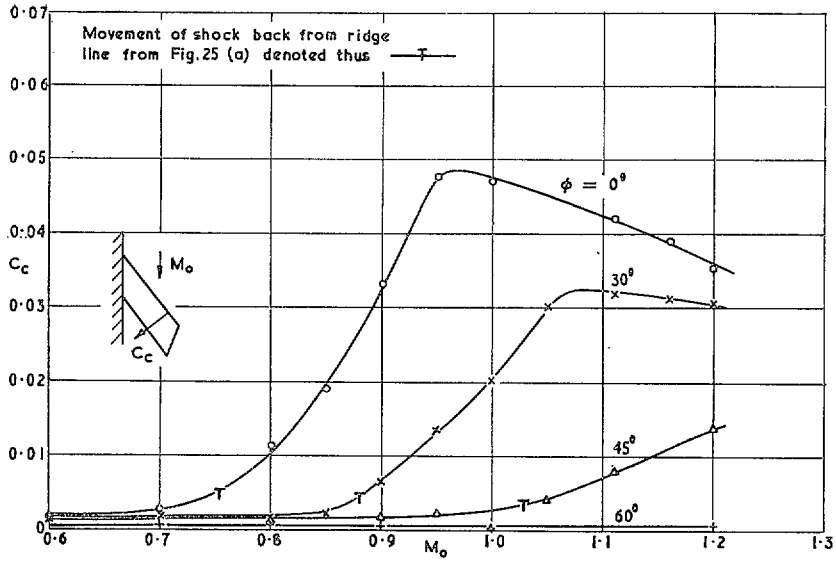

FIG. 35a. Chordwise pressure-force coefficients for double-wedge profile at zero incidence.

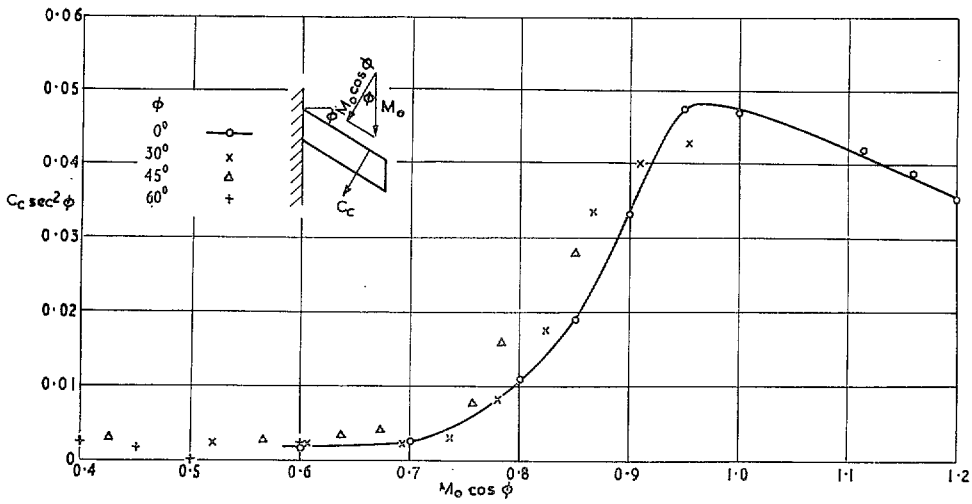

FIG. 35b. Correlation of reduced chordwise pressure-force coefficient for double-wedge profile at zero incidence.

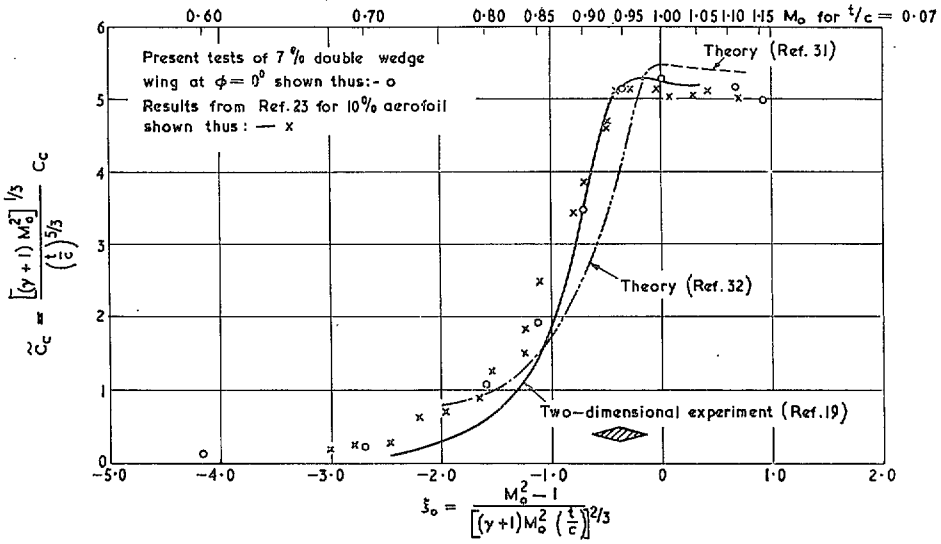

FIG. 36. Variation of chordwise pressure-force coefficient with Mach number for $\phi = 0°$, plotted in transonic similarity form.

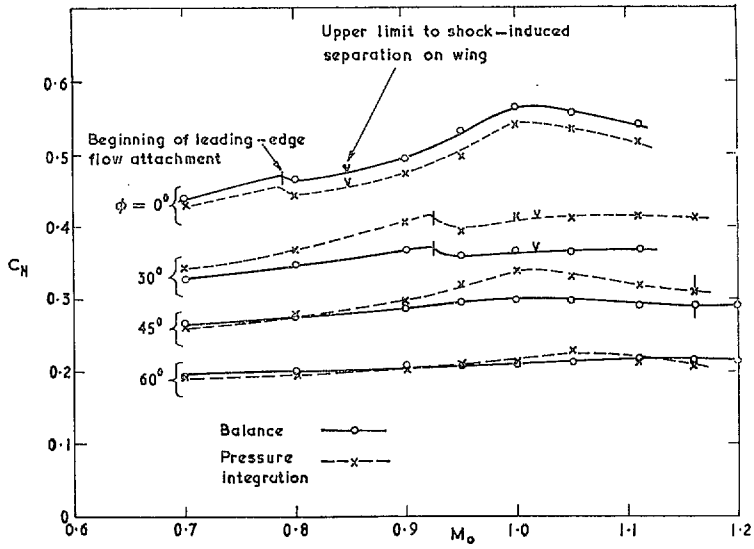

FIG. 37. Comparison of overall wing normal-force coefficient (balance) with that obtained from integration of pressure distributions at $\alpha = 4·0°$ (single-wedge wing).

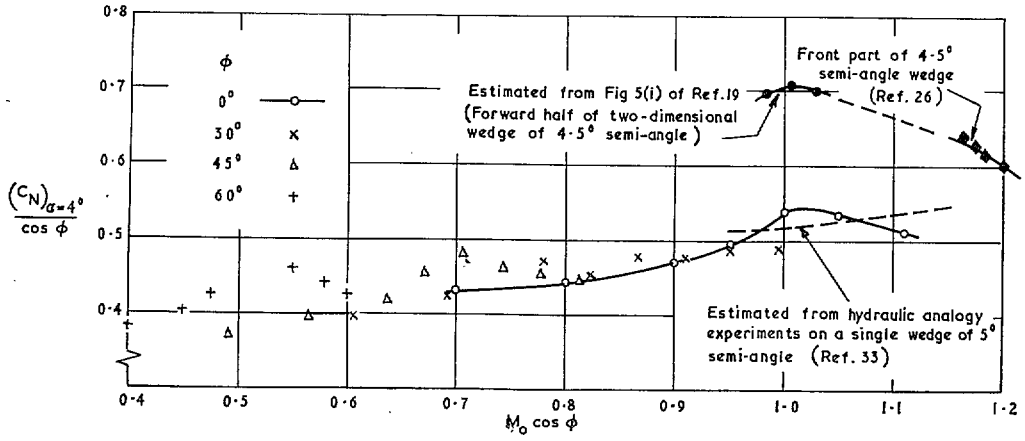

FIG. 38. Correlation of normal-force coefficients for single-wedge section at wing incidence of 4·0°.

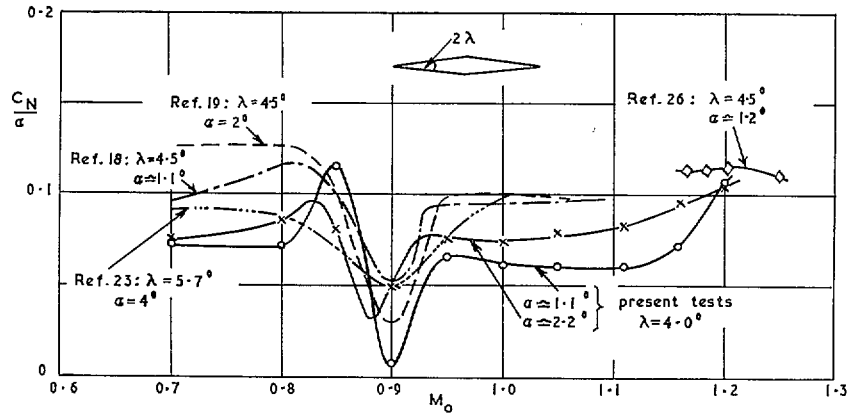

FIG. 39. Comparison of normal-force-coefficient slope at small incidences with two-dimensional data (double-wedge section).

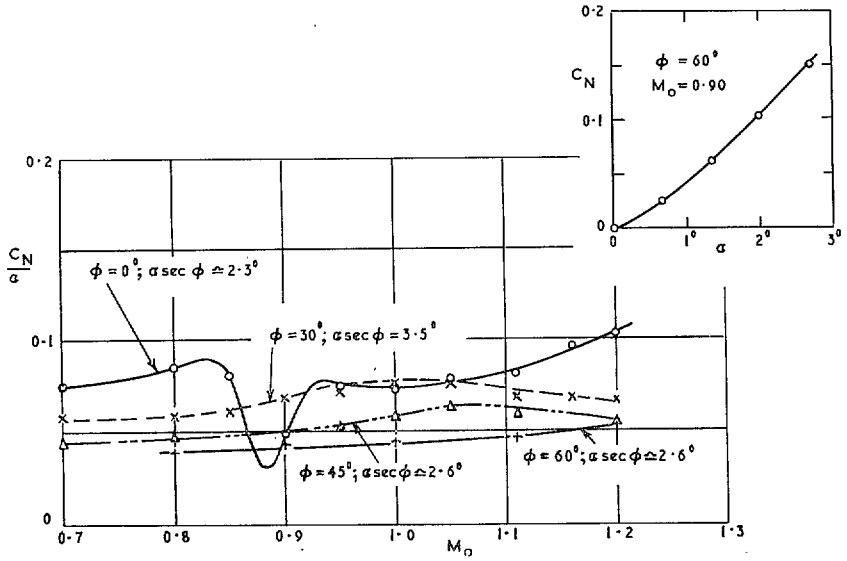

FIG. 40. Section normal-force coefficient for four sweepback angles (double-wedge wing).

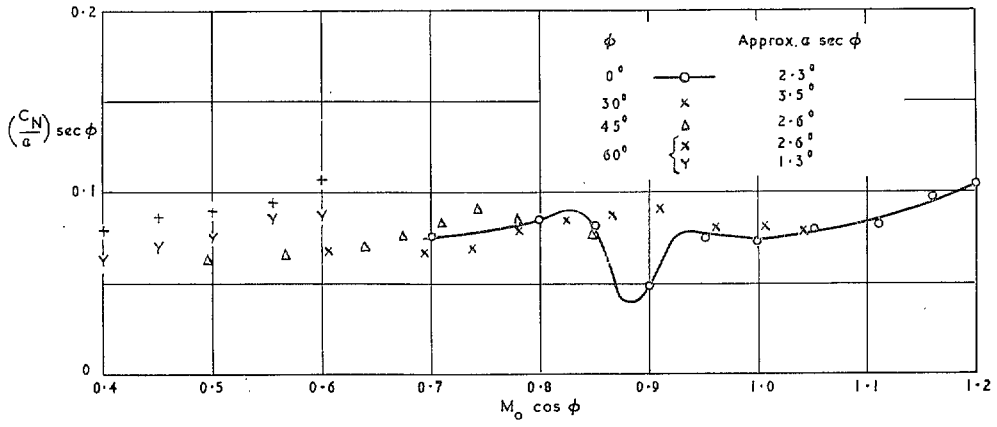

FIG. 41. Correlation of normal-force coefficients for double-wedge section.

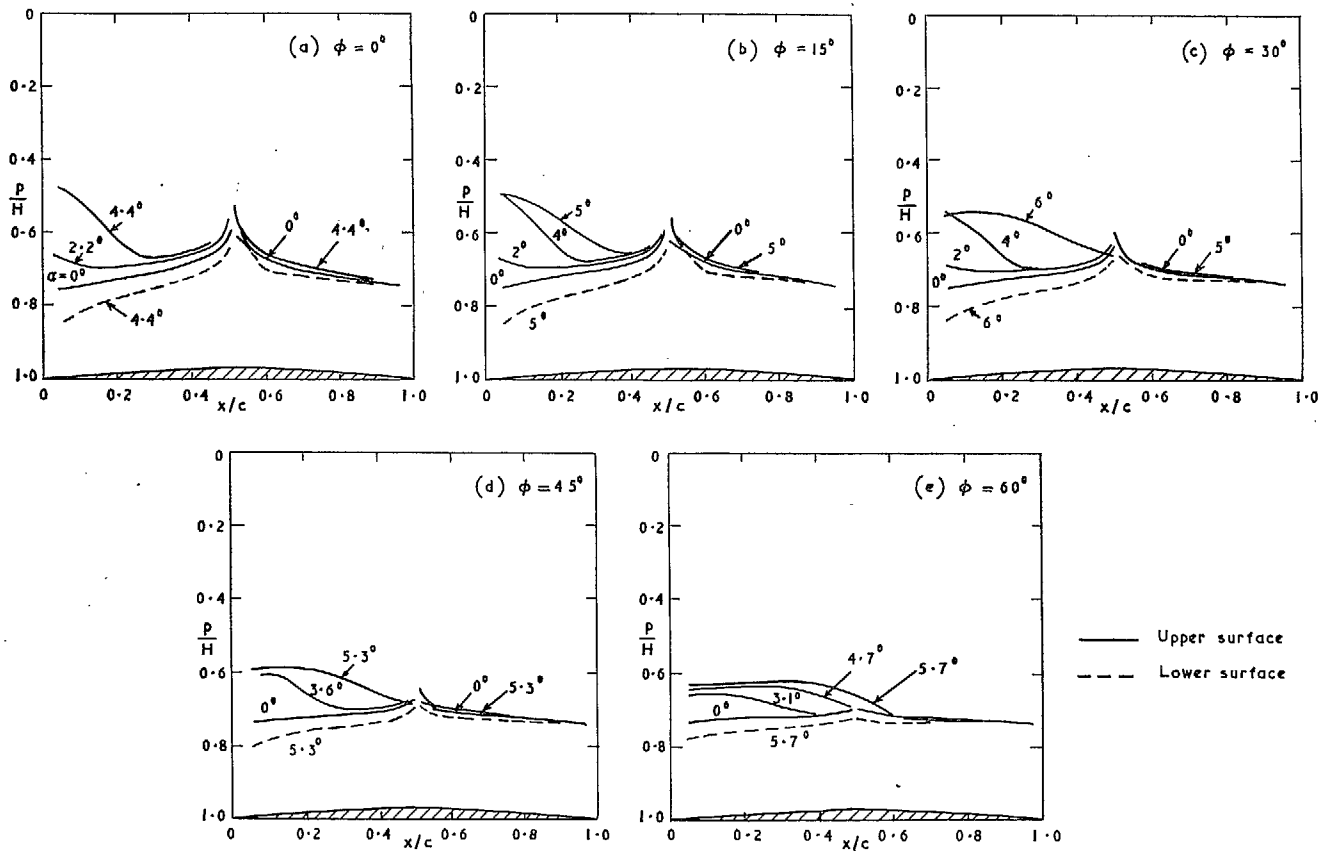

FIG. 42. Pressure distributions on double-wedge section at $M_0 = 0{\cdot}70$.

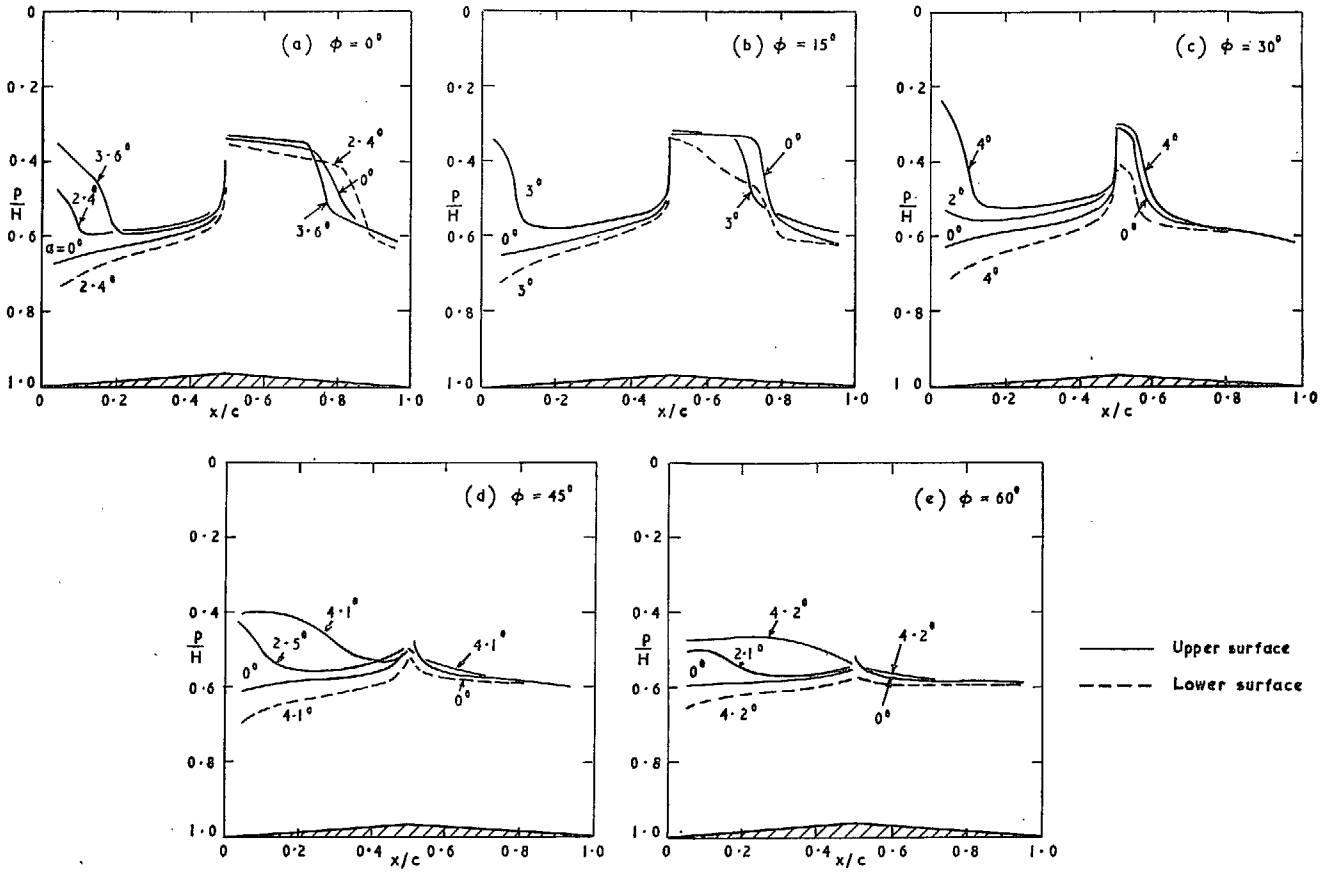

FIG. 43. Pressure distributions on double-wedge section at $M_0 = 0{\cdot}90$.

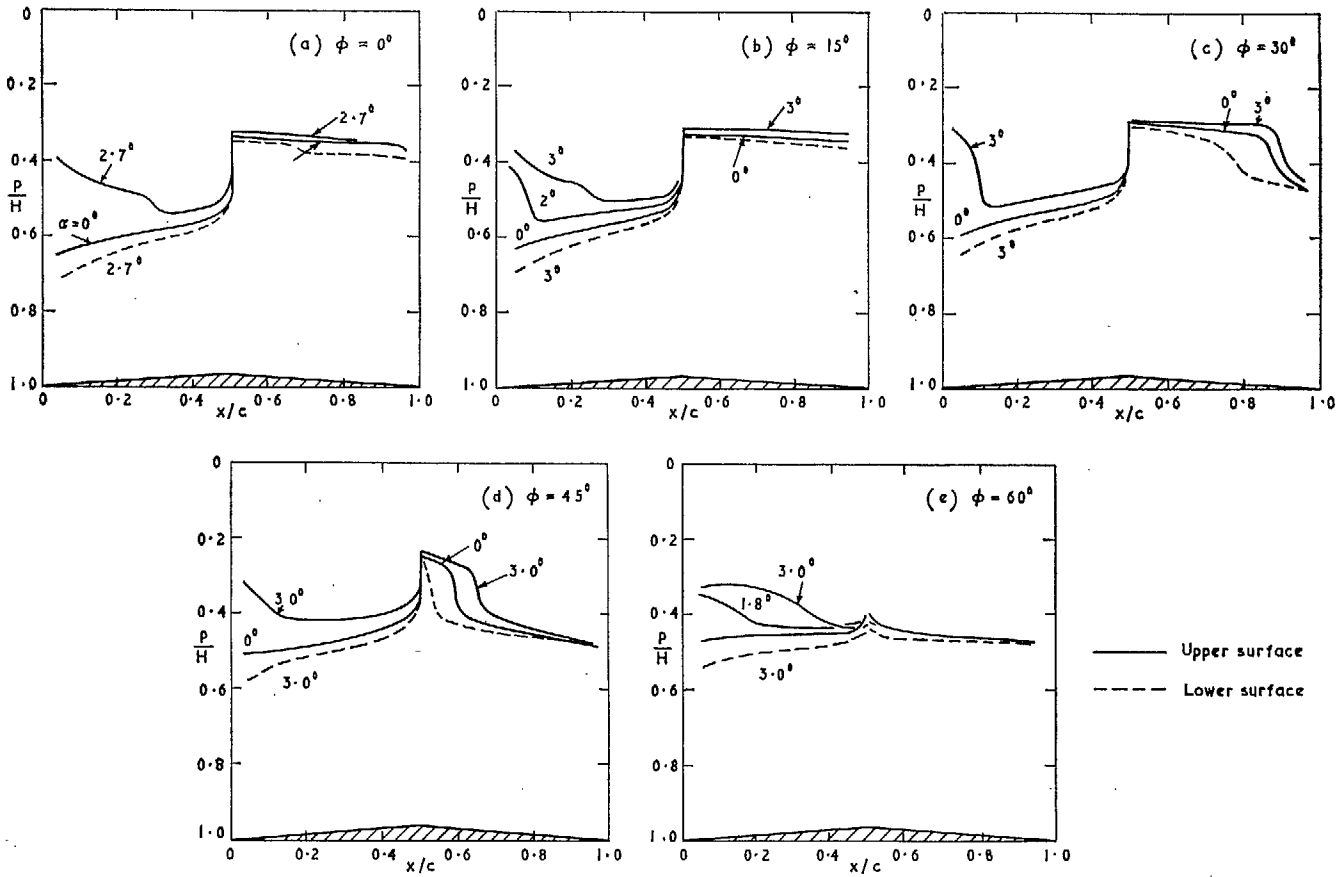

FIG. 44. Pressure distributions on double-wedge section at $M_0 = 1{\cdot}11$.

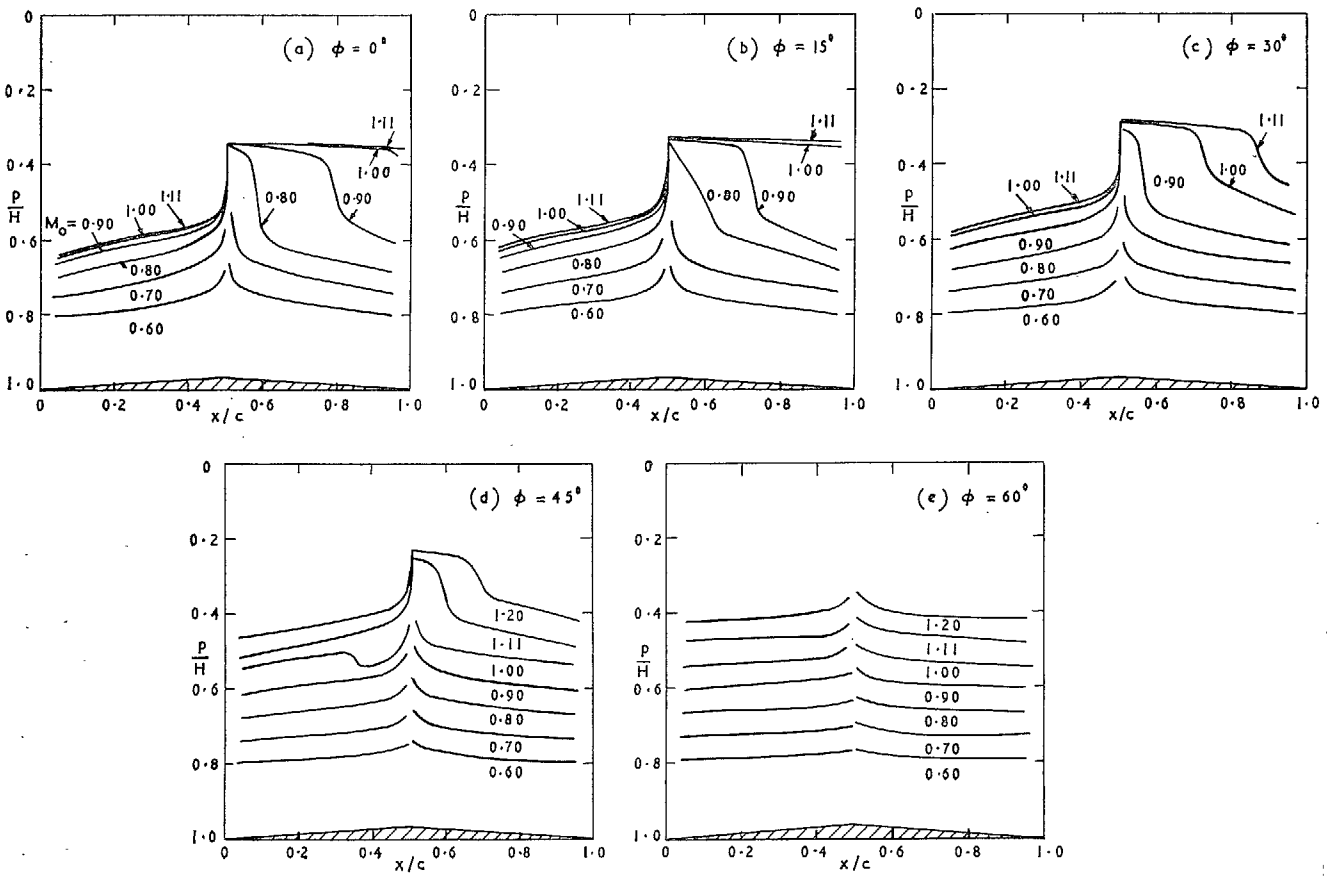

FIG. 45. Pressure distributions on double-wedge section at $\alpha = 0°$.

(88242)

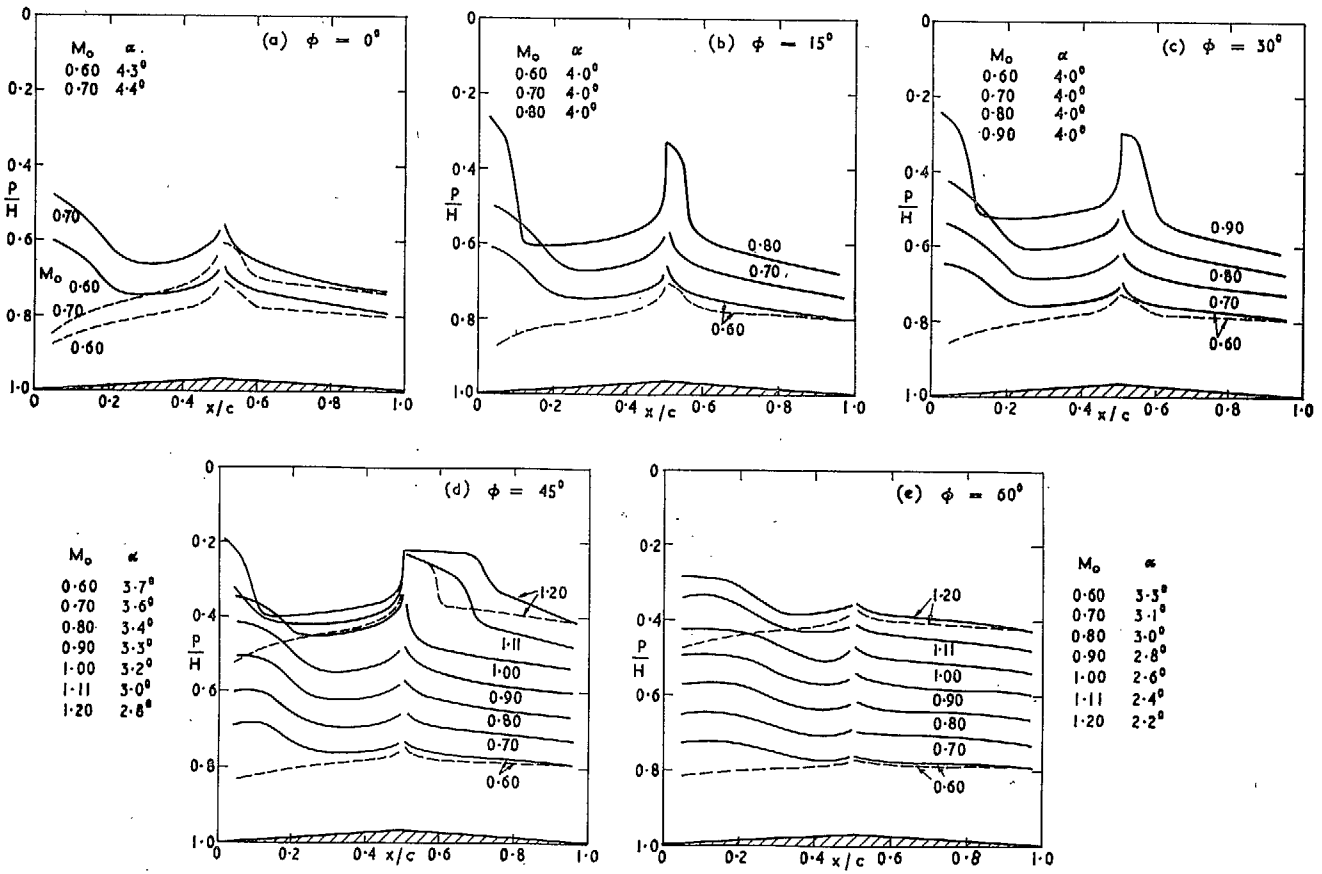

FIG. 46. Pressure distributions on double-wedge section at nominal incidence of 4·0°.

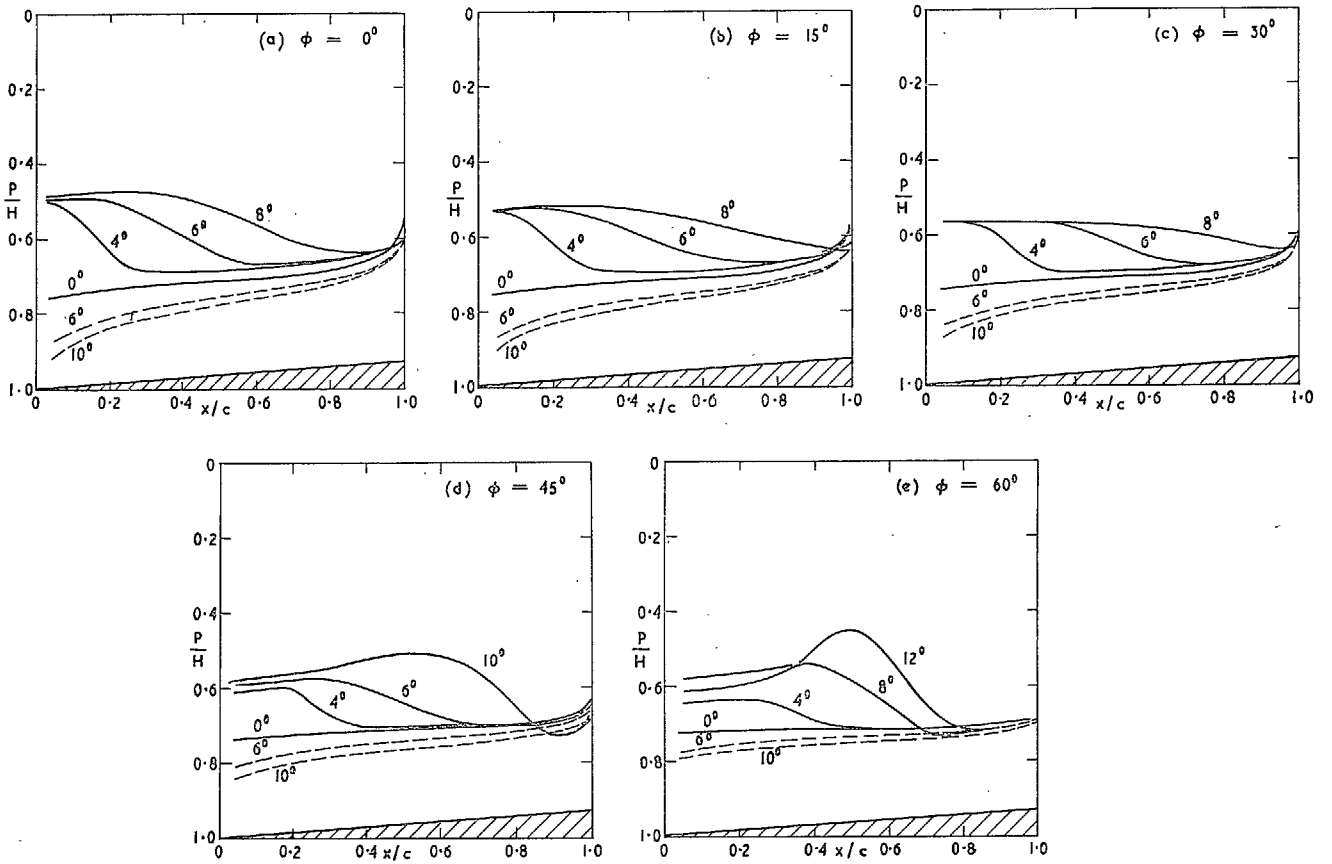

FIG. 47. Pressure distributions on single-wedge section at $M_0 = 0{\cdot}70$.

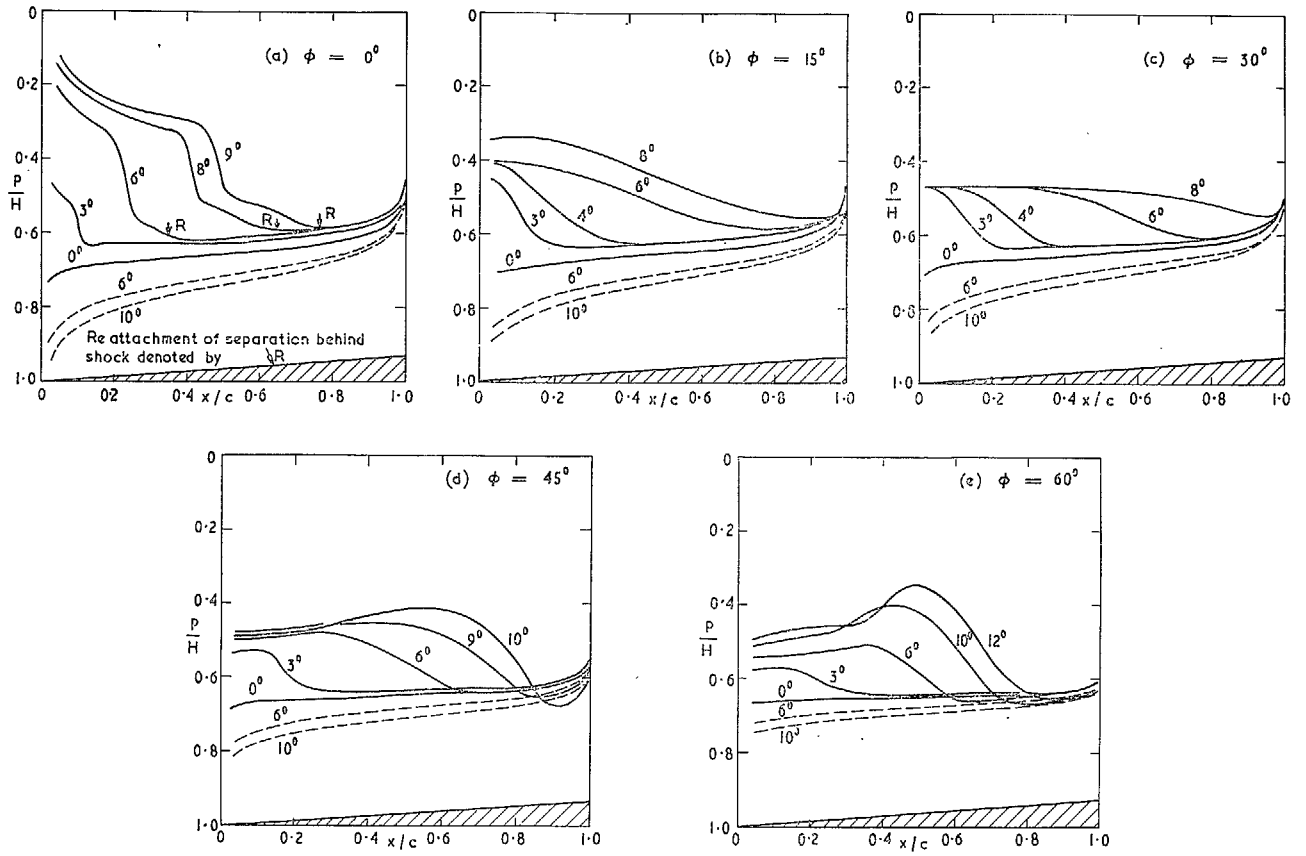

FIG. 48. Pressure distributions on single-wedge section at $M_0 = 0{\cdot}80$.

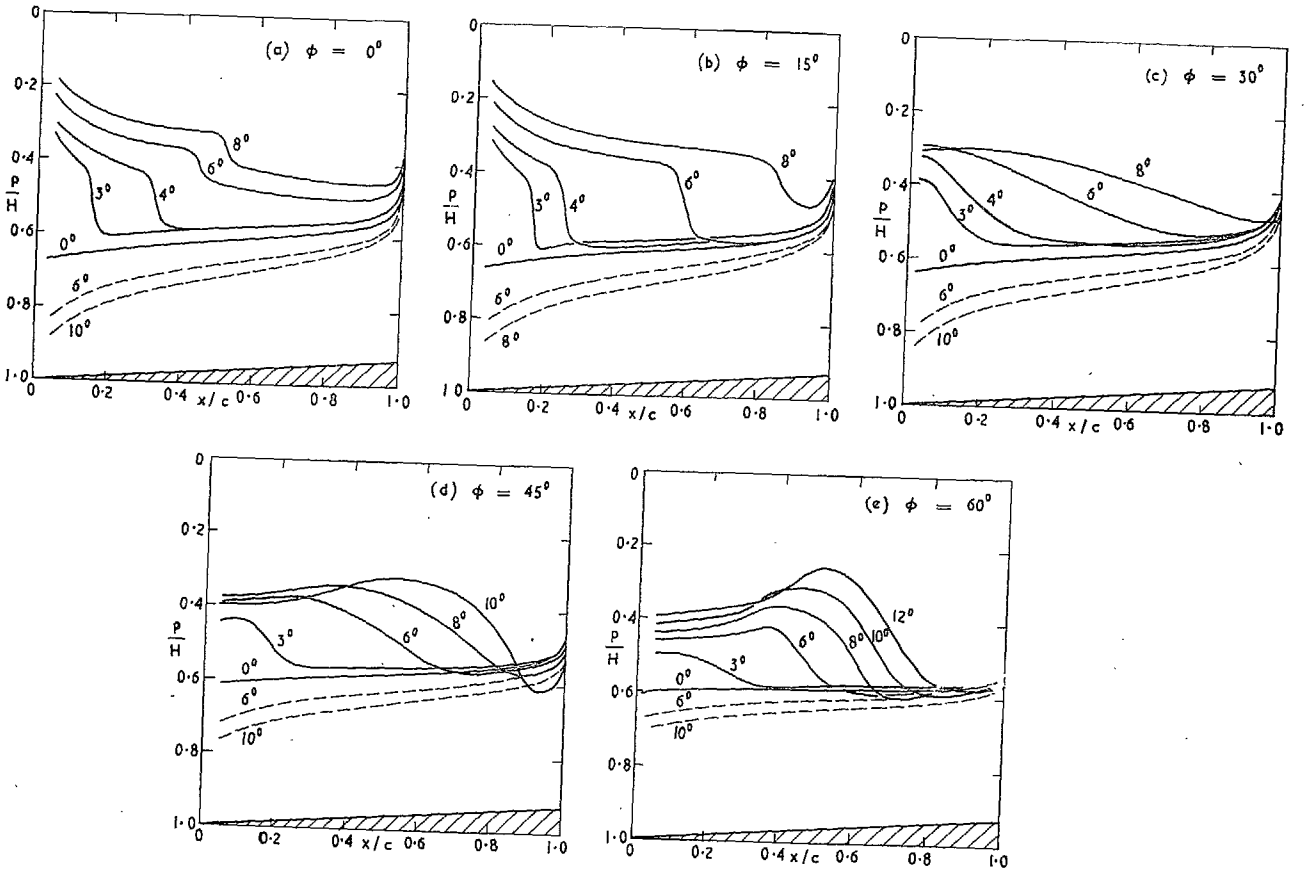

FIG. 49. Pressure distributions on single-wedge section at $M_0 = 0{\cdot}90$.

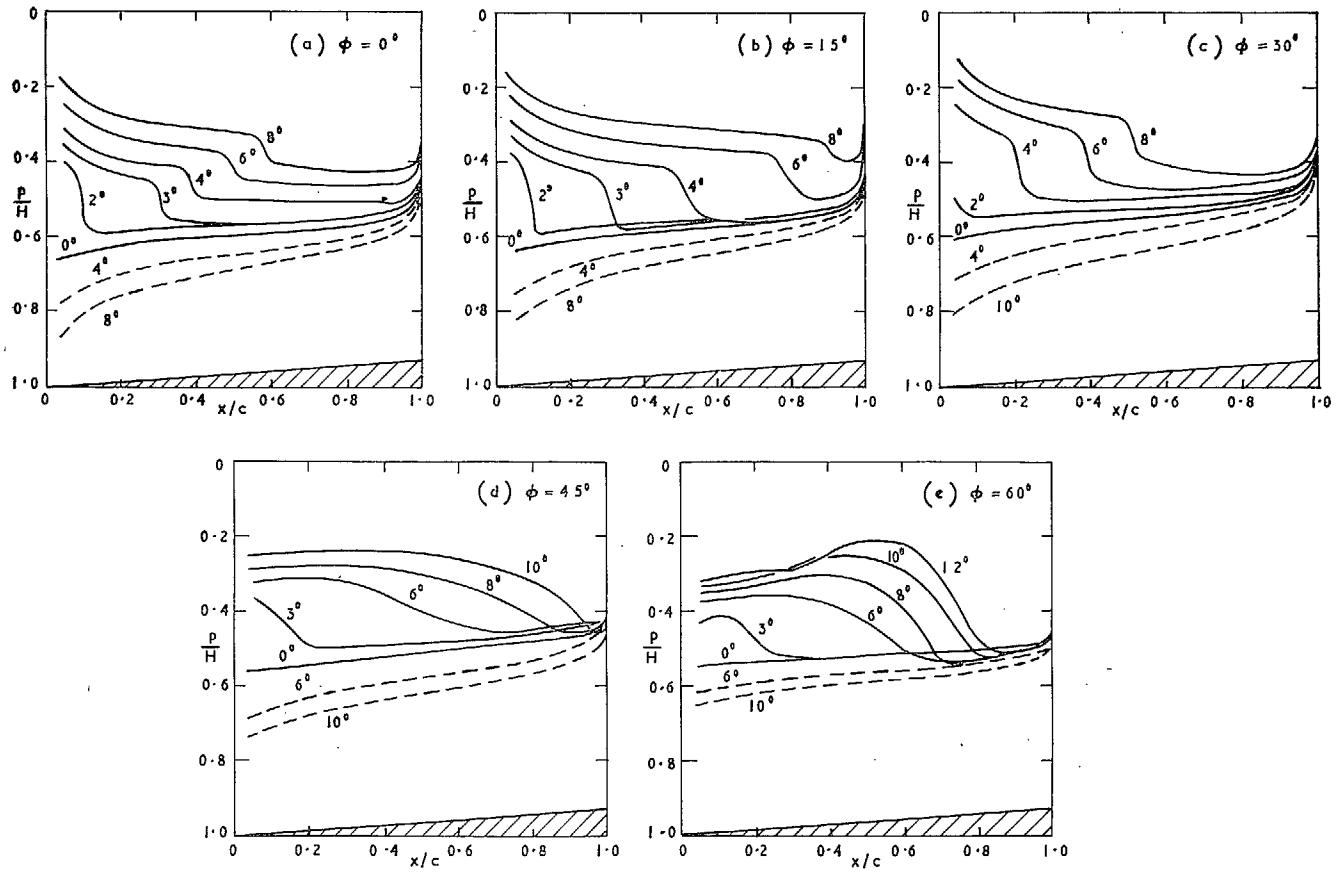

FIG. 50. Pressure distributions on single-wedge section at $M_0 = 1{\cdot}00$.

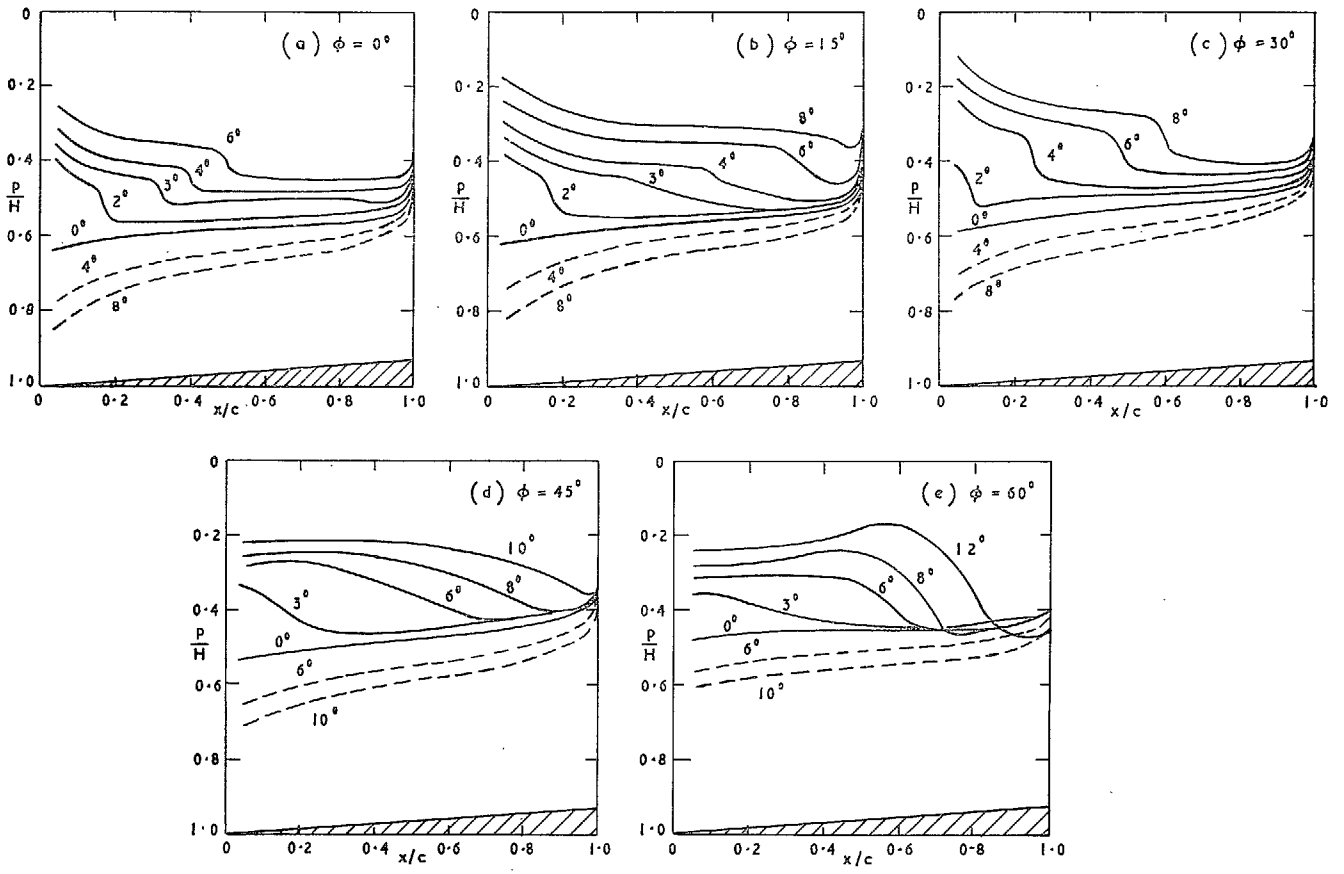

FIG. 51. Pressure distributions on single-wedge section at $M_0 = 1{\cdot}11$.

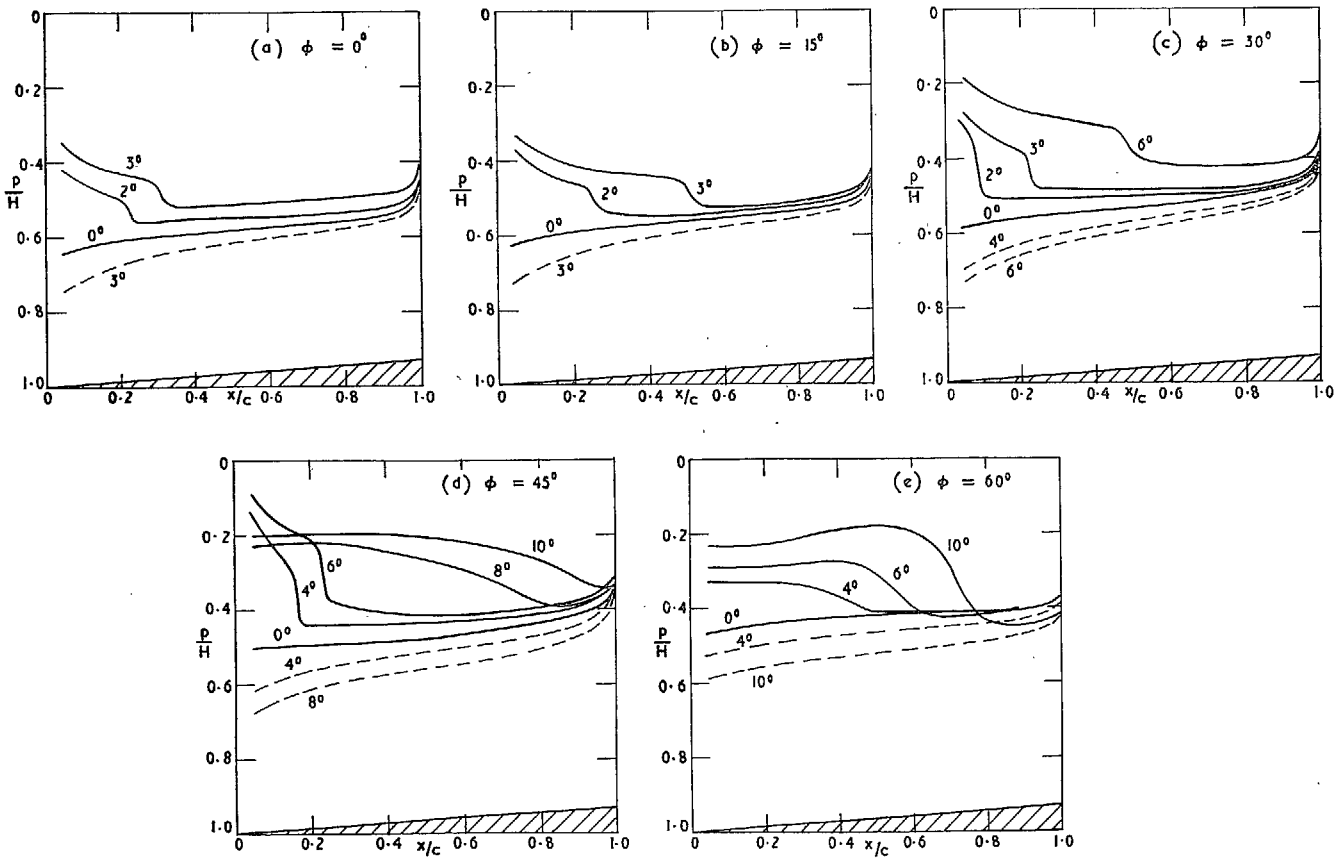

FIG. 52. Pressure distributions single-wedge section at $M_0 = 1{\cdot}16$.

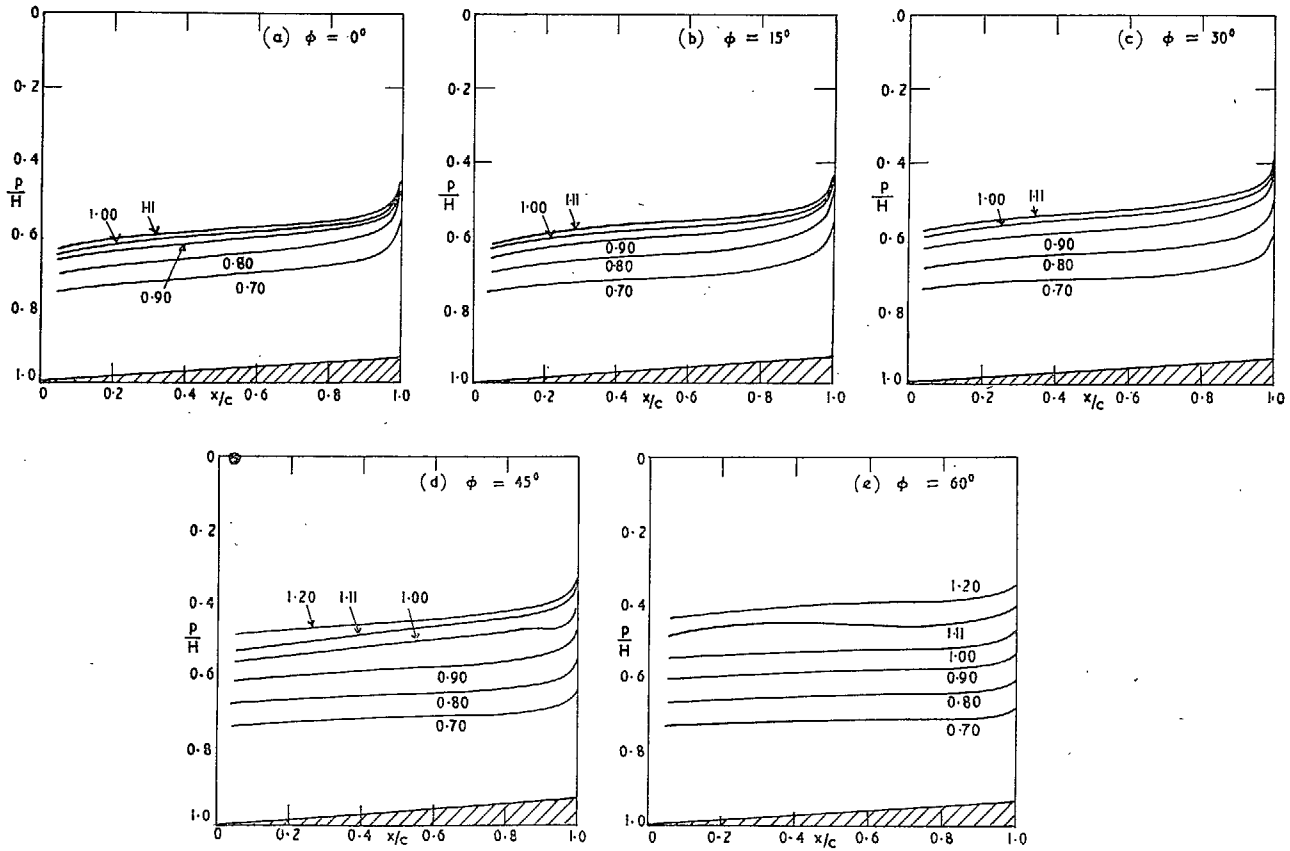

FIG. 53. Pressure distributions single-wedge section at $\alpha = 0°$.

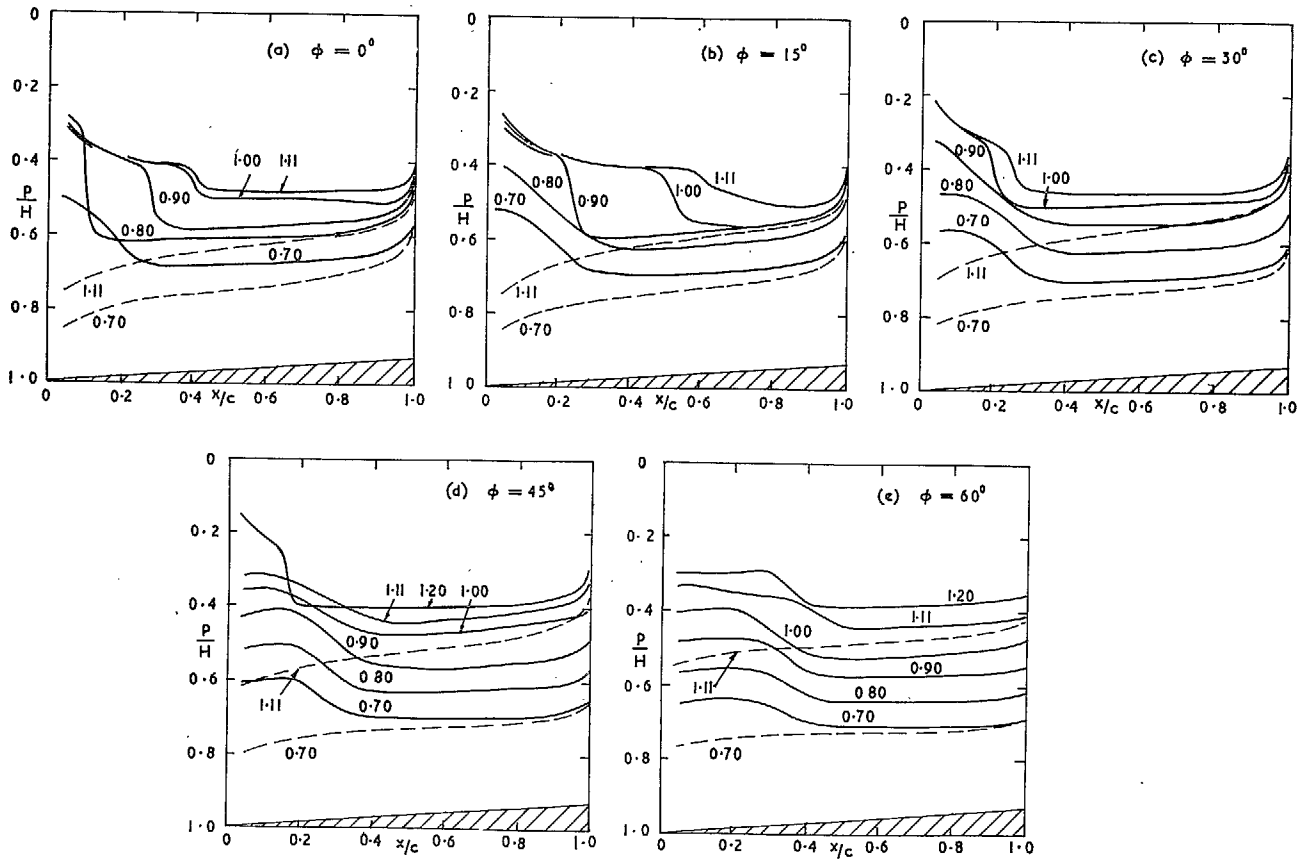

FIG. 54. Pressure distribution on single-wedge section at $\alpha = 4°$.

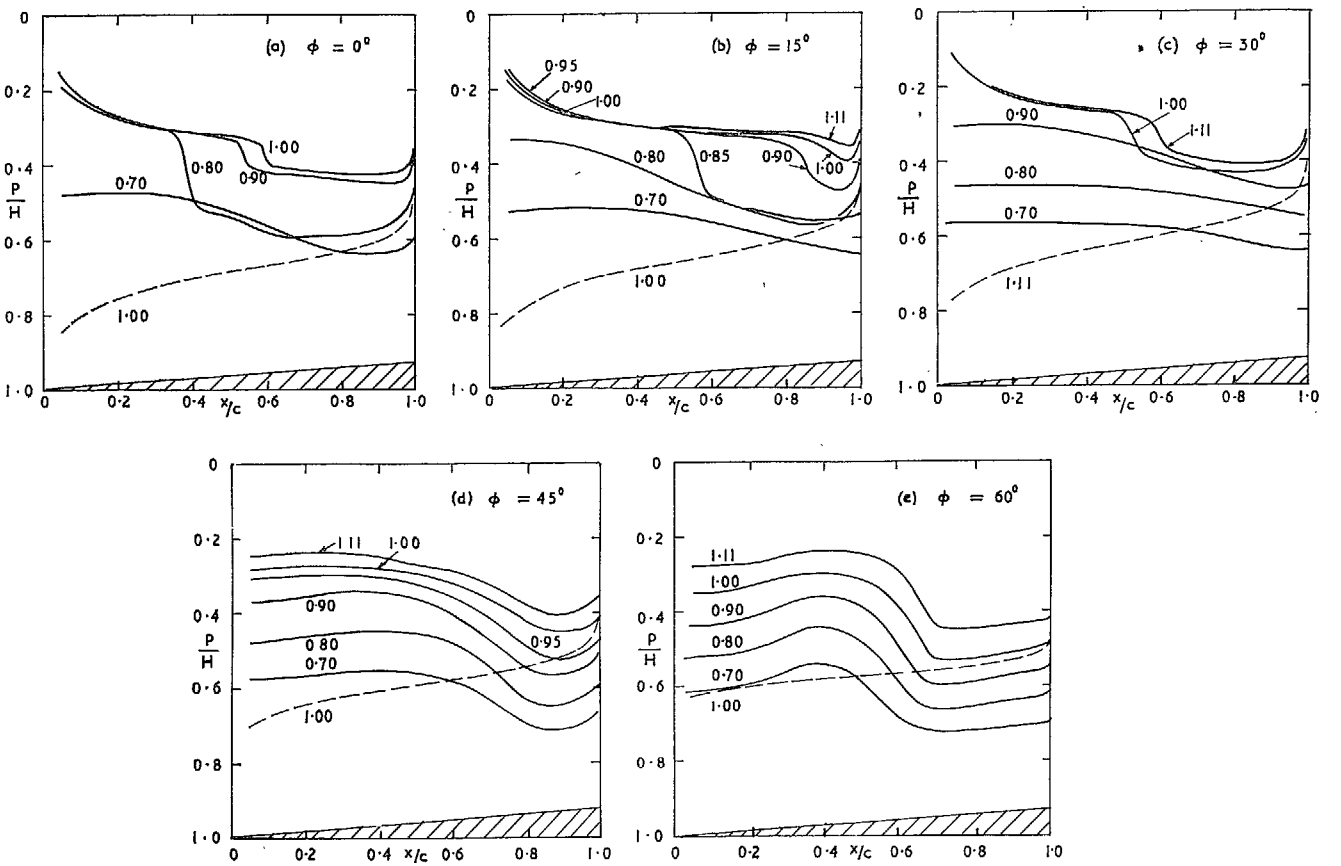

FIG. 55. Pressure distributions on single-wedge section at $\alpha = 8°$.

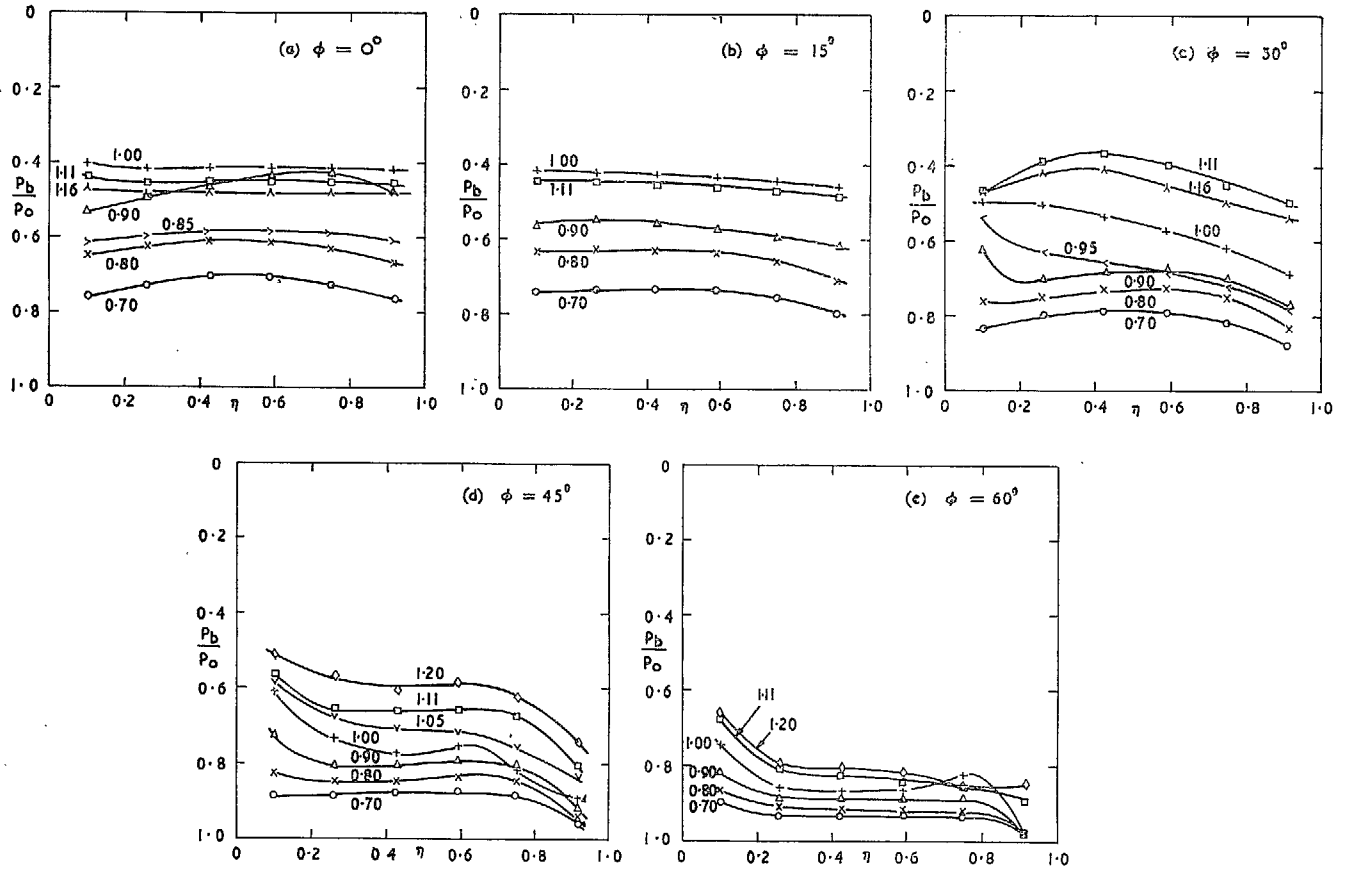

FIG. 56. Distribution of base pressure on single-wedge section at $\alpha = 0°$.

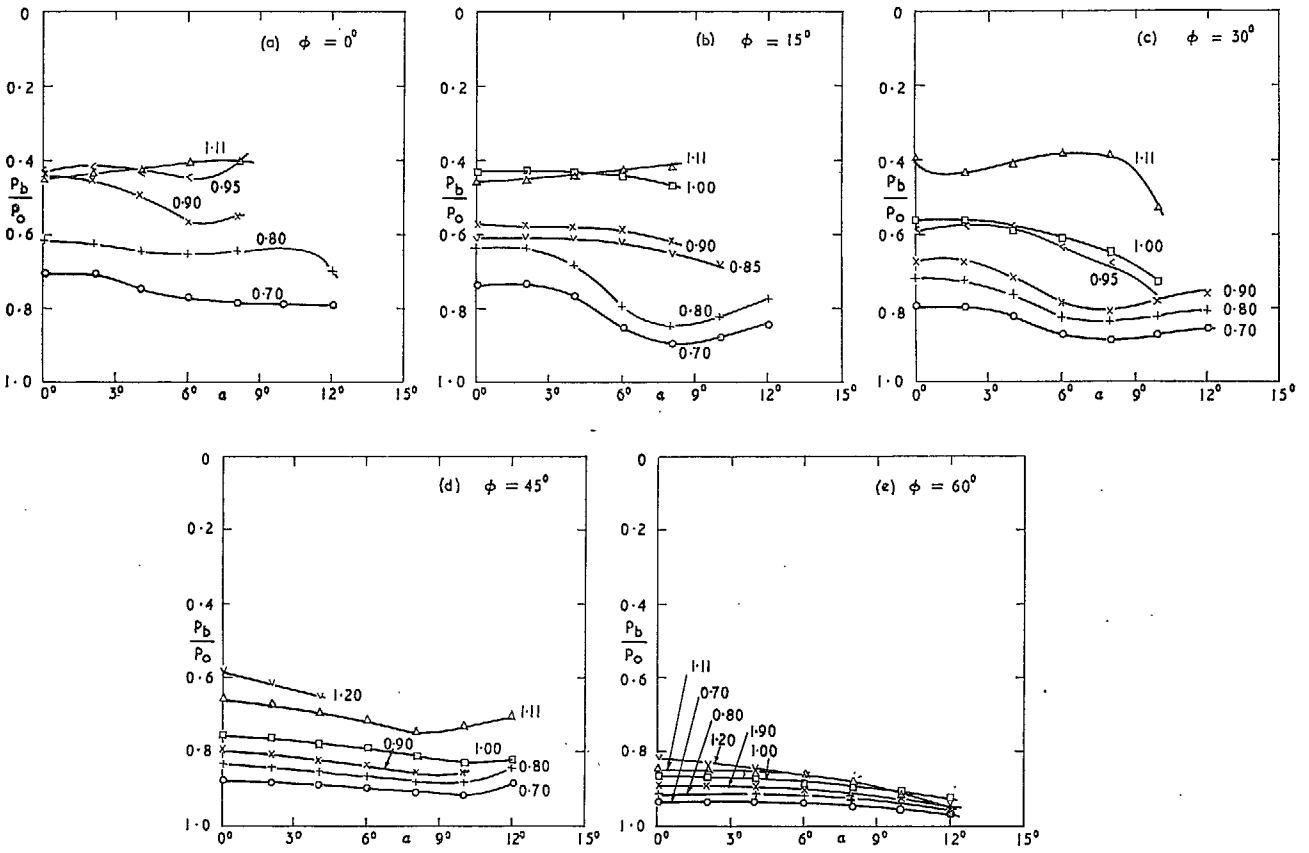

FIG. 57. Variation of base pressure on single-wedge section at 0·59 of the base semi-span.

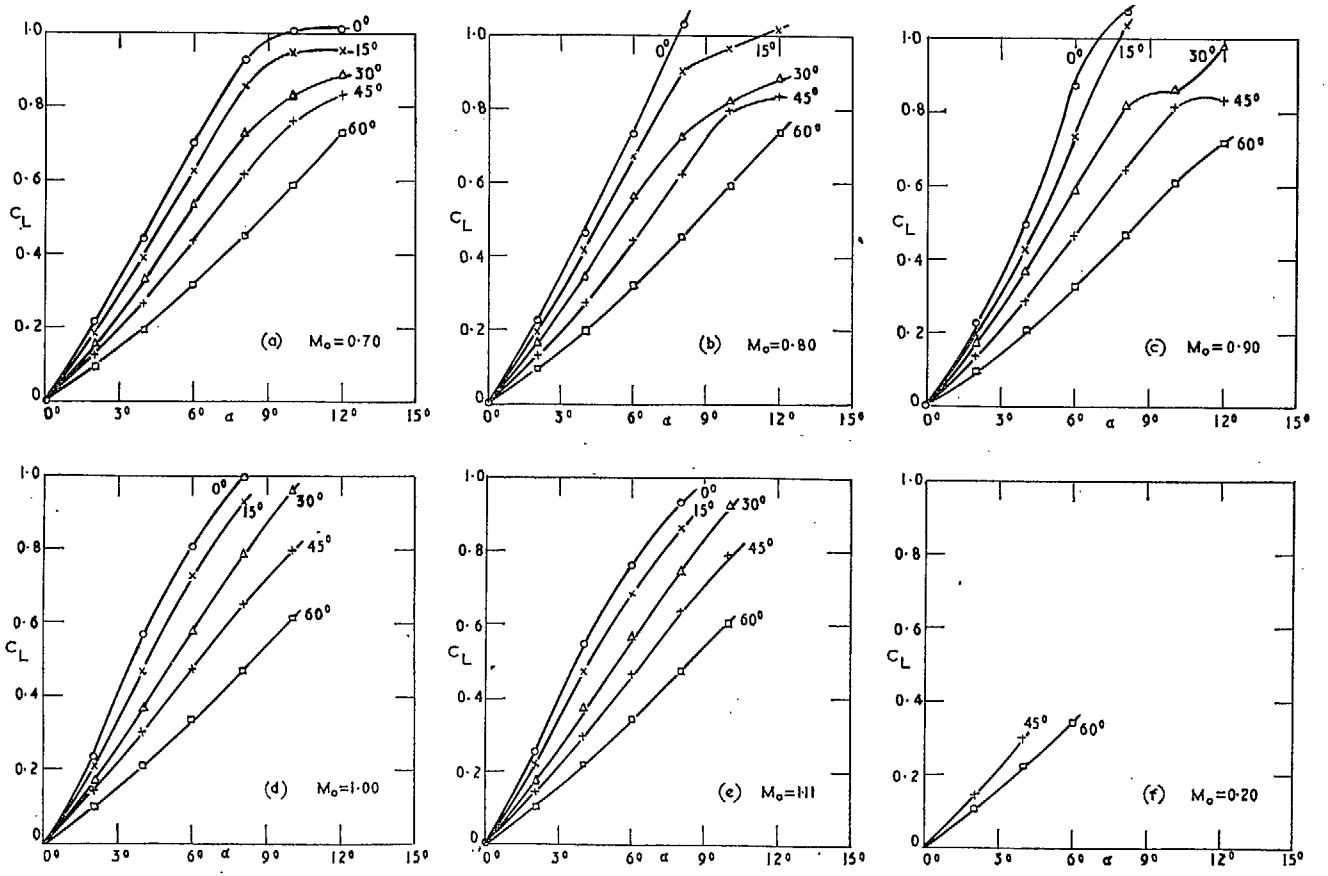

FIG. 58. Overall lift coefficients of single-wedge wing (from balance measurements).

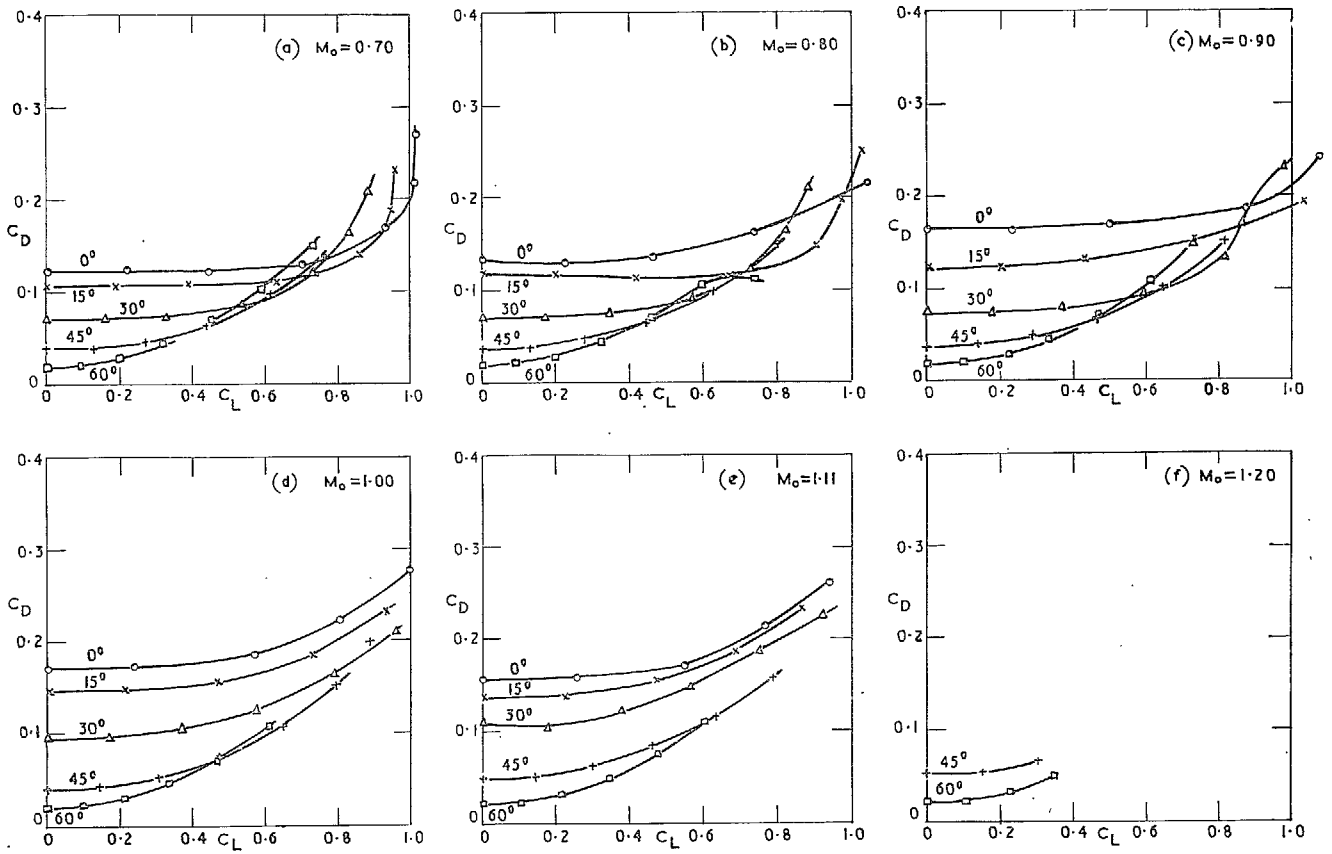

FIG. 59. Overall drag curves for single-wedge wing (from balance measurements).

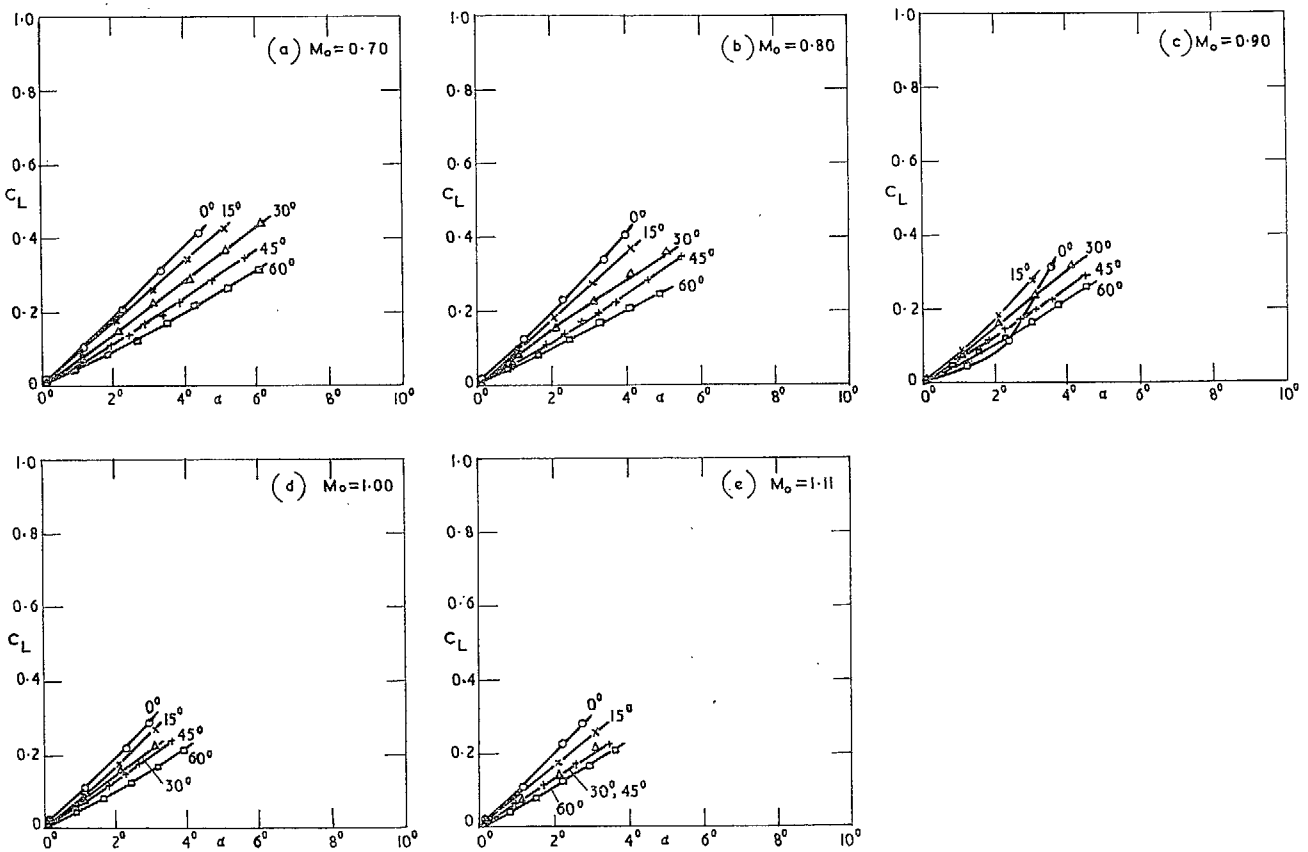

FIG. 60. Overall lift coefficients of double-wedge wing (from balance measurements).

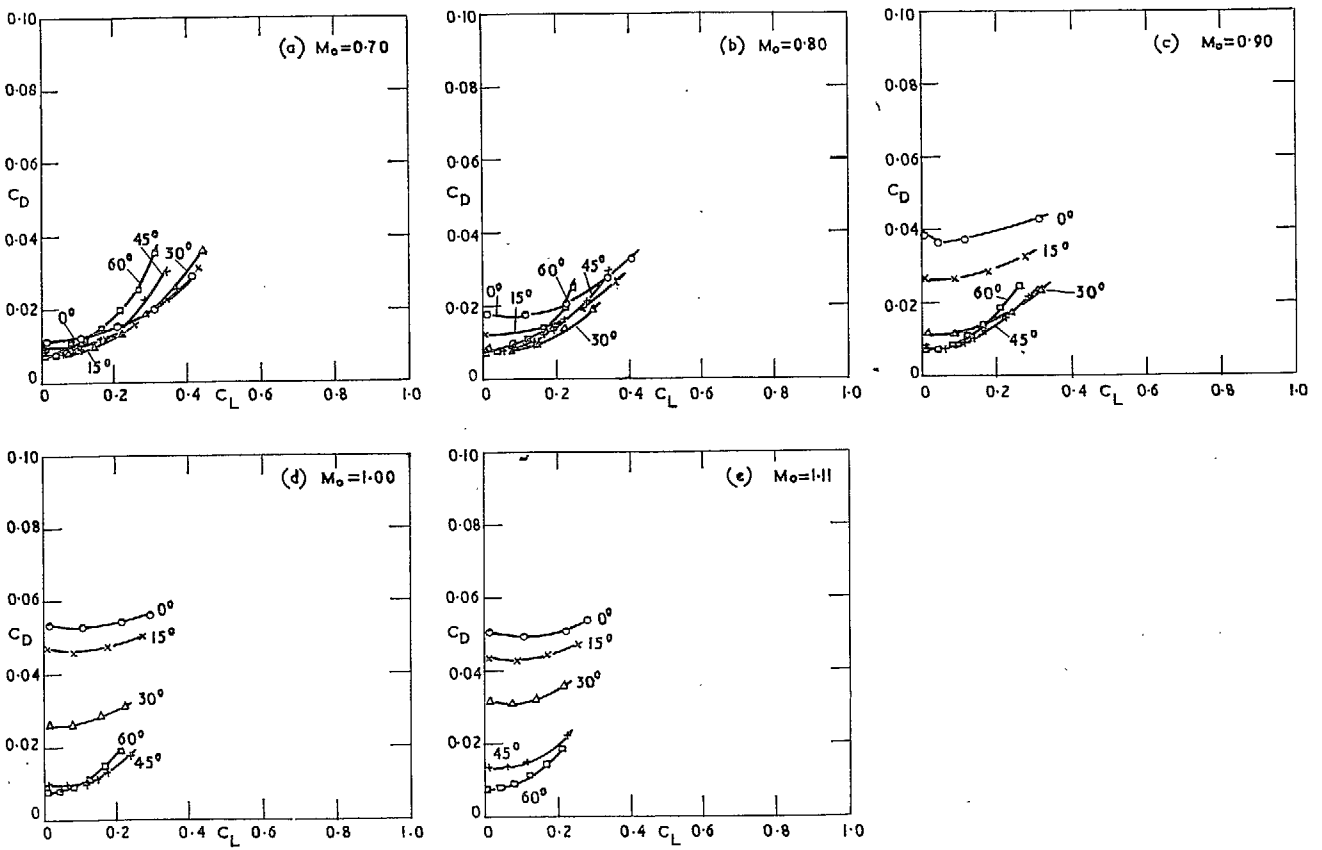

FIG. 61. Overall drag curves for double-wedge wing (from balance measurements).

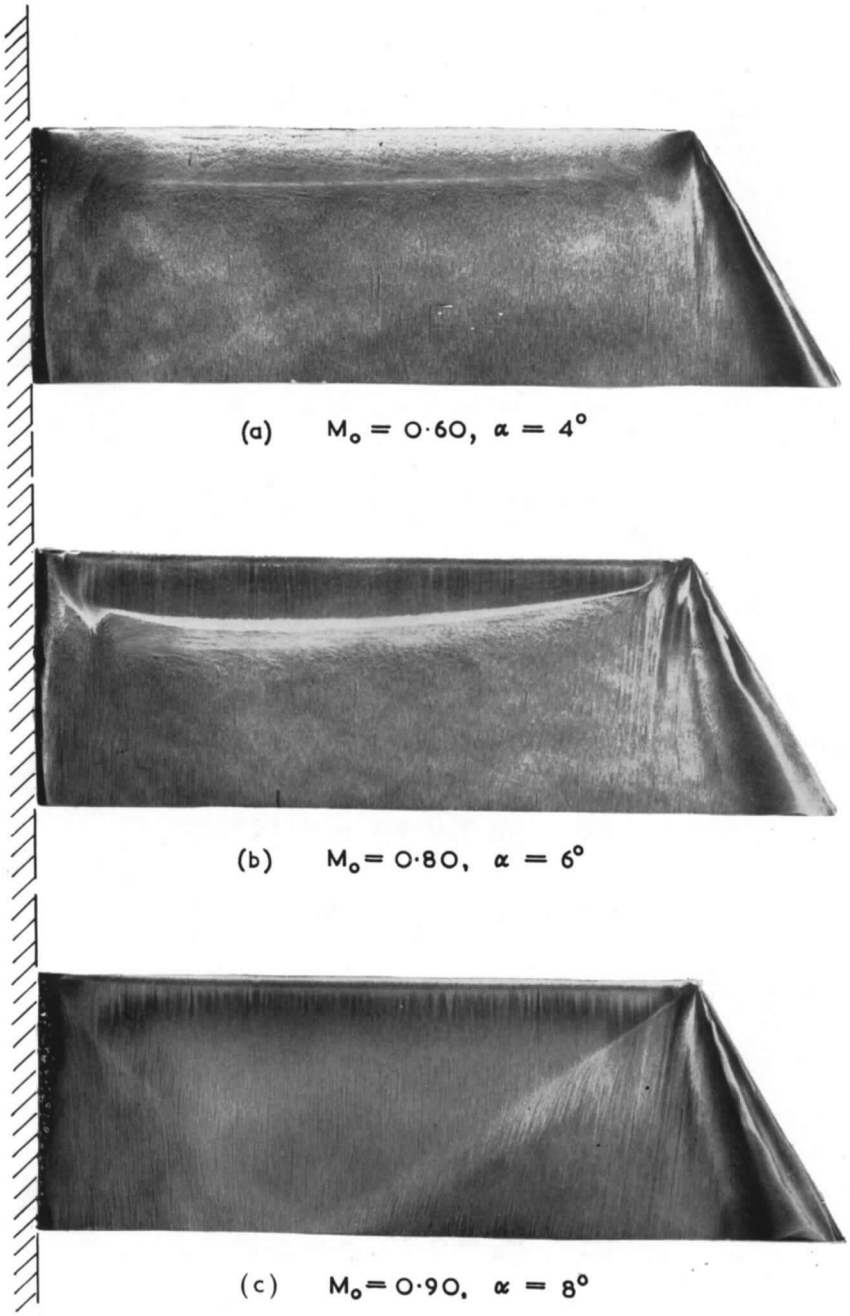

FIG. 62. Oil patterns on upper surface of single-wedge wing at $\phi = 0°$.

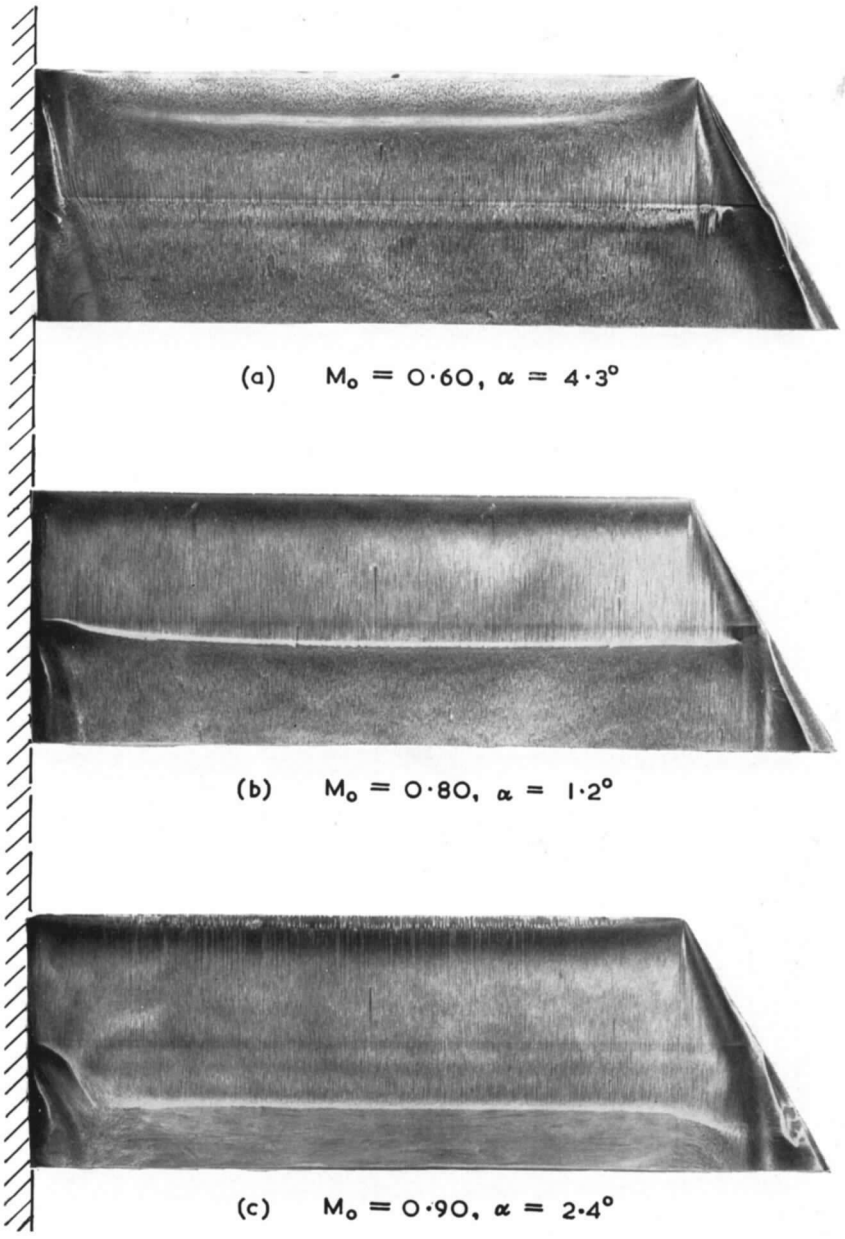

FIG. 63. Oil patterns on upper surface of double-wedge wing at $\phi = 0°$.

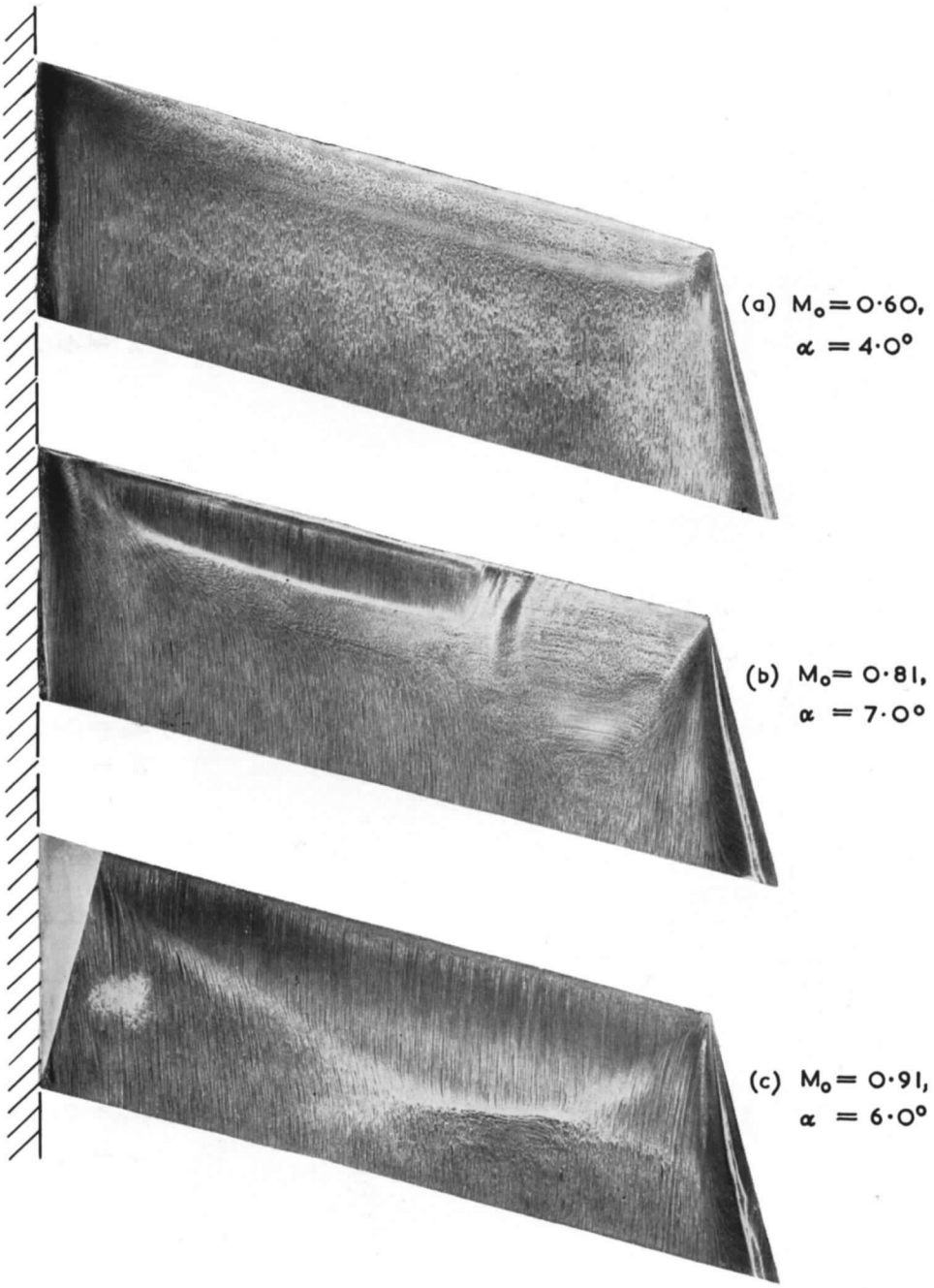

FIG. 64. Oil patterns on upper surface of single-wedge wing at $\phi = 15°$.

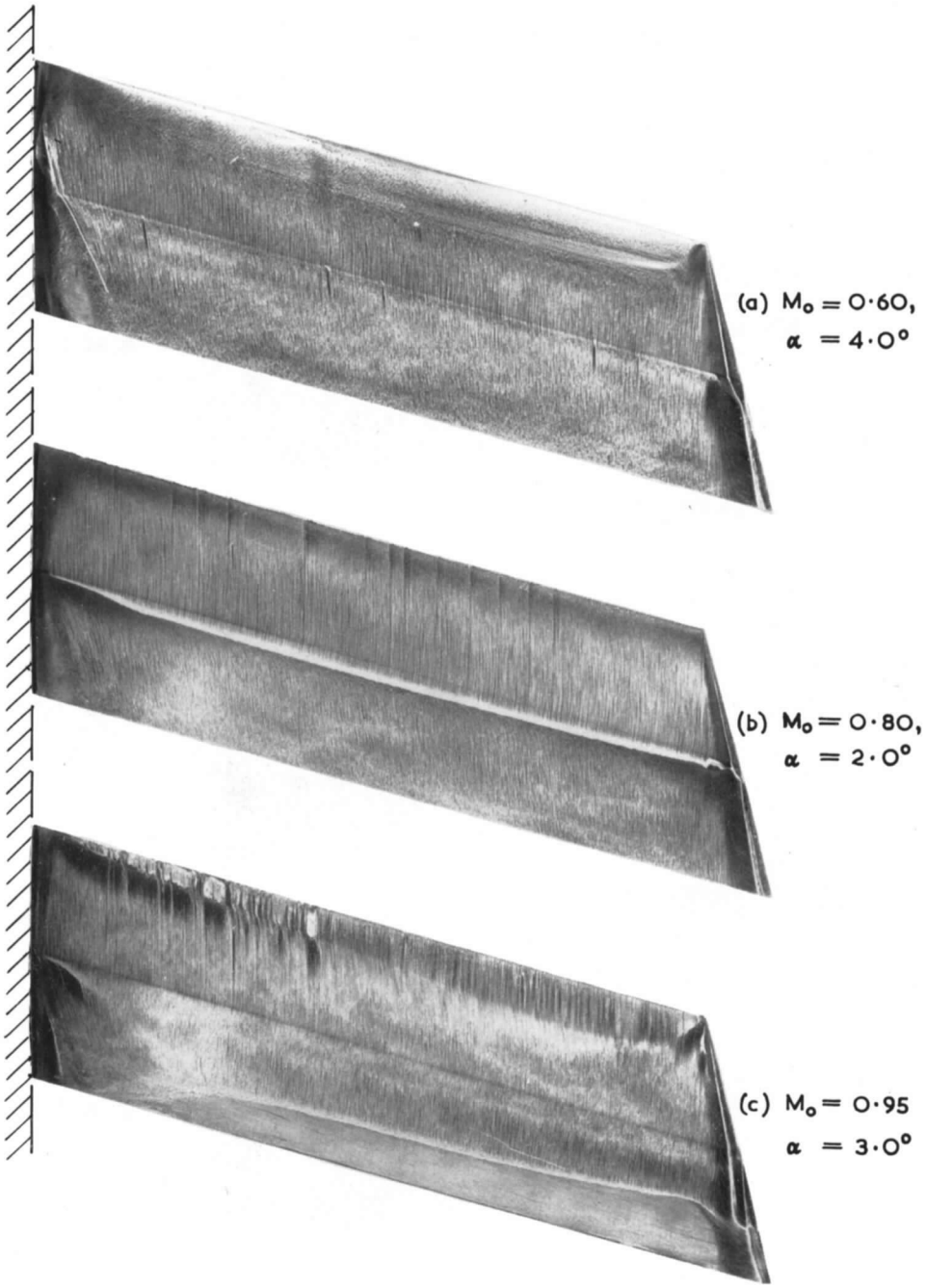

FIG. 65. Oil patterns on upper surface of double-wedge wing at $\phi = 15°$.

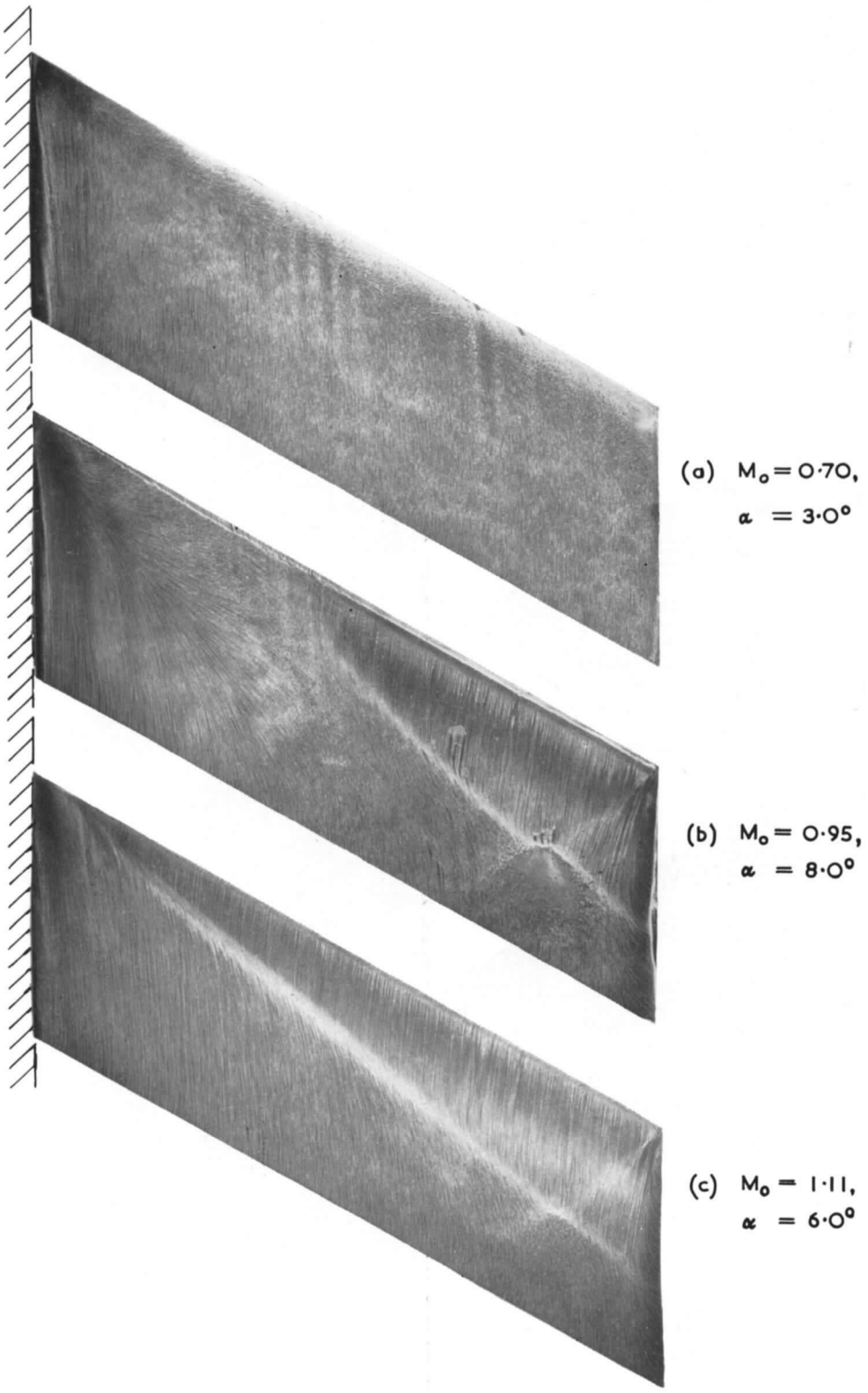

FIG. 66. Oil patterns on upper surface of single-wedge wing at $\phi = 30°$.

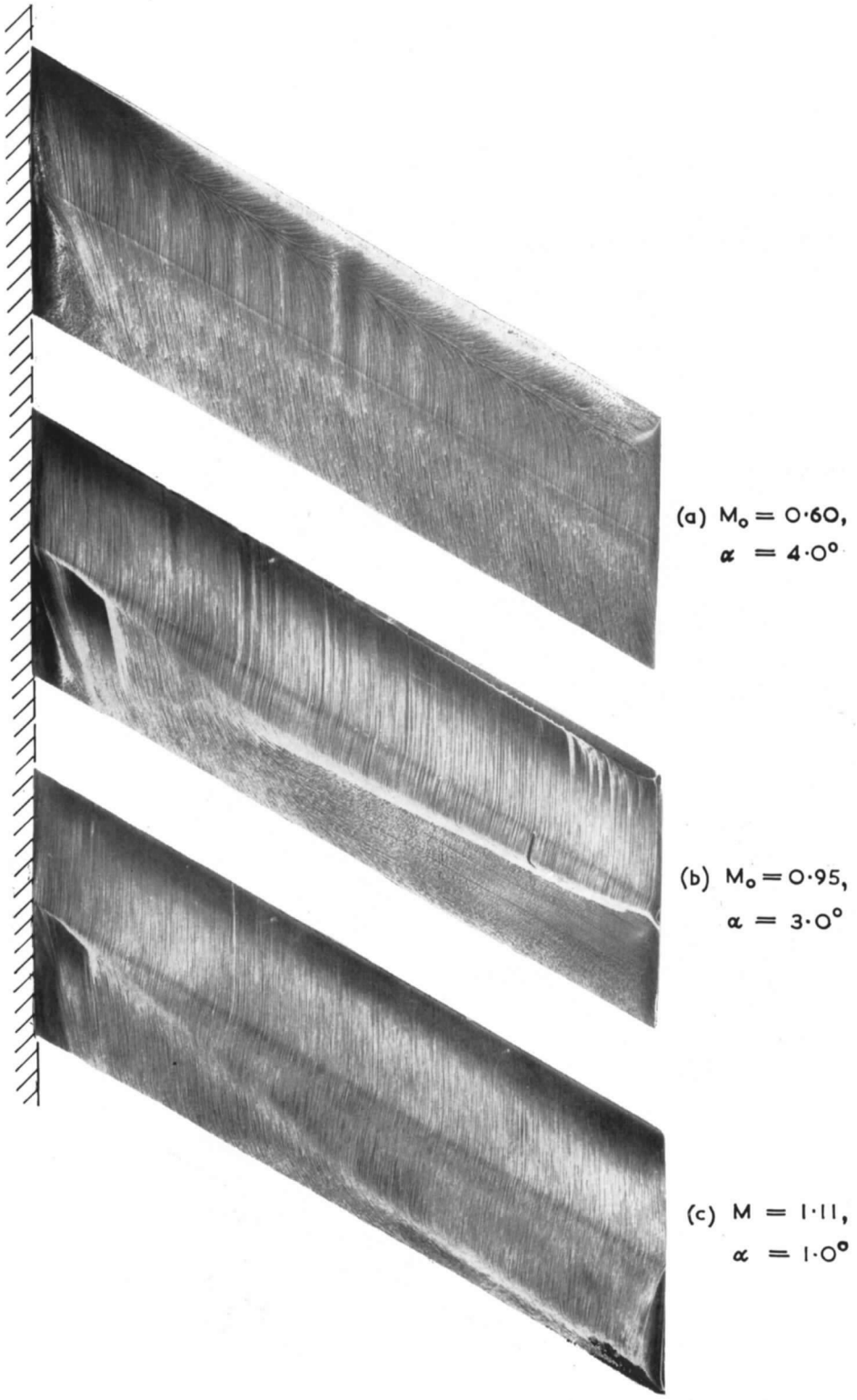

FIG. 67. Oil patterns on upper surface of double-wedge wing at $\phi = 30°$.

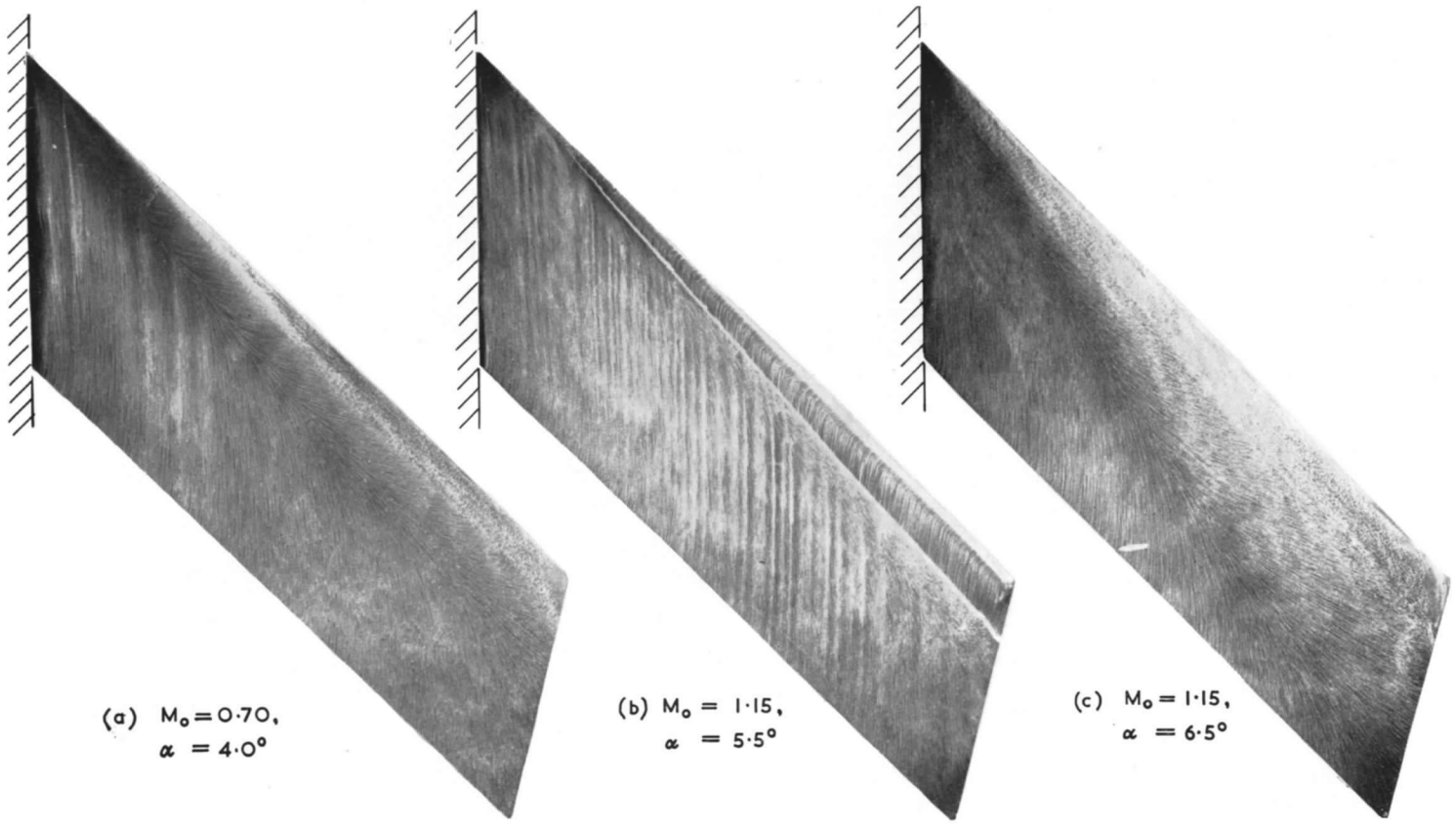

FIG. 68. Oil patterns on upper surface of single-wedge wing at $\phi = 45°$.

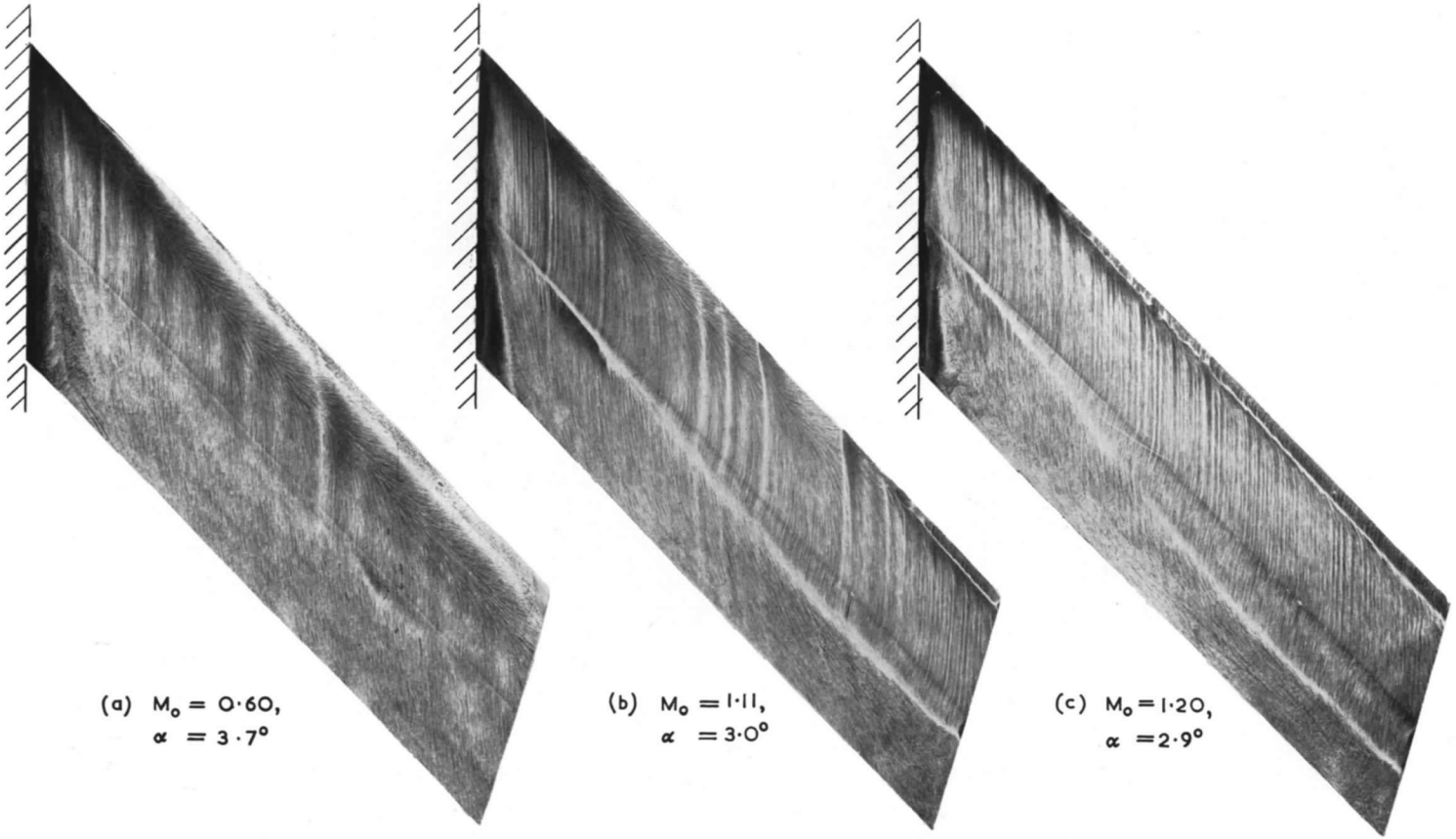

FIG. 69. Oil patterns on upper surface of double-wedge wing at $\phi = 45°$.

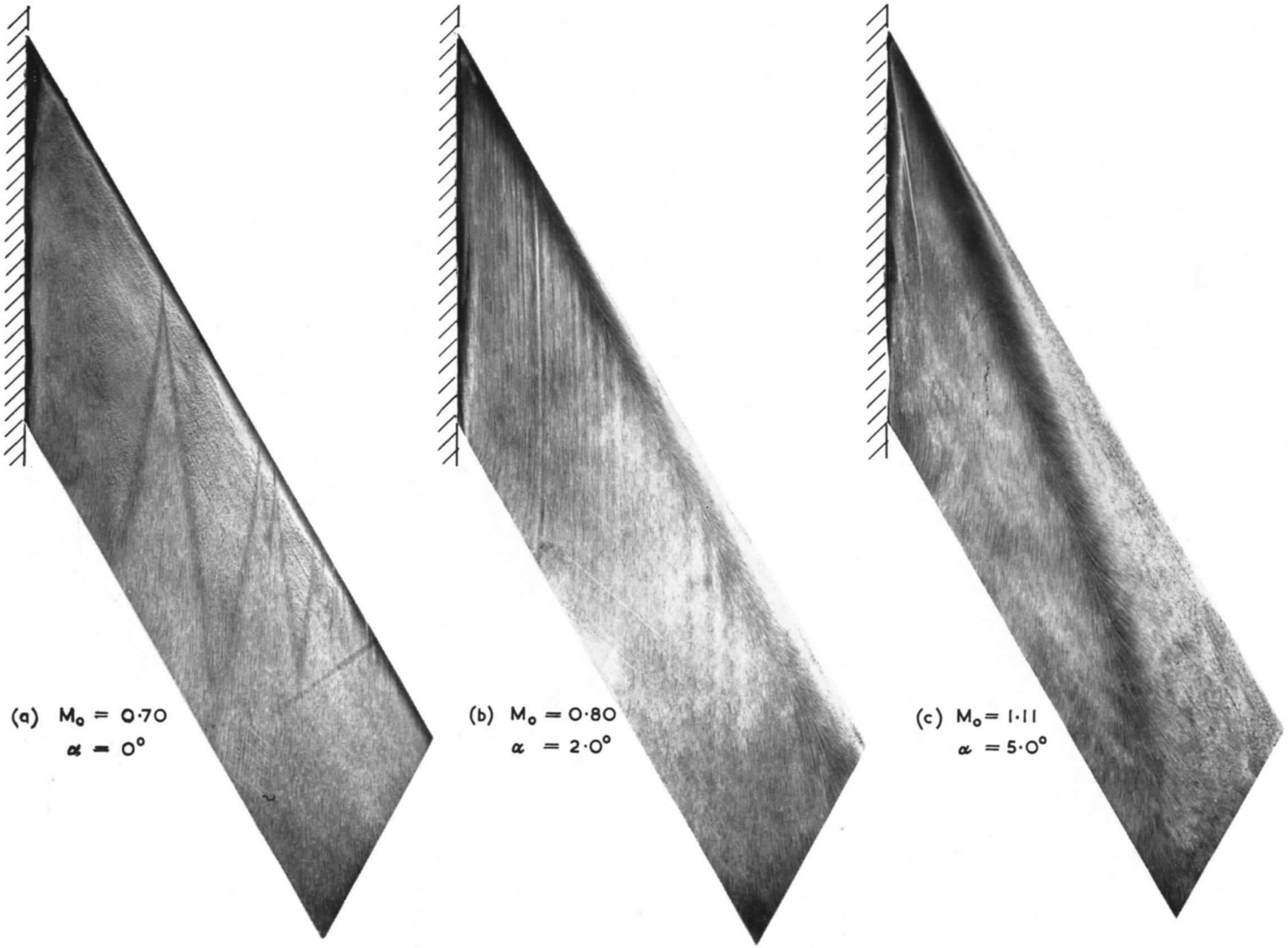

FIG. 70. Oil patterns on upper surface of single-wedge wing at $\phi = 60°$.

(88242) Wt. 65/1418 K.5 12/63 Hw.

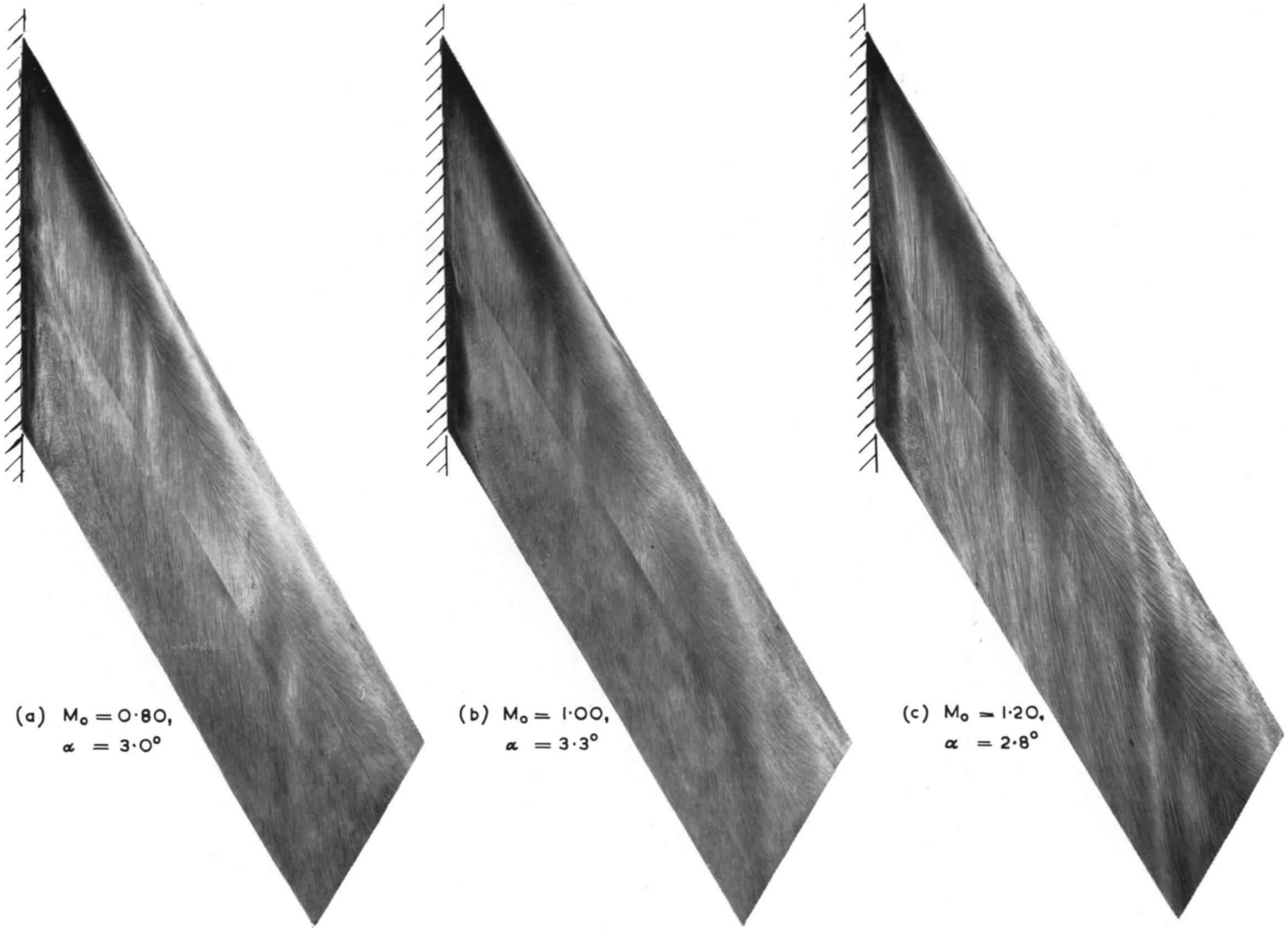

FIG. 71. Oil patterns on upper surface of double-wedge wing at $\phi = 60°$.

Publications of the Aeronautical Research Council

ANNUAL TECHNICAL REPORTS OF THE AERONAUTICAL RESEARCH COUNCIL (BOUND VOLUMES)

1942 Vol. I. Aero and Hydrodynamics, Aerofoils, Airscrews, Engines. 75*s.* (post 2*s.* 9*d.*)
Vol. II. Noise, Parachutes, Stability and Control, Structures, Vibration, Wind Tunnels. 47*s.* 6*d.* (post 2*s.* 3*d.*)

1943 Vol. I. Aerodynamics, Aerofoils, Airscrews. 80*s.* (post 2*s.* 6*d.*)
Vol. II. Engines, Flutter, Materials, Parachutes, Performance, Stability and Control, Structures. 90*s.* (post 2*s.* 9*d.*)

1944 Vol. I. Aero and Hydrodynamics, Aerofoils, Aircraft, Airscrews, Controls. 84*s.* (post 3*s.*)
Vol. II. Flutter and Vibration, Materials, Miscellaneous, Navigation, Parachutes, Performance, Plates and Panels, Stability, Structures, Test Equipment, Wind Tunnels. 84*s.* (post 3*s.*)

1945 Vol. I. Aero and Hydrodynamics, Aerofoils. 130*s.* (post 3*s.* 6*d.*)
Vol. II. Aircraft, Airscrews, Controls. 130*s.* (post 3*s.* 6*d.*)
Vol. III. Flutter and Vibration, Instruments, Miscellaneous, Parachutes, Plates and Panels, Propulsion. 130*s.* (post 3*s.* 3*d.*)
Vol. IV. Stability, Structures, Wind Tunnels, Wind Tunnel Technique. 130*s.* (post 3*s.* 3*d.*)

1946 Vol. I. Accidents, Aerodynamics, Aerofoils and Hydrofoils. 168*s.* (post 3*s.* 9*d.*)
Vol. II. Airscrews, Cabin Cooling, Chemical Hazards, Controls, Flames, Flutter, Helicopters, Instruments and Instrumentation, Interference, Jets, Miscellaneous, Parachutes. 168*s.* (post 3*s.* 3*d.*)
Vol. III. Performance, Propulsion, Seaplanes, Stability, Structures, Wind Tunnels. 168*s.* (post 3*s.* 6*d.*)

1947 Vol. I. Aerodynamics, Aerofoils, Aircraft. 168*s.* (post 3*s.* 9*d.*)
Vol. II. Airscrews and Rotors, Controls, Flutter, Materials, Miscellaneous, Parachutes, Propulsion, Seaplanes, Stability, Structures, Take-off and Landing. 168*s.* (post 3*s.* 9*d.*)

1948 Vol. I. Aerodynamics, Aerofoils, Aircraft, Airscrews, Controls, Flutter and Vibration, Helicopters, Instruments, Propulsion, Seaplane, Stability, Structures, Wind Tunnels. 130*s.* (post 3*s.* 3*d.*)
Vol. II. Aerodynamics, Aerofoils, Aircraft, Airscrews, Controls, Flutter and Vibration, Helicopters, Instruments, Propulsion, Seaplane, Stability, Structures, Wind Tunnels. 110*s.* (post 3*s.* 3*d.*)

Special Volumes

Vol. I. Aero and Hydrodynamics, Aerofoils, Controls, Flutter, Kites, Parachutes, Performance, Propulsion, Stability. 126*s.* (post 3*s.*)
Vol. II. Aero and Hydrodynamics, Aerofoils, Airscrews, Controls, Flutter, Materials, Miscellaneous, Parachutes, Propulsion, Stability, Structures. 147*s.* (post 3*s.*)
Vol. III. Aero and Hydrodynamics, Aerofoils, Airscrews, Controls, Flutter, Kites, Miscellaneous, Parachutes, Propulsion, Seaplanes, Stability, Structures, Test Equipment. 189*s.* (post 3*s.* 9*d.*)

Reviews of the Aeronautical Research Council

1939–48 3*s.* (post 6*d.*) 1949–54 5*s.* (post 5*d.*)

Index to all Reports and Memoranda published in the Annual Technical Reports

1909–1947 R. & M. 2600 (out of print)

Indexes to the Reports and Memoranda of the Aeronautical Research Council

Between Nos. 2351–2449	R. & M. No. 2450	2*s.* (post 3*d.*)
Between Nos. 2451–2549	R. & M. No. 2550	2*s.* 6*d.* (post 3*d.*)
Between Nos. 2551–2649	R. & M. No. 2650	2*s.* 6*d.* (post 3*d.*)
Between Nos. 2651–2749	R. & M. No. 2750	2*s.* 6*d.* (post 3*d.*)
Between Nos. 2751–2849	R. & M. No. 2850	2*s.* 6*d.* (post 3*d.*)
Between Nos. 2851–2949	R. & M. No. 2950	3*s.* (post 3*d.*)
Between Nos. 2951–3049	R. & M. No. 3050	3*s.* 6*d.* (post 3*d.*)
Between Nos. 3051–3149	R. & M. No. 3150	3*s.* 6*d.* (post 3*d.*)

HER MAJESTY'S STATIONERY OFFICE

from the addresses overleaf

Printed and published by
HER MAJESTY'S STATIONERY OFFICE

To be purchased from
York House, Kingsway, London W.C.2
423 Oxford Street, London W.1
13A Castle Street, Edinburgh 2
109 St. Mary Street, Cardiff
39 King Street, Manchester 2
50 Fairfax Street, Bristol 1
35 Smallbrook, Ringway, Birmingham 5
80 Chichester Street, Belfast 1
or through any bookseller

Printed in England

S.O. Code No. 23-3348